AIRCRAFT AGILITY

by

Brian G. Thompson

Thesis submitted to the faculty of the
Virginia Polytechnic Institute and State University
in partial fulfillment of the requirements for the degree of

Master of Science

in

Aerospace and Ocean Engineering

APPROVED:

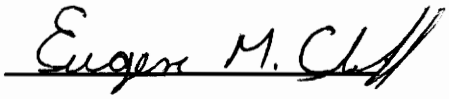

Dr. E.M. Cliff, Chairman

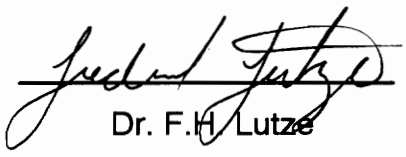

Dr. F.H. Lutze

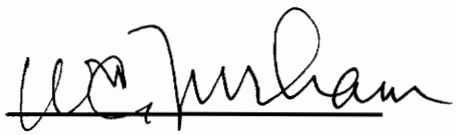

Dr. W.C. Durham

December 4, 1992
Blacksburg, Virginia

C.2

AIRCRAFT AGILITY

by

Brian G. Thompson

Dr. E.M. Cliff, Chairman

Aerospace and Ocean Engineering

(ABSTRACT)

A definition of an aircraft agility vector is given as the time rate-of-change of the applied forces acting on an aircraft and agility is characterized as being representable by instantaneous and integral time-scales. A unified framework for evaluating instantaneous and integral agility is developed based on the notion of a new dynamic model for aircraft motions. This model may be viewed as intermediate between a point-mass model, in which the body attitude angles are control-like, and a rigid-body model, in which the body attitude angles evolve according to Newton's Laws. Specifically, we consider the case of symmetric flight and construct a model in which the body roll-rate and pitch-rate are the controls. Accordingly, we refer to this new dynamics model as the *body-rate model, (BRM).*

Instantaneous agility is presented as the locus of achievable agility vectors and the construction of such *agility sets* is demonstrated from aerodynamic and propulsive data for a modern jet fighter. Figures depicting this locus are displayed with indications of the limiting control. An integral performance flight problem is presented and subsequently solved via the optimal control theory. *Agility metrics* are suggested for this problem based on the transients which exist between the dynamics of the *BRM* and those of the point-mass model. Suggestions are also provided on the use of instantaneous *agility sets* and integral *agility metrics* in the design of aircraft and in performance comparisons of competing aircraft.

ACKNOWLEDGEMENTS

First and foremost I would like to thank Dr. E.M. Cliff for his assistance and infinite patience throughout the writing of this thesis. I have known Dr. Cliff for over seven years now, during that time I have learned a great deal about not only Flight Dynamics and Control but, also about what it means to be a gentleman and a highly respected professional. If, in the course of my career, I can achieve a fraction of the reputation and respect that Dr. Cliff has achieved, I will truly be able to consider myself a success. Dr. F.H. Lutze also deserves special thanks for his guidance on this project and for the fond memories that I have of the times we spent flying and "talking flying". Thanks are also due to Dr. W.C. Durham, for serving on my committee, and to the staff and students associated with the Interdisciplinary Center for Applied Math (ICAM) for providing a relaxed yet serious atmosphere for research.

In acknowledging assistance in completing my Master of Science degree, I certainly cannot neglect to mention my wife, Cathy, who insisted on leaving the job, friends and home she loved to allow me to return to school to pursue this degree. I will be forever grateful for this tremendous sacrifice. I also want to thank my son Alexander Jacob, for being born and thereby forcing me to face reality and subsequently complete this thesis, and my parents, in-laws, family and friends who have all provided me with moral support.

Finally, on the economic side, I would like to thank both the Aerospace and Ocean Engineering Department at Virginia Tech, for providing me with assistantships and tuition waivers throughout the time I was resident in Blacksburg, and NASA Langley Research Center for providing funds to support research on aircraft agility under contract NAG-1-1405.

TABLE OF CONTENTS

LIST OF FIGURES

CHAPTER 5: INTEGRAL AGILITY

APPENDIX B: THE AIRCRAFT MODEL

LIST OF SYMBOLS

AGILITY-RELATED VARIABLES

$\vec{\mathbf{a}}$	Aircraft Acceleration Vector	ft/s^2
$\vec{\mathbf{A}}$	Aircraft Kinetic Agility Vector	lbf/s or g/s
A_x, A_y, A_z	Axial, Lateral and Normal Agility Components	lbf/s or g/s
f	Reference to Generic Coordinate Frame	N/A
$\vec{\mathbf{F}}$	Aircraft Force Vector	lbf
I	Reference to Inertial Coordinate Frame	N/A
$\vec{\mathbf{J}}$	Aircraft Kinematic Agility Vector (Jerk)	ft/s^3
$\vec{\mathbf{V}}$	Aircraft Velocity Vector	ft/s

AIRCRAFT STATE & CONTROL-RELATED VARIABLES

h	Altitude or height	ft
M	Mach Number	none
n	Lateral Load-Factor	$g's$
p, q, r	Body-Axis Roll, Pitch and Yaw-Rates	deg/s or rad/s
p_w, q_w, r_w	Wind-Axis Roll, Pitch and Yaw-Rates	deg/s or rad/s
$\vec{\mathbf{T}}$	Thrust Vector	lbf
T_n	Net Thrust	lbf
$\dot{T}$	Thrust-Rate	lbf/s or g/s
$\vec{\mathbf{u}}$	Vector of Controls	N/A
V	Velocity	ft/s
V_C	Corner Velocity	ft/s
x	Downrange Position	ft
$\vec{\mathbf{x}}$	Vector of States	N/A
$\dot{\vec{\mathbf{x}}}$	Vector of State-Rates	N/A
y	Crossrange Position	ft
α	Angle-of-Attack	deg

β	Sideslip-Angle	deg
χ	Heading-Angle (Velocity Yaw)	deg
$\vec{\delta}$	Vector of Control Surface Deflections	deg
$\delta_A, \delta_S, \delta_R, \delta_T$	Aileron, Stabilator, Rudder and Throttle Deflections	deg
γ	Flight Path Angle (Velocity Pitch)	deg
μ	Bank-Angle (Velocity Roll)	deg
$\vec{\omega}$	Body-Axes Angular Velocity Vector	deg/s or rad/s
$\vec{\omega}_w$	Wind-Axes Angular Velocity Vector	deg/s or rad/s

AIRCRAFT AERODYNAMIC AND PHYSICAL PROPERTIES VARIABLES

b	Wingspan	ft
$\overline{c}$	Mean Aerodynamic Chord	ft
C_D, C_L	Drag and Lift Force Coefficients	none
$C_{D_\alpha}, C_{L_\alpha}$	Drag and Lift Coefficient Derivatives with α	deg^{-1}
C_{D_M}, C_{L_M}	Drag and Lift Coefficient Derivatives with Mach	none
C_l, C_m, C_n	Roll, Pitch and Yaw Moment Coefficients	none
$C_{l_{\delta_A}}, C_{m_{\delta_S}}, C_{n_{\delta_R}}$	Roll, Pitch and Yaw Surface Deflection Derivatives	deg^{-1}
$C_{l_p}, C_{m_q}, C_{n_r}$	Roll, Pitch and Yaw Damping Derivatives	none
D, L, Q	Drag, Lift and Side Forces	lbf
I_x, I_y, I_z	Mass Moment-of-Inertia About (x,y,z) Body-Axes	$slug - ft^2$
L, M, N	Roll, Pitch and Yaw Moments	$ft - lbf$
m	Mass	$slugs$
S	Reference Area	ft^2
W	Weight	lbf

OPTIMAL CONTROL-RELATED VARIABLES

f	Vector of State Equations (state-rates)	N/A
H	Variational-Hamiltonian	none
H_{CD}	Control Dependent Hamiltonian Terms	none
J	Performance Index	deg
r	Radius Control for Circular Control Bound	none
S	Switching Function	N/A
ϕ	Cost Functional	N/A

λx	Influence Function for State Variable x	N/A
ν	Adjoint Variable for (p,q) Control Constraint	rad/s
π	Jump Vector for Co-States	none
θ	Adjoint Variable for α State Constraint	none
σ	Angular Control for Circular Control Bound	rad

MISCELLANEOUS VARIABLES

a	Atmospheric Sonic Speed	ft/s
a_h	Sonic Speed Derivative with Altitude	s^{-1}
g	Acceleration Due to Gravity	ft/s^2
n	Aircraft Lateral Load-Factor	$g's$
$\bar{q}$	Dynamic Pressure	lbf/ft^2
t	Time	s
ρ	Atmospheric Density	sl/ft^3
ρ_h	Density Derivative with Altitude	sl/ft^4

CHAPTER 1
INTRODUCTION AND BACKGROUND

1.1: Motivations for Agility Research

Aircraft designers have always been interested in comparing flying characteristics of competing designs. Historically, these have been comparisons of performance parameters or flying qualities characteristics. Flight performance comparisons can generally be separated into the following two distinct categories in terms of time-scales (see Miele [25], p. 117):

- Point (instantaneous) performance
- Integral performance

Where instantaneous performance examines properties at a given instant in time and, integral performance examines properties over a finite length of time.

For early, low-performance fighter aircraft the instantaneous performance measures-of-merit generally included maximum rate-of-climb, maximum turn-rate and maximum level-flight speed while endurance and range were the primary integral performance measures. Figure 1.1 displays several measures of instantaneous turning performance vs. aircraft velocity and altitude. From this plot one can determine the aircraft velocity required to achieve maximum turn-rate, $\dot{\chi}$, minimum turn-radius, r_{min}, maximum load-factor, n_{max}, or maximum bank angle, μ_{max}, as a function of altitude.

As aircraft technology advanced, and new weapons such as air-to-air missiles appeared on the scene, missions became more complex and the early standards of performance comparison were seen to be deficient resulting in a search for new measures-of-merit. Such requirements led to the introduction of energy-maneuverability and cruise-dash methods which are currently used in evaluating fighter aircraft performance [2,4,5,9,16,23,29,30,33]. Figure 1.2 depicts an energy-

maneuverability hodograph for a modern fighter aircraft. As indicated on the figure the key points on the hodograph are the points of maximum energy-rate (A), maximum sustainable turn-rate (B) and, maximum turn-rate (C). Recent developments in aircraft and missile technology, such as all-aspect missiles, thrust vectoring, electronic countermeasures, stealth and digital flight control, are once again requiring that designers seek new performance measures-of-merit. Whereas earlier performance measures have primarily been based on point mass dynamics, this model is obviously inadequate for describing measures-of-merit associated with evolving tactics, such as post-stall or point-and-shoot maneuvers, which may be important for future air combat success. For maneuvers of this type some account must be made of the rigid-body dynamics. Efforts in this direction have led researchers to introduce a notion which is commonly referred to as *agility*. An expanded summary of McAtee's description [see Figure 2, ref. 24] of the evolution of aircraft and weapon characteristics and corresponding performance measures is presented in Figure 1.3. In the following sections we present a brief summary of existing agility concepts and an overview which describes the purpose of the present analysis.

1.2: Existing Notions of Agility

Agility research has been ongoing since at least 1985 [31]. Since that time a number of so-called *agility metrics* have been proposed by industry, government and academic researchers [11,14,17,24,31,32,34]. A qualitative description of several of these concepts is provided in Figure 1.4. While the diversity of these ideas is obvious, there are also many similarities. Other researchers have attempted to organize and classify the proposed metrics or analyze them and compare them with existing flying qualities parameters [3,12,15,22,26,27,28,36]. Two summaries of existing agility metrics which attempt to organize the subject are those done by Dorn [12] and Bitten [3].

In [12] Dorn states that agility can, and has been, "associated with transients, controllability, maneuverability, pointing ability, acceleration, dynamics, flying qualities and performance". He then goes on to suggest that, due to the overwhelming number of agility definitions, it may be best to "undefine" agility and proceed to redefine it in an orderly, scientific fashion. Dorn advocates classifying agility in terms of "state-change activity" versus maneuver time and then choosing generalized agility metrics associated with three characteristic time bands:

(1) Instantaneous rates,

(2) Small-amplitude tasks (1-2 second maneuvers)

(3) Large-amplitude tasks (10-20 second maneuvers)

He defines the complete set of time bands as an "agility spectrum". A depiction of this agility spectrum is shown in Figure 1.5. As Dorn mentions, the purpose of his paper is to *stimulate ideas* relative to the establishment of an "Agility Science", as such he offers no precise definitions of generalized agility metrics.

In an analysis of existing agility metrics conducted concurrently with Dorn's analysis, Bitten notes in [3] that most researchers agree that agility can be described by considering three "agility components" consisting of:

(1) Longitudinal/Axial agility in the direction of the velocity vector

(2) Pitch/Curvature/Normal agility contained in the maneuver plane

(3) Roll/Torsional/Lateral agility representing rotation of the lift vector

He also notes that the proposed metrics can be related to either the maneuver state or its first or second derivative and in terms of maneuver time-scales may be classified as being either transient (instantaneous or short duration integral) or functional (long duration integral). Figure 1.6 classifies several existing agility concepts according to Bitten's "agility spectrum".

From the papers by Dorn and Bitten, as well as the works of other researchers, it is obvious that there are two basic schools of thought regarding agility metrics, after Miele [25] they can most simply be described as:

- Instantaneous agility
- Integral agility

Where instantaneous agility may be associated with notions of a jerk vector which can be evaluated at any point along the aircraft path and integral agility may be characterized by "time-to" metrics such as point-and-shoot or roll reversal maneuvers. In lieu of the "agility spectra" proposed by other researchers, the terms instantaneous and integral will be used in this paper to describe two basic types of agility metrics.

1.3: A Unified Approach to Agility

Although the agility metrics discussed in the previous section are all useful measures-of-merit in their own right, it is obvious that a need exists for a unifying agility framework which is based on a solid mathematical foundation. In fact, Dorn [12] states the following; "There seems to be little work ongoing to look at instantaneous agility. This can be disconcerting when one considers that this is the building block of the other time-scales ... ", he then goes on to mention that "there may be alternative approaches [to agility] that use different reference frames or state variables ...". With Dorn's statement in mind, the purposes of this paper can be revealed as providing:

- A *sharp definition* of agility beginning with the notion of instantaneous agility, and
- A *unifying mathematical framework* in which one can assess the agility inherent in a given aircraft design.

Before these goals can be realized, a few words on "total aircraft agility" are warranted. As noted by Riley and Drajeske [26], many notions about agility are based on success in the aerial-combat arena. Within this scenario one must consider threat aircraft and missiles, avionics, stealth, weaponry and pilot technique. Due to this complexity, we cannot offer a *precise* definition of total aircraft agility. However, the definition of agility presented herein *is* based on well-founded concepts in flight mechanics and can be used to provide some useful, *computable* measures of agility.

An obvious starting point for building the framework of agility is Newton's 2nd Law. By considering the inertial time rate-of-change of *both* sides of Newton's equation it is possible to not only assess the agility at each point of a specific maneuver in terms of kinematics (*ie* the acceleration rate or jerk vector), but to also derive "agility sets" by determining the locus of all achievable instantaneous force-rate vectors. Figure 1.7 depicts a conceptual notion of agility sets as compared to a single jerk vector. The concept under consideration is that an aircraft has a certain potential for agility which may be described by a 3-dimensional agility set. As the aircraft changes flight conditions, its potential agility and thus the shape of the agility set will change. If the boundary of the agility set of one aircraft exceeds that of another, then one may be able to say, independently of maneuver choice, that the first aircraft has more agility than the other at that point in the flight envelope. Comparisons over several points in the flight envelope would

reveal regions which yield the greatest advantages or disadvantages. Most significantly, in regions where an agility margin is not satisfactory, limiting controls can be identified thereby aiding the design process. Moreover, these ideas are extendable to integral time-scales wherein *optimal* maneuvers can be flown by continually operating the aircraft at the limits of the agility set. This is in contrast to most existing notions of integral or functional agility in which the maneuvers are usually not flown in an optimal manner. These ideas on instantaneous and integral agility performance are examined in detail in the remaining chapters.

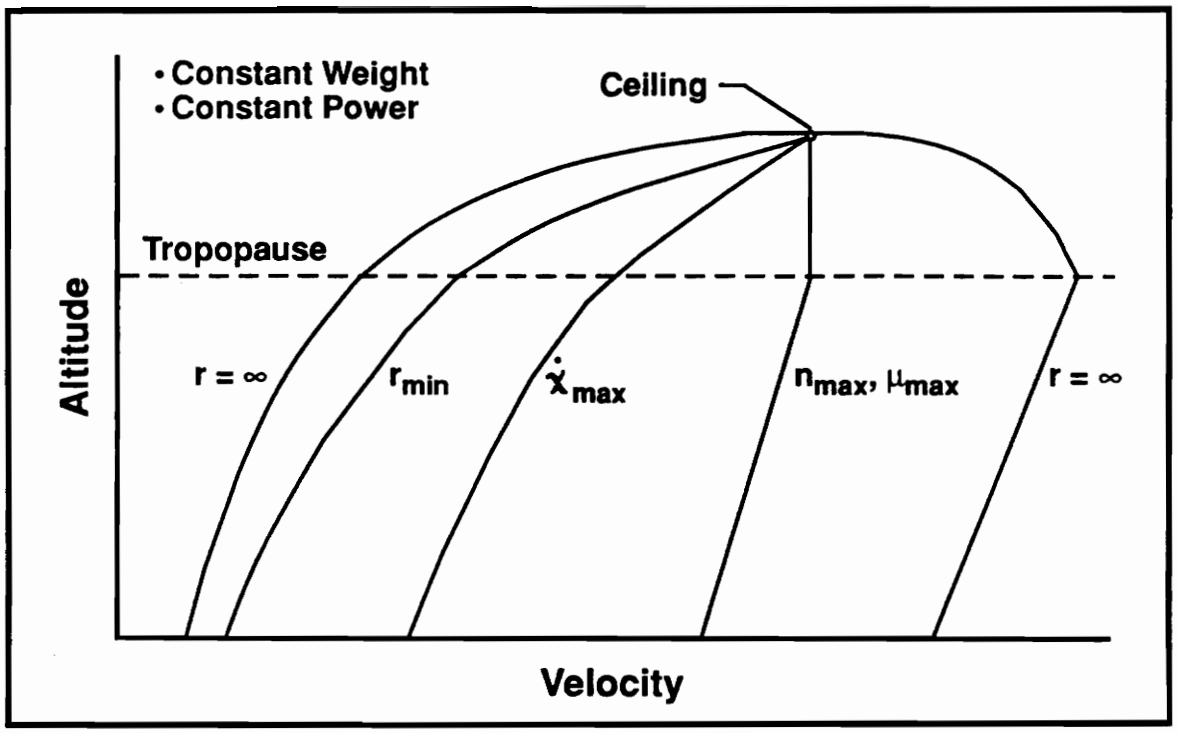

Figure 1.1. Instantaneous Turning Performance

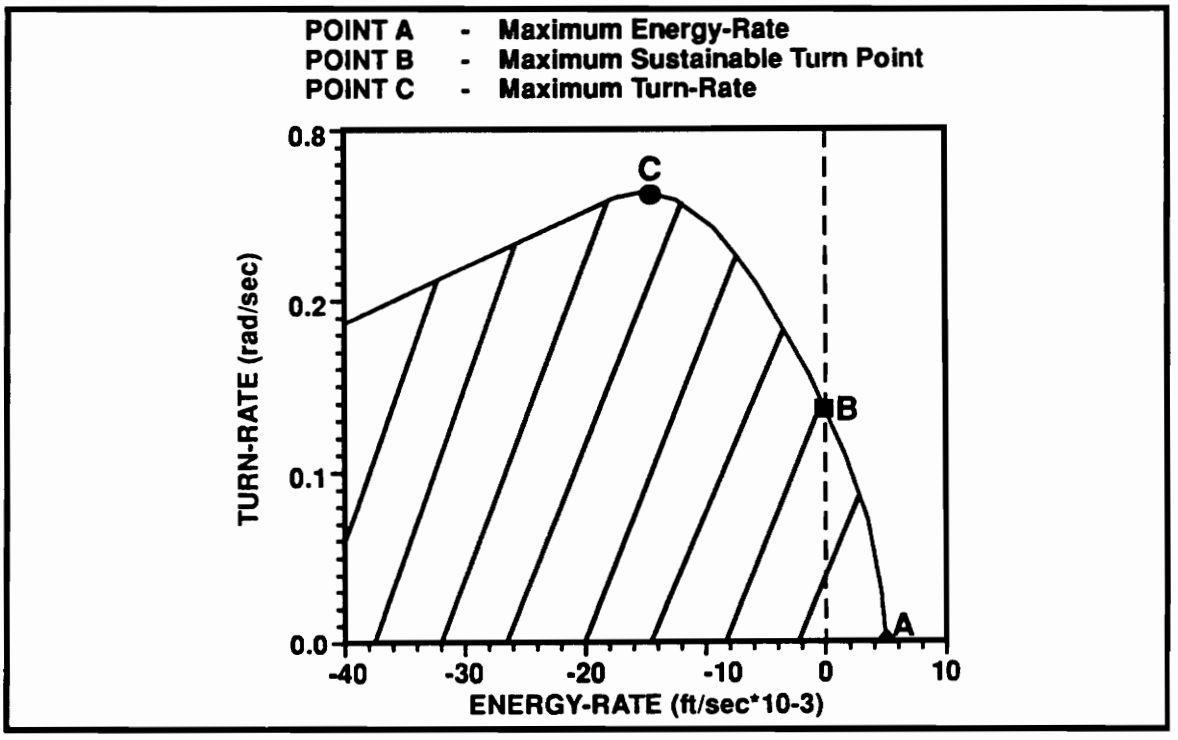

Figure 1.2. Energy-Maneuverability Hodograph

ERA	AIRCRAFT CHARACTERISTICS	WEAPON CHARACTERISTICS	PERFORMANCE METRIC
WW I	• Low Tech Prop • Slow Speeds • Very High Turn-Rates • Short Range	• Small Caliber Guns • Small Gravity Bombs	• Limited Measures of Performance
WW II	• High Tech Prop • Moderate Speeds • Very High Turn-Rate • Long Range	• Small Caliber Guns • Large Gravity Bombs • Improved Weapon Release/Aiming	• Emphasis on Instantaneous Capabilities, Range and Endurance
Korea	• Early Jets • High Speeds • High Turn-Rates • Long Range	• Improved Guns • Unguided Missiles • No Significant Gains in Weapon Control	• Energy-Maneuverability and Cruise-Dash Techniques
Vietnam	• High Performance Jets • Very High Speeds • Low Turn-Rates • Very Long Range	• State-of-Art Guns • Guided Bombs • BVR Guided Missiles • Rear Aspect IR Missiles	• Energy-Maneuverability and Cruise-Dash Techniques
1990's	• Basic Performance Similar to Vietnam Era • Electronic Displays • Digital Flight Control • Thrust Vectoring	• Advanced BVR Missiles • All Aspect Missiles • Fire & Forget • Countermeasures	• Advances in Technology Dictate New Measures of Performance ••• AGILITY •••

Figure 1.3. Evolution of Performance Metrics

SOURCE	METRIC	DESCRIPTION
Herbst (MBB)	• Tangential Agility • Curvature Agility • Torsion Agility	• Rate-of-change of longitudinal acceleration • Rate-of-change of lateral acceleration • Angular rotation of the Lift vector
Skow (Eidetics)	• Energy Rate • Pitch Agility • Turn Agility	• Change in axial acceleration • Time-to-achieve change in lateral g-level • Time-to-capture specified roll angle
AFFTC	• Airspeed Capture • Pitch Capture • Bank Capture	• Time-to-achieve final airspeed • Time-to-achieve final pitch angle • Time-to-achieve final bank angle
McAtee (General Dynamics	• Dynamic Speed Turn • Supermaneuver Controllability	• Acceleration capability as function of velocity • Turn-rate vs velocity bleed-rate • Capability to achieve high α and $\dot{\alpha}$ while maintaining control of aircraft
Kalviste (Northrop)	• DT Parameter • Roll Reversal	• Combined measure of turn time-radius • Capability to reverse turn direction quickly

Figure 1.4. A Sampling of Proposed Agility Metrics

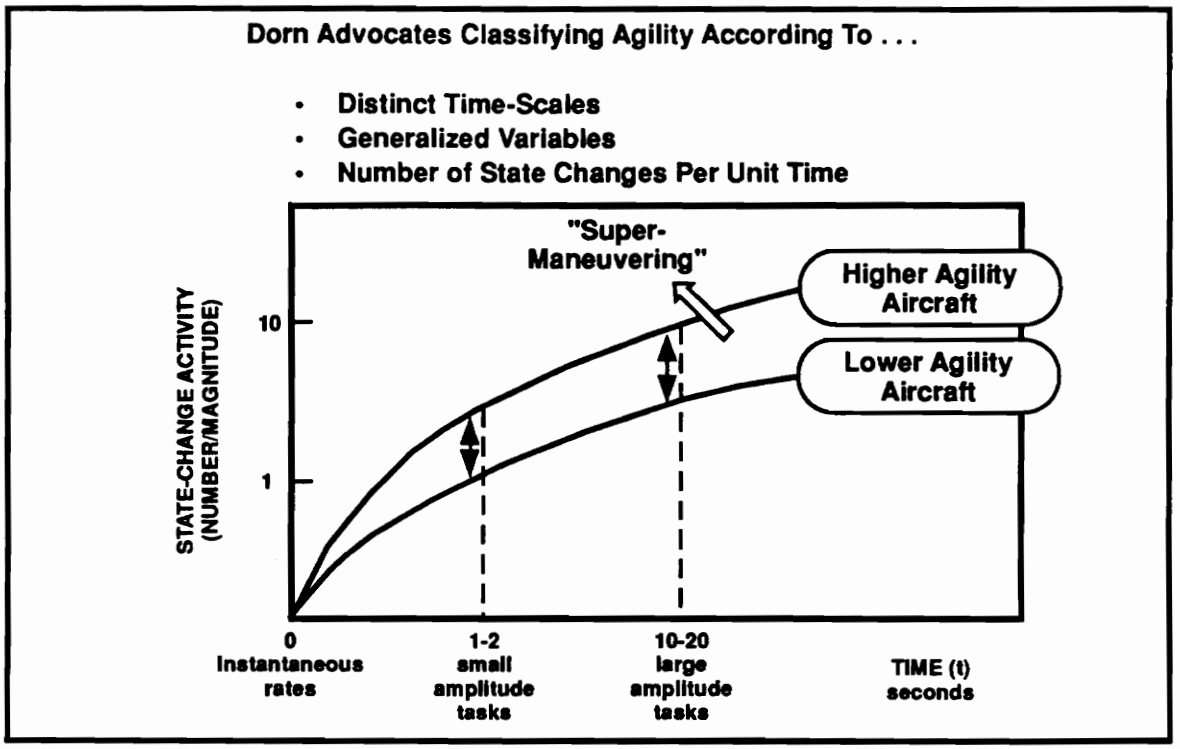

Figure 1.5. Dorn's "Agility Spectrum"

Bitten Classifies Agility With . . .

- Nondistinct Time-Scales
- Agility Components

Agility Component	*General Dynamics*	*AFFTC*	*Eidetics*	*MBB*	*Working Definition*
Longitudinal (Axial)	Dynamic Speed	Time To Final Air Speed	Energy Rate	A_j	$\dot{N}_x$
Curvature (Pitch)	Turn	Time To Capture θ or ψ	Time To Pitch	A_k	$\dot{N}_z$
Torsional (Roll)	p, q, r At High α	Time To Bank	Turn Agility	A_t	$\dot{P}_{stab}$

Functional — Transient

Maneuverability — Agility

Figure 1.6. Bitten's "Agility Spectrum"

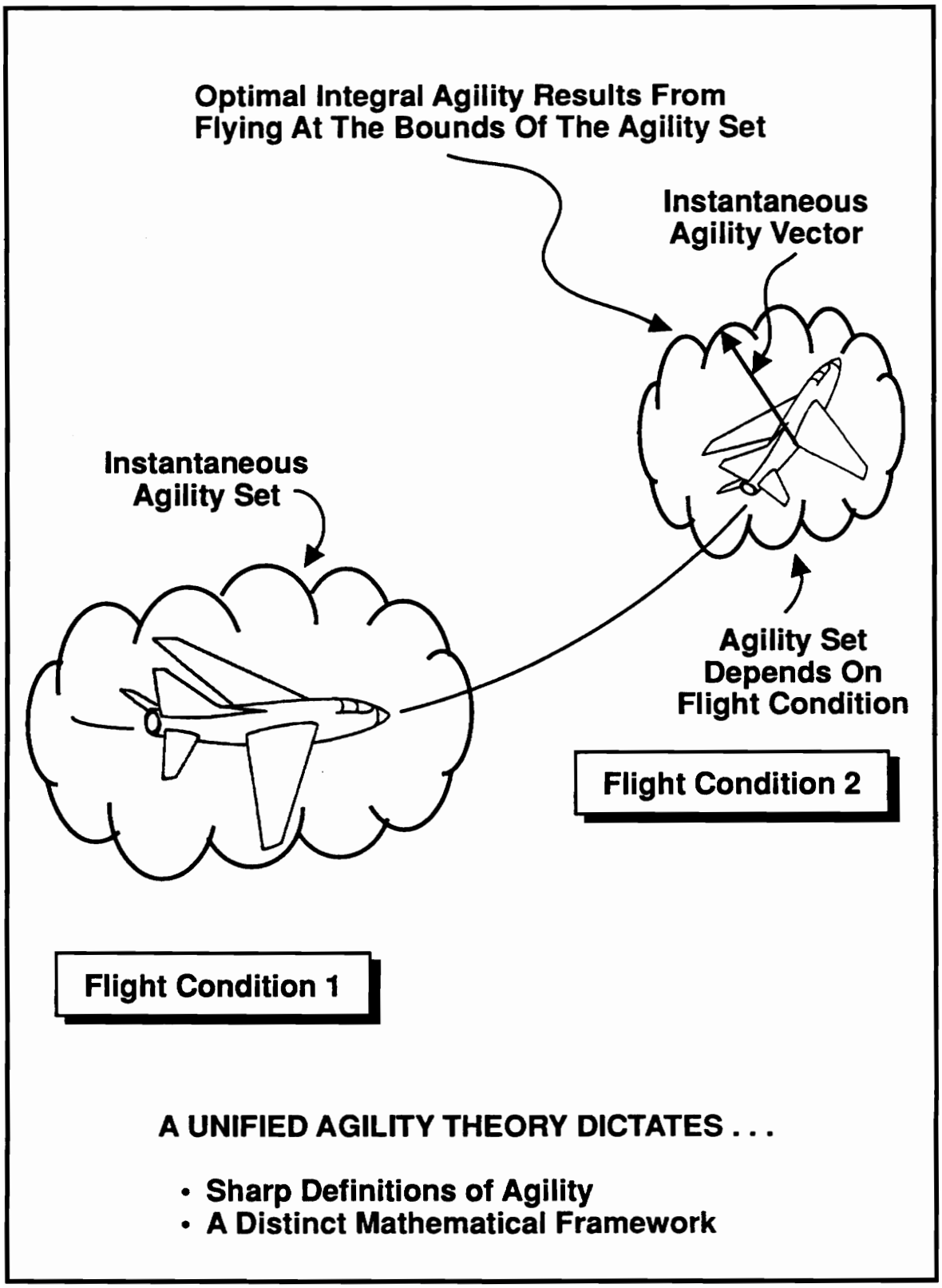

Figure 1.7. A Unified Theory of Aircraft Agility

CHAPTER 2
QUANTIFYING AGILITY

2.1: The Agility Vector

Previous researchers, such as Herbst [14], have proposed that agility be defined as the time derivative of the acceleration vector. This notion could appropriately be described as "kinematic agility" since the emphasis is placed on the properties of the flight path and one is not directly concerned with the forces acting on an aircraft. Kinematic agility is intuitively pleasing and very useful if one wishes to *analyze* the agility displayed during a particular maneuver or tactic. On the other hand, to *predict* the agility of a proposed vehicle, one is led to consider "kinetic agility" where the focus is on the aircraft force-rates instead of the acceleration-rates. In this view it is possible to estimate not only a single "agility vector" but, also an "agility set" the boundary of which is determined by the locus of the limiting values of all achievable force-rate vectors. This concept could prove to be quite useful in the design of agile aircraft since it can be related to control effectiveness. Based on Newton's 2nd Law, it is possible to incorporate the notions of "kinematic" and "kinetic" agility into a single unifying definition resulting directly from the most basic of the principles of flight mechanics. As such, the author feels that this definition of agility can provide the foundation for the "agility science" advocated by Dorn.

In order to derive the "agility vector" we start by recalling Newton's 2nd Law as follows:

$$\bar{\mathbf{F}} = m \frac{d\bar{\mathbf{V}}}{dt} \Big|_I \tag{2.1}$$

The subscript I indicates that the time derivative of the velocity is taken with respect to an inertial reference frame which is necessary for the Law to remain valid. However, it is noted that the force, velocity and acceleration vectors may be *represented* in any reference frame whether it be inertial or non-inertial. The best choice for such a reference system is not clear and is usually a matter of convenience. Coordinate systems will be discussed in more detail in Section 2.2.

Note that the aircraft mass is considered to remain constant, this is a reasonable approximation given the short maneuver time-spans associated with agility-type maneuvers.

By concentrating on the left-hand side of equation (2.1) one is led to compute agility as the time rate of change of the applied forces acting on an aircraft (kinetic agility) as follows:

$$\vec{\mathbf{A}} = \frac{d\vec{\mathbf{F}}}{dt}\Big|_f \tag{2.2}$$

where the *f* indicates that the derivative may be taken with respect to any desired frame of reference since equation (2.2) represents a *definition* rather than a physical law. In an analogous manner, one may also compute agility relative to the time rate of change of the acceleration (kinematic agility) by concentrating on the right-hand side of (2.1), *ie*:

$$\vec{\mathbf{A}} = \frac{d}{dt}\left[m \frac{d\vec{\mathbf{V}}}{dt}\Big|_I \right]\Big|_f \tag{2.3}$$

Once again the choice for the system *f* is not restricted. However, if one wishes to relate agility to a *true* jerk vector , where:

$$\vec{\mathbf{J}} = \frac{d^2\vec{\mathbf{V}}}{dt^2}\Big|_I \tag{2.4}$$

then the time derivative in equations (2.2) and (2.3) must be taken with respect to an inertial reference frame. As such, we choose to define the coordinate system *f* as the inertial system I and to carry out the time derivatives in (2.2) and (2.3) accordingly. This leads to an agility vector which is *defined* by the equation:

$$\vec{\mathbf{A}} = \frac{d\vec{\mathbf{F}}}{dt}\Big|_I = m\vec{\mathbf{J}} \tag{2.5}$$

where the vector $\vec{\mathbf{A}}$ represents kinetic agility (lbf/sec) and the vector $\vec{\mathbf{J}}$ represents kinematic agility (ft/sec^3). Note that since the aircraft mass is considered to be constant, it is a simple matter to convert from kinetic agility to kinematic agility or vice versa. It is therefore convenient to retain the separate notions of kinetic and kinematic agility. However, the reader should keep in mind that the definition of agility, and the resulting agility vector presented herein, are based on

the time differentiation of Newton's 2nd Law as given in equation (2.1) and are therefore representative of kinetic agility. The details of the differentiation operation are discussed in Sections 2.3 and 2.4.

2.2: Coordinate System Considerations

As mentioned in the previous section, the choice of the best reference system on which to represent the force and velocity vectors (and therefore the agility vector) is not intuitively obvious, it depends on how one would define "best". Since the choice does not change the agility vector itself, it seems to come down to a decision based on utility or convenience. The three coordinate systems which immediately come to mind are the:

- Body-fixed axes
- Wind axes
- Frenet or "natural" axes.

Where the body-fixed and wind systems are probably the most commonly employed reference frames in flight mechanics applications and the Frenet system forms the basis of the study of space curves known as differential geometry [25,35]. The body-fixed and wind systems are compared to each other in Figure 2.1, and the Frenet system is depicted in Figure 2.2. One might note from these figures that both the wind and Frenet systems are defined relative to the velocity vector and therefore move with respect to the aircraft. The body-fixed axes are, of course, rigidly fixed within the aircraft. Specifically, the axes of these systems are aligned as follows:

Body-Fixed System

x_B : contained in the aircraft plane of symmetry and positive forward.

z_B : perpendicular to the x_B-axis, contained in the aircraft plane of symmetry, and positive downward for a normal flight attitude.

y_B : perpendicular to the aircraft plane of symmetry and oriented such that the system is right-handed.

Wind System

x_w : tangent to flight path (velocity) and positive in direction of flight.

z_w : perpendicular to the x_w-axis, contained in the aircraft plane of symmetry, and positive downard for a normal flight attitude.

y_w : perpendicular to the x_w-z_w plane and oriented such that the system is right-handed.

Frenet System

t : *tangent vector*, tangent to the flight path and positive forward.

n : *principal normal*, perpendicular to the tangent vector, contained in the osculating plane, directed along the instantaneous radius of curvature of the flight path, and positive toward the center of curvature.

b : *binormal*, perpendicular to the osculating plane, right-handed system.

In trying to determine which coordinate system is best-suited for a study of agility, it is noted that agility, as defined herein, has close connections with the velocity vector. It therefore seems reasonable to choose a coordinate system with an orientation which is directly related to the velocity vector rather than being strictly associated with aircraft geometry. The body-fixed system has not been chosen for the present study for primarily this reason. However, it is worth noting that a body-fixed system may be preferable for other studies of agility. An example of such a situation would be a flight test where acceleration-rates might be measured with respect to body-fixed axes.

Having eliminated the body-fixed system from immediate consideration, attention is now focused on the wind and Frenet systems. Consider the aircraft velocity vector as it is represented in the wind and Frenet systems respectively:

(2.6) $\vec{\mathbf{V}} = V\,\mathbf{i}_w = V\,\mathbf{t}$

Both of these reference frames satisfy our requirement that the triad orientation be directly related to the velocity vector, further consideration is therefore needed in order to determine the ideal frame of reference. In referring back to the description of these triads and comparing Figures 2.1 and 2.2, one will note that the Frenet system orientation is strictly defined by the instantaneous curvature of the flight path. In fact, for the case of lineal flight, both the principal normal and binormal vectors are undefined since the radius of curvature is infinite. Just as it was undesirable to choose a reference system which is strictly associated with the airframe it is also undesirable to choose a system which is strictly associated with the flight path. This is due to the

fact that it would be difficult to represent aircraft forces and force-rates (kinetic agility) in such a system. For this reason we feel that the Frenet system is not well-suited for the present study of agility, on the other hand, the wind system is well-suited since the triad is not only directly related to the velocity vector but, the force and force-rate components are in the familiar directions of lift, drag and side force.

Having weighed the considerations listed above, the wind-axes have been chosen as the local moving reference system for this paper since it is equally well-suited for studies of both kinetic and kinematic agility. Of course, as indicated earlier, this decision does not mean that the wind-axes are the "best" choice for all situations but, they do seem to provide the most utility and convenience for this study.

Since our choice of wind-axes is unique among the existing notions of agility, it is worthwhile to associate a descriptive name with each component of the agility vector which was first defined in equation (2.5) and which may be represented on the wind-axes as:

(2.7) $\bar{\mathbf{A}} \equiv A_x \mathbf{i}_w + A_y \mathbf{j}_w + A_z \mathbf{k}_w$

Accordingly, the three components of the agility vector, as defined by equation (2.7), will be referred to as follows for the remainder of the study.

$A_x \Rightarrow$ Axial Agility (along x-wind axis)
$A_y \Rightarrow$ Lateral Agility (along y-wind axis)
$A_z \Rightarrow$ Normal Agility (along z-wind axis)

Note that the term axial agility, which is a result of changes in the magnitude of the tangential component of the acceleration vector, has been retained from previous agility studies [14,16] since it is essentially unchanged. However, the terms lateral and normal agility are new and have been chosen to better describe agility relative to the wind-axes system since these components are not equivalent to the previously defined notions of roll/torsional agility and pitch/curvature agility respectively. The agility components are depicted in Figure 2.3 and their characteristics

are described in greater detail in following sections.

2.3: Kinematic Agility

Although the focus of the present study has been placed on the analysis of agility from the view point of force-rates, in the interest of completeness it is worthwhile to derive the acceleration-rate terms so that they may be compared to those obtained by other researchers. The acceleration-rate vector (kinematic agility) is derived by differentiating the velocity vector twice with respect to time. Since these time derivatives are taken relative to an inertial system, the fact that the wind-axes themselves are rotating must be taken into account [13,25]. The first derivative of the velocity naturally gives the acceleration which is:

$$\vec{\mathbf{a}} = \dot{V}\,\mathbf{i}_w + V\left(\frac{d\mathbf{i}_w}{dt}\right)\Big|_I \tag{2.8}$$

where the time rate-of-change of the unit vector is given by Poisson's formula as:

$$\left(\frac{d\mathbf{i}_w}{dt}\right) = \vec{\omega}_w \times \mathbf{i}_w \tag{2.9}$$

and $\vec{\omega}_w$ is the angular velocity vector of the wind-axes with respect to a fixed inertial reference frame. Using Miele's [1] notation, the wind-axes angular velocity vector may be written as:

$$\vec{\omega}_w = p_w\,\mathbf{i}_w + q_w\,\mathbf{j}_w + r_w\,\mathbf{k}_w \tag{2.10}$$

where p_w is the velocity roll-rate, q_w is the velocity pitch-rate, and r_w is the velocity yaw-rate. The derivation of these angular velocity components is discussed in Chapter 3 and Appendix A. Now, returning to equation (2.9), taking the cross product, and substituting the result into (2.8) gives the acceleration vector, written with respect to the wind-axes, as:

$$\vec{\mathbf{a}} = \dot{V}\,\mathbf{i}_w + Vr_w\,\mathbf{j}_w - Vq_w\,\mathbf{k}_w \tag{2.11}$$

Finally, differentiating the acceleration vector (2.11) with respect to time will yield the jerk vector, $\vec{\mathbf{J}}$, which was defined in equation (2.4) and has been described herein as representing kinematic

agility. The jerk vector assumes the following form when represented on the wind-axes:

$$\text{(2.12)}\quad \bar{\mathbf{J}} = \left[\ddot{V} - V\left(r^2{}_w + q^2{}_w\right)\right]\mathbf{i}_w + \left[\dot{V}r_w + V\left(\dot{r}_w + p_w q_w\right)\right]\mathbf{j}_w - \left[\dot{V}q_w + V\left(\dot{q}_w - p_w r_w\right)\right]\mathbf{k}_w$$

It is worthwhile to note that the only difference between this vector, which is represented in the wind system, and a jerk vector represented in the Frenet system is that the angular velocity and angular acceleration components which appear in (2.12) would be those of the Frenet system instead of the wind system and the unit vectors would, of course, be those of the Frenet system. For instance, in the Frenet system the component of angular velocity in the binormal direction is a measure of the rotation-rate of the axes within the osculating plane, and hence indicative of the *curvature* of the path, while the other two components are measures of the rotation of the osculating plane itself and are indicative of the *torsion* of the path. The use of the Frenet system in flight mechanics is discussed by Miele [25] and Walden [35].

Although other researchers have proposed that agility be defined as an acceleration-rate, the jerk vector given by equation (2.12) differs from these concepts in that it is defined relative to the wind system and has been derived with respect to inertial space. For instance, the notion of agility suggested by Herbst is based on representing agility in the Frenet system and defining it relative to a non-inertial reference frame. That is, Herbst's agility components amount to a choice of a non-inertial reference frame "*f* " in equation (2.2) or (2.3). In particular, the rotation of the Frenet-axes is ignored when differentiating the standard Frenet acceleration vector; as such, this vector is not a true jerk vector. The components of Herbst's "agility vector" are given below for comparison purposes only:

$$A_{\text{Tangential}} = \ddot{V}$$
$$A_{\text{Curvature}} = -V\dot{\omega} - \dot{V}\omega$$
$$A_{\text{Torsional}} = \ddot{\theta} - \ddot{\chi}\sin\gamma - \dot{\chi}\dot{\gamma}\cos\gamma$$

Here θ represents the angular position of the osculating plane relative to the vertical direction, ω is the rotation-rate of the tangent and principal normal axes within the osculating plane (turn-rate), γ is the velocity flight-path angle, and χ is the velocity heading angle. One may note that Herbst's torsional agility component is not a measure of acceleration-rate. Instead, it represents the angular acceleration of the osculating plane about the velocity vector. It was necessary for

Herbst to "pick" a measure of torsional agility since he did not account for the rotation of the Frenet-axes when differentiating the acceleration vector, and therefore could not obtain the "natural" measure of lateral (torsional) agility as given in equation (2.12). Herbst's torsional agility component represents the "quickness of warping the maneuver plane", and was selected "to provide a realistic measure of combat agility" [14].

As mentioned earlier, kinematic agility is best-suited for the analysis of maneuvers once they have been flown rather than for predicting the agility characteristics of an aircraft. For example, an aircraft which is pulling g's in the vertical plane obviously displays agility along the axial and normal axes but will not exhibit any agility along the lateral axis since the wind-axes roll and yaw-rates will be zero (see equation 2.12). Similarly, an aircraft performing an unloaded roll will exhibit lateral agility but will not exhibit axial or normal agility (so long as $\ddot{V}$ and γ are respectively zero). Maneuvers such as these are easily analyzed in hindsight but do not necessarily meet any optimality criteria. One goal of this study is to develop such an optimal criteria by predicting aircraft performance from the viewpoint of the potential force-rates. Accordingly, we will now begin our study of kinetic agility.

2.4: Kinetic Agility

In studying kinetic agility, attention is focused on computing the time rate-of-change of the applied forces rather than the acceleration. Recall the usual decomposition of the applied forces acting on an aircraft as:

$$\vec{F} = \vec{F}_a + \vec{F}_p + \vec{F}_g$$

where the force vectors are defined as follows:

$\vec{F} \Rightarrow$ the net external force

$\vec{F}_a \Rightarrow$ the net aerodynamic force

$\vec{F}_p \Rightarrow$ the net propulsive force

$\vec{F}_g \Rightarrow$ the net gravitational force

Note that for flight over a flat earth the gravitational force vector $\vec{F}_g$ is a constant in inertial space, its contribution to the agility vector is therefore zero and it need not be considered further. The

aerodynamic force vector, represented in its usual form on the wind-axes, is shown graphically in Figure 2.1 and takes the following vector form:

(2.13) $\vec{\mathbf{F}}_a = -(D\,\mathbf{i}_w + Q\,\mathbf{j}_w + L\,\mathbf{k}_w)$

If the gross thrust vector is assumed to act in a fixed direction relative to the aircraft geometry, *ie* along the body *x*-axis, then the net propulsive force vector represented on the wind-axes is given as:

$$\vec{\mathbf{F}}_p = \vec{\mathbf{T}}_g - D_R\,\mathbf{i}_w$$

where $\vec{\mathbf{T}}_g$ is the gross thrust vector, and $D_R = \dot{m}_a V$ is the ram drag experienced by the propulsive system. Here, $\dot{m}_a$ is the mass flow-rate of the air through the engine. Transforming the gross thrust vector to the wind-axes yields the following net propulsive force vector:

(2.14) $\vec{\mathbf{F}}_p = (T_g \cos\alpha \cos\beta - D_R)\,\mathbf{i}_w + T_g \cos\alpha \sin\beta\,\mathbf{j}_w + T_g \sin\alpha\,\mathbf{k}_w$

Finally, the agility vector is obtained by summing equations (2.13) and (2.14) and taking the time derivative of the resulting vector. Recall that the motion of the wind-axes must be accounted for during the differentiation process. Carrying out these operations yields an agility vector of the form shown in equation (2.7), where the individual components are given as follows:

(2.15) Axial Agility

$$A_x = \dot{T}_g \cos\alpha \cos\beta - T_g\left(\dot{\alpha} \sin\alpha \cos\beta + \dot{\beta} \cos\alpha \sin\beta\right) - \dot{D}_R - \dot{D} - q_w(T_g \sin\alpha + L) - r_w(T_g \cos\alpha \sin\beta - Q)$$

(2.16) Lateral Agility

$$A_y = \dot{T}_g \cos\alpha \sin\beta - T_g\left(\dot{\alpha} \sin\alpha \sin\beta - \dot{\beta} \cos\alpha \cos\beta\right) - \dot{Q} + r_w(T_g \cos\alpha \cos\beta - D_R - D) + p_w(T_g \sin\alpha + L)$$

(2.17) Normal Agility

$$A_z = \dot{T}_g \sin\alpha - T_g\dot{\alpha} \cos\alpha + p_w(T_g \cos\alpha \sin\beta - Q) - \dot{L} - q_w(T_g \cos\alpha \cos\beta - D_R - D)$$

Although the components of the agility vector are quite involved in the form given above, they may be greatly simplified with the following assumptions:

- the aircraft maintains symmetric flight at all times ... $(\beta = \dot{\beta} = 0)$
- the net thrust always acts along the flight path ... $\left(\vec{F}_p = T_n \mathbf{i}_w\right)$

where T_n is the magnitude of the net thrust. The first of these assumptions simply limits the scenario since it rules out the application of side forces to enhance agility; in this sense it is a strong assumption. The second assumption is reasonable only so long as the angle-of-attack remains small; however, it will be shown later that the effect of thrust and thrust-rate on the magnitude of the agility vector is quite small in comparison to the effect of the aerodynamic forces and force-rates. With the assumptions listed above, the net force vector (with the gravity terms omitted) reduces to:

$$\vec{F} = (T_n - D)\mathbf{i}_w - L\,\mathbf{k}_w$$

Taking the time derivative of this force vector yields the following simplified components of the agility vector:

(2.18) $A_x = \dot{T}_n - \dot{D} - q_w L$ (Axial Agility)

(2.19) $A_y = p_w L + r_w(T_n - D)$ (Lateral Agility)

(2.20) $A_z = -\dot{L} - q_w(T_n - D)$ (Normal Agility)

The terms in equations (2.18)-(2.20) which are of primary interest to a study of agility are those which are affected by the aircraft controls. It will be shown in Chapter 4 that determining the limits of control effectiveness can be directly related to determining the limits of the agility vector and thereby deriving the agility sets which were previously discussed. However, before this operation can be carried out, it is necessary to choose a mathematical model of the aircraft dynamics wherein the states and controls are precisely defined. Modeling is discussed in Chapter 3.

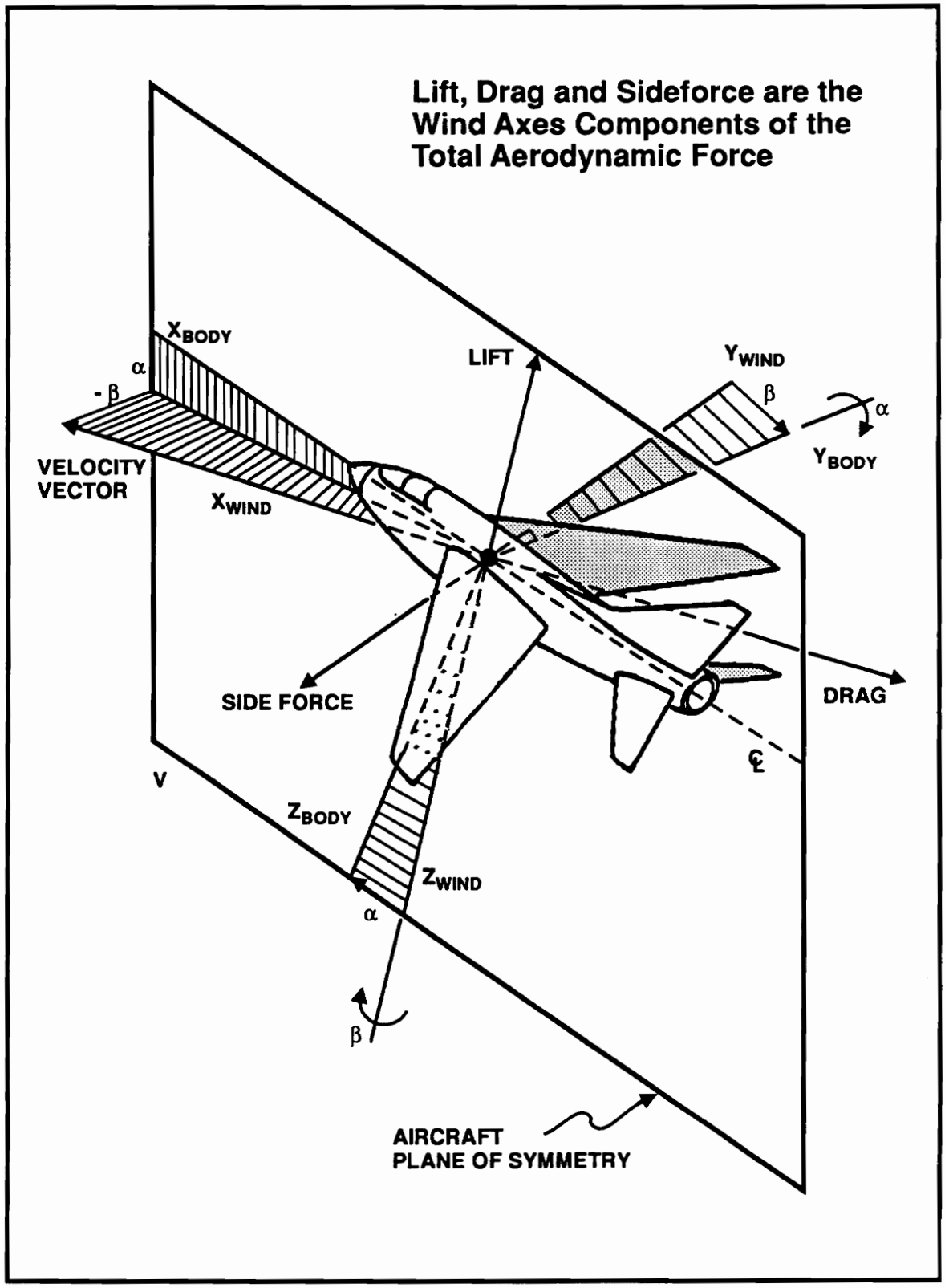

Figure 2.1. Body-Fixed vs. Wind Coordinates

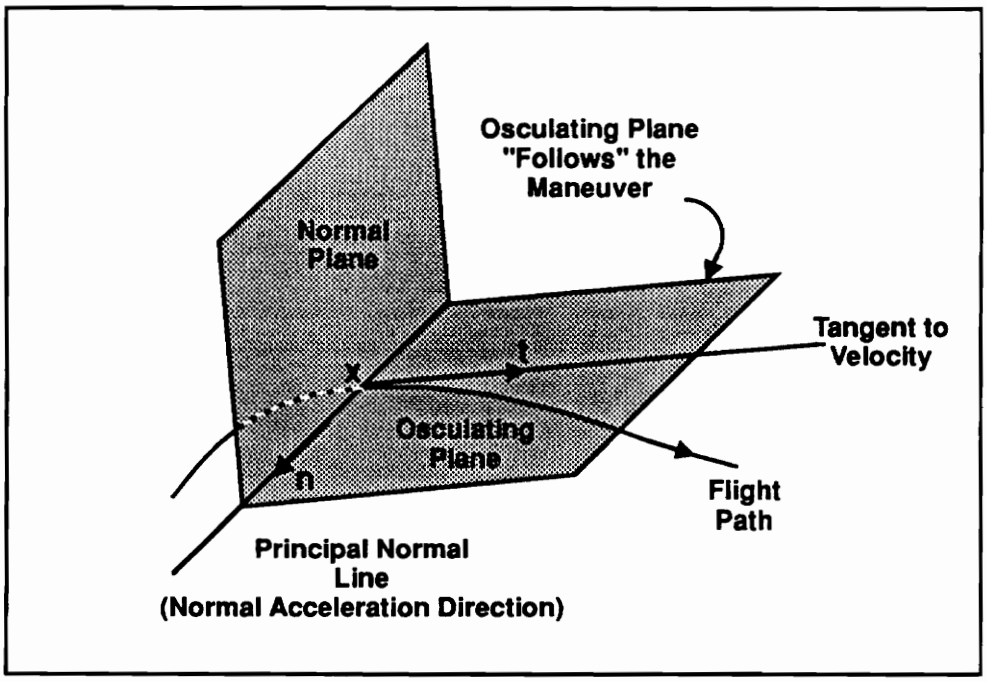

The Maneuver Plane

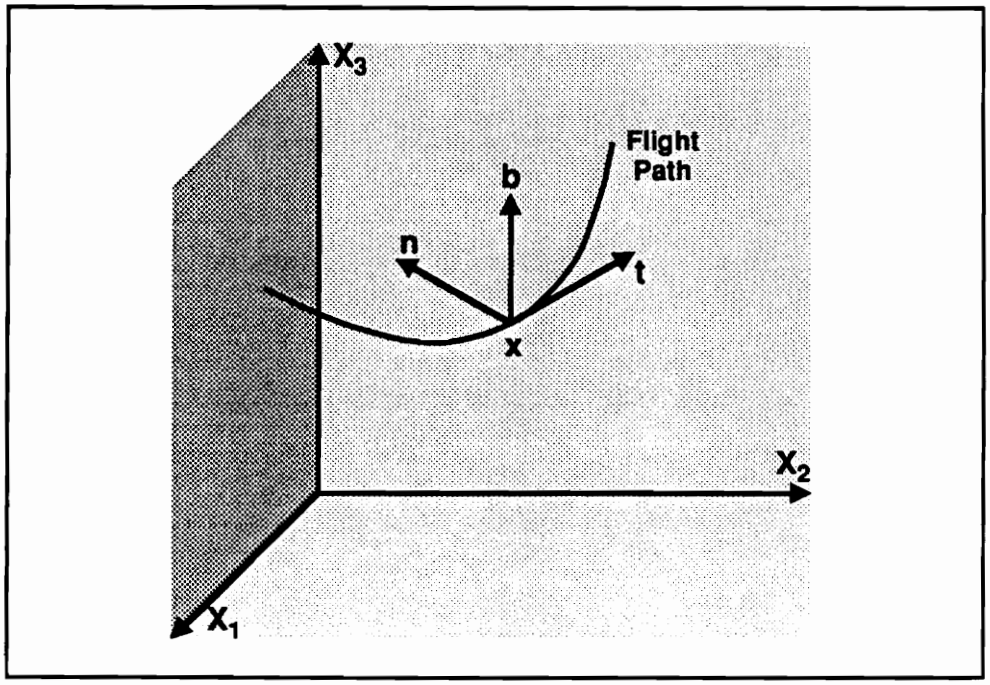

The Moving Triad

Figure 2.2. Frenet Coordinates

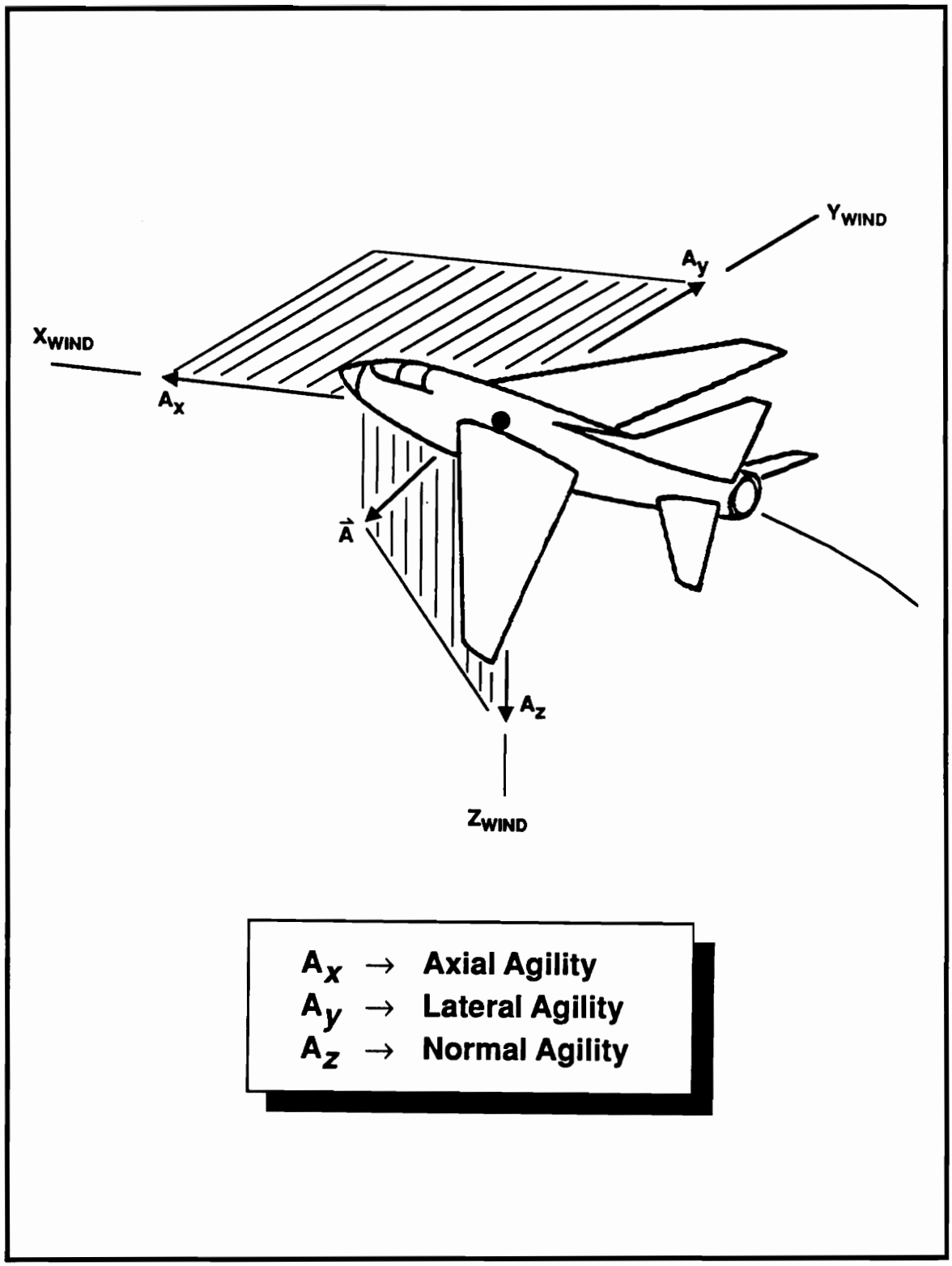

Figure 2.3. Components of the Agility Vector

CHAPTER 3
AGILITY MODELING CONSIDERATIONS

3.1: Fundamental Thoughts

For the purpose of developing the notion of aircraft agility it is important to put the problem in perspective. It is most convenient to do this in the context of the mathematical model which will be used to represent the aircraft dynamics. Before such a model is defined, it should be noted that it is impossible to model *real* aircraft exactly, care must therefore be taken in the formulation of the mathematical model which will be used to *represent* the aircraft. A mathematical model for aircraft performance is based on the dynamical equations which describe the motion of the aircraft. A first order dynamical model of the motion can most generally be represented by the relation:

$$\dot{\vec{X}} = f\left(\vec{X}, \vec{U}\right) \tag{3.1}$$

where $\vec{X}$ is a vector consisting of the aircraft state variables, $\dot{\vec{X}}$ is the vector of state-rates and, $\vec{U}$ is the vector of aircraft controls. Note that the control variables play the role of forcing functions in the equations of motion and can be thought of as being instantly achievable upon selection. The level of sophistication to which the dynamics are modeled usually depends on the type of problem under consideration. It is desirable to employ a model with as few states and controls as possible, while maintaining an acceptable level of accuracy, so that resulting analyses are not unnecessarily complicated. The question one might ask at this point is, *what choice of states and controls is sufficient for a study of aircraft agility ?*

Since some account of the aircraft rigid-body dynamics will be required for a meaningful study of agility, a logical model to consider initially is the rigid-body model (RBM). A minimum of 12 state variables would be required for an agility analysis employing a RBM of the dynamics. One choice for these variables is:

x,y,h : position coordinates
V : speed
γ : flight path elevation angle
χ : flight path heading angle
p : body-axis roll rate
q : body-axis pitch rate (S)
r : body-axis yaw rate
α : angle-of-attack
β : side-slip angle
μ : velocity bank angle

An additional state variable would be required to model changes in aircraft weight if maneuvers are sufficiently long in duration. However, since maneuvers associated with agility are characteristically short, we may reasonably assume that the aircraft weight is constant. It should also be noted that this choice of state variables is not unique for a RBM. For instance, in some applications one may wish to replace the aerodynamic angles (α,β,μ) with the body attitude angles (θ,ϕ,ψ). We have chosen the aerodynamic angles as states since we are concerned with computing force-rates in our study of agility. It will subsequently be shown that the force-rates are strong functions of the aerodynamic angular rates. On the other hand, we will not be directly concerned with the attitude of the aircraft with respect to the inertial reference system and hence there will be no specific requirement for computing the attitude angles.

The first six variables in the list of states (S) describe the point mass motions of the aircraft. The evolution in time of V, γ, and χ is determined from Newton's Laws (2.1) which yields equations that describe the motion of the aircraft center-of-mass. The trajectory equations relate these variables to the time rate-of-change of the position variables x, y and h. The remaining six variables describe the rigid-body motions of the aircraft. The evolution in time of p, q and r is also based on Newton's Laws (torque equals time rate-of-change of angular momentum). These body-rates may then be related to the angular rates of the aerodynamic angles α, β and μ through the so-called "kinematic equations". The differential equations of motion for the set of state variables (S) are provided in Appendix A. Note that since the aerodynamic forces acting on an aircraft depend on the body attitude (specifically α and β), it is reasonable to interpret the rigid-body motions as providing the dynamical equations which describe how the forces evolve in time. This confirms our previous statement that some model of the rigid-body motion is required

for a study of agility since we are directly concerned with the evaluation of force-rates.

The set of control variables for a RBM typically includes a throttle setting and deflection angles for the various aerodynamic surfaces as indicated below:

δ_T : throttle position
δ_A : aileron deflection angle
δ_S : stabilator deflection angle
δ_R : rudder deflection angle (C)
δ_F : flap deflection angle

A more detailed control set might include secondary aerodynamic surfaces, such as leading edge flaps and speed brakes, and allow for non-symmetric deflection of the aerodynamic control surface pairs such as the stabilator and rudder surfaces. A graphical depiction of the RBM states and controls described in (S) and (C) is provided in Figures 3.1 and 3.2.

Upon considering the shear number of states and controls required by the full rigid-body model, as well as the non-linearity of the equations of motion, one realizes that it would be an extremely difficult task to implement such a model in any analysis involving optimization techniques. Since a goal of this study is to perform such analyses, simplification of the model is essential. In the following section we will identify a new type of dynamic model which will serve our purposes in terms of modeling rigid-body motions while also reducing the number of states and controls required by the full RBM.

3.2: The Body-Rate Dynamic Model

Previous studies in approximating aircraft performance have used ideas of singular perturbation theory to reduce the number of states in the analysis [1,18]. Our problem requires that we maintain a reasonable model of the rigid-body motion. This requirement eliminates the possibility of employing models which assume instantaneous changes in body attitude. For instance, the point-mass model is inappropriate for studies of agility since this model assumes that the aerodynamic angles (α,β,μ), and hence the aerodynamic forces, are instantly achievable upon selection. It is obvious that with such a model the force-rate terms contained in the agility

vector would be meaningless.

A compromise between the full RBM and existing lesser models, which do not account for rigid-body motions, can be realized by choosing an intermediate model based on the use of the aircraft body-rates p, q and r as a form of aerodynamic control and thrust-rate as a propulsive control. For purposes of clarity this model will henceforth be referred to as the body-rate dynamic model, abbreviated BRM. The BRM concept is intended to improve the approximation of the dynamics of lower order models, at least in part, by accounting for the fact that the body attitude cannot be changed instantly. However, one should keep in mind that the most important modeling feature, in terms of agility analysis, is not body attitude *per se*, but the forces which result from these attitudes. *The unifying idea is to consider the rate at which one can change the net force acting on the vehicle.*

The basic BRM effectively reduces the number of states required in the analysis from twelve to nine by assuming that the body-rates are control-like. If we also impose the conditions of symmetric flight and thrust along the path, then the resulting model is further simplified. Applying these conditions to the rigid-body equations listed in Appendix A leads to the following set of state equations for the body-rate model:

(3.2) $$\dot{x} = V \cos\gamma \cos\chi$$

(3.3) $$\dot{y} = V \cos\gamma \sin\chi$$

(3.4) $$\dot{h} = V \sin\gamma$$

(3.5) $$\dot{V} = g\left[\frac{(T - D)}{W} - \sin\gamma\right]$$

(3.6) $$\dot{\gamma} = \left[\frac{L}{W}\cos\mu - \cos\gamma\right]$$

(3.7) $$\dot{\chi} = \frac{g}{V}\frac{L}{W}\frac{\sin\mu}{\cos\gamma}$$

(3.8) $$\dot{\alpha} = q + \frac{g}{V}\left[\cos\mu\cos\gamma - \frac{L}{W}\right]$$

(3.9) $$\dot{\beta} = 0 = p \sin\alpha + r \cos\alpha + \frac{g}{V} \sin\mu \cos\gamma$$

(3.10) $$\dot{\mu} = \frac{p}{\cos\alpha} + \frac{g}{V} \sin\mu \left[\frac{L}{W} \tan\gamma + \tan\alpha \cos\gamma \right]$$

Note that the symmetric flight condition effectively reduces the number of state variables from nine to eight since β will be constant. In addition, this condition results in the constraint equation (3.9) which must be satisfied. The effect of equation (3.9) is to reduce the number of independent body-rate controls from three (*p,q,r*) to two. We have chosen to use this equation to eliminate the yaw-rate as an independent control. Solving (3.9) for *r* yields the following relation:

(3.11) $$r = p\tan\alpha + \frac{g}{V} \frac{\sin\mu\cos\gamma}{\cos\alpha}$$

As a final note in regard to the BRM state equations we mention the fact that the horizontal position coordinates (*x,y*) are ignorable, since they are not coupled with any of the other states, and may therefore be neglected if they are not required in the analysis. Similarly, if *x* and *y* are not required in the analysis, then the heading angle χ becomes ignorable and may be neglected if it is not needed.

In terms of the BRM controls we now have *p* and *q* as independent aerodynamic controls and thrust-rate as a propulsive control. A simple propulsive model, with thrust-rates corresponding to extreme changes in throttle position (*ie* throttle-slam and throttle-chop), will be sufficient for initial modeling of the effect of engine response limits on agility. However, determining admissible values for *p* and *q* is not as simple since the body-rates are coupled to the physical control surfaces through the moment equilibrium equations in the following manner:

(3.12) $$\begin{Bmatrix} (I_y - I_z)qr \\ (I_z - I_x)pr \\ (I_x - I_y)qp \end{Bmatrix} + [M\zeta] \begin{Bmatrix} p \\ q \\ r \end{Bmatrix} + [M\delta]\bar{\delta} = \bar{0}$$

Here $M\zeta$ is a matrix of damping derivatives, $M\delta$ is a matrix of control derivatives and $\bar{\delta}$ is the vector of control surface deflections. In principle, the system of equations in (3.12) can be solved

for the body-rates in terms of the surface deflections. Recall however, that there are only two degrees-of-freedom here since the yaw rate is constrained by equation (3.11). Since the aircraft control surface deflections $\bar{\delta}$ will be physically bounded, it is clear that equation (3.12) induces bounds on the body-rates p and q. For preliminary design studies, where detailed aircraft data is not available, one could simply parameterize p and q or limit them based on the characteristics of historically similar aircraft. Computation of these bounds will be discussed in detail in Chapter 4. The states and controls of the BRM are depicted in Figures 3.2 and 3.3.

3.3: Evaluating the Force-Rate Terms

With the choice of states and controls clear in our minds, we can now evaluate the components of the agility vector in greater detail. Since we have imposed the conditions of symmetric flight and thrust along the path on the analysis, we will only be concerned with evaluating the terms in the simplified agility vector which is listed in component form in equations (2.18-2.20). In particular, we are interested in deriving relations for the wind-axes angular rates (p_w, q_w, r_w) and the time derivatives of the applied forces $(\dot{L}, \dot{D}, \dot{T}_n)$ in terms of the BRM states and controls. Once this task has been accomplished we will be able to proceed with the numerical analyses in the remaining chapters.

Recall that the aerodynamic forces are usually presented in terms of non-dimensional coefficients in the following manner:

(3.13) $$F_a = C_F(\alpha, M)\bar{q}S$$

where $\bar{q}$ is the dynamic pressure, S is a characteristic reference area and, it has been assumed that the force coefficients are primarily dependent on angle-of-attack and Mach number. Taking the time derivative of equation (3.13) yields the following general expression for the lift and drag force-rate terms:

(3.14) $$\dot{F}_a = \left[\dot{\alpha}\left(\frac{\partial C_F}{\partial \alpha}\right) + \dot{M}\left(\frac{\partial C_F}{\partial M}\right)\right]\bar{q}S + \dot{\bar{q}}C_F S$$

where the partial derivatives are stability derivatives which depend on the characteristics of the aircraft in question. Data for these derivatives has been provided in Appendix B. The other derivatives in equation (3.14) include the time rate-of-change of the angle-of-attack, which was defined in equation (3.8) and, the time rate-of-change of the Mach number and the dynamic pressure, where both of these variables depend on the aircraft velocity and altitude. By applying the chain rule we obtain the following relations for the time derivatives of Mach number and dynamic pressure respectively:

$$\dot{M} = \frac{\dot{V}}{a} - \frac{V}{a^2}\frac{da}{dh}\dot{h} \tag{3.15}$$

$$\dot{\bar{q}} = \frac{V^2}{2}\frac{d\rho}{dh}\dot{h} + \rho V\dot{V} \tag{3.16}$$

where a is the speed of sound, ρ is the atmospheric density and, $\dot{h}$ and $\dot{V}$ were previously defined in equations (3.4) and (3.5) respectively. Note that the aerodynamic force-rates, equation (3.14) are influenced by the body pitch-rate q through the equation for angle-of-attack rate, (equation 3.8). Since q is considered a control variable in the BRM, it may therefore be used to directly effect both the axial and normal agility components which depend on the drag-rate and lift-rate, respectively.

As mentioned in the previous section, we have chosen a simple model for the propulsive system wherein we consider only extreme throttle movements. In this case the value for the thrust-rate term, which appears only in the axial agility component, is parameterized as either a maximum (throttle-slam), a minimum (throttle-chop) or zero (no movement).

With the applied forces and their rates defined we turn our attention to the remaining undefined terms in the agility vector which are the components of the wind-axes angular velocity vector (p_w, q_w, r_w). The derivation of these terms is presented in Appendix A for the case of non-symmetric flight over a flat earth. With the assumption of symmetric flight the components are simplified to the following forms:

$$p_w = \frac{p}{\cos\alpha} + \sin\mu\cos\gamma\tan\alpha \tag{3.17}$$

(3.18) $$q_w = \frac{g}{V}\left[\frac{L}{W} - \cos\mu\cos\gamma\right]$$

(3.19) $$r_w = \frac{g}{V}\sin\mu\cos\gamma$$

Note that the only term which contains a control variable is p_w, which is directly affected by the body roll rate, and in turn appears in the lateral agility component.

In summary, we see that there are four terms $(\dot{L}, \dot{D}, \dot{T}_n, p_w)$ in the agility vector which depend on the independent BRM control variables p, q and $\dot{T}_n$. The other terms depend only on the maneuver state. With a bit of algebraic manipulation we may write the agility components in the following form:

(3.20) $$A_x = \dot{T}_n + c_1 \cdot q + c_2$$

(3.21) $$A_y = c_3 \cdot p + c_4$$

(3.22) $$A_z = c_5 \cdot q + c_6$$

where the c_i terms are constant for a particular maneuver state and are given by the following relations:

(3.23) $$c_1 = -\bar{q}SC_{D_\alpha}$$

(3.24)

$$c_2 = q_w\bar{q}S(C_{D_\alpha} - C_L) + \sin\gamma\frac{S}{2}\left[2\bar{q}M^2a_\alpha C_{D_M} - V^3C_{D\rho_\alpha}\right] + \frac{\bar{q}S}{mV}\left[(C_{D\bar{q}}S - T_n) + mg\sin\gamma\right](2C_D + MC_{D_M})$$

(3.25) $$c_3 = \frac{C_L\bar{q}S}{\cos\alpha}$$

(3.26) $$c_4 = \frac{g}{V}\sin\mu\cos\gamma\left[\bar{q}S(C_L\tan\alpha - C_D) + T_n\right]$$

(3.27) $c_3 = -\bar{q}SC_{L_\alpha}$

(3.28)

$$c_6 = q_w\bar{q}S(C_{D_\alpha} - C_L) - q_wT_n + \sin\gamma\frac{S}{2}\left[2\bar{q}M^2a_\alpha C_{L_M} - V^3C_L\rho_h\right] + \frac{\bar{q}S}{mV}\left[(C_D\bar{q}S - T_n) + mg\sin\gamma\right](2C_L + MC_{L_M})$$

where the subscripts α, M, and h denote that a derivative has been taken with respect to the indicated variable.

The components of the agility vector, as represented on the wind-axes, have now been defined completely and a functional form for these components, in terms of the body-rate dynamic model states and controls, has been identified. In fact, we see that for the simplified BRM the agility components become affine functions of the body-rates p and q. In the following chapter we will employ analytic techniques to show that the limits of an aircraft's instantaneous agility capabilities (agility sets) is directly related to determining the admissible bounds on the control variables p and q. Then in Chapter 5, we will employ the body-rate dynamic model to formulate and solve an integral agility optimal control problem.

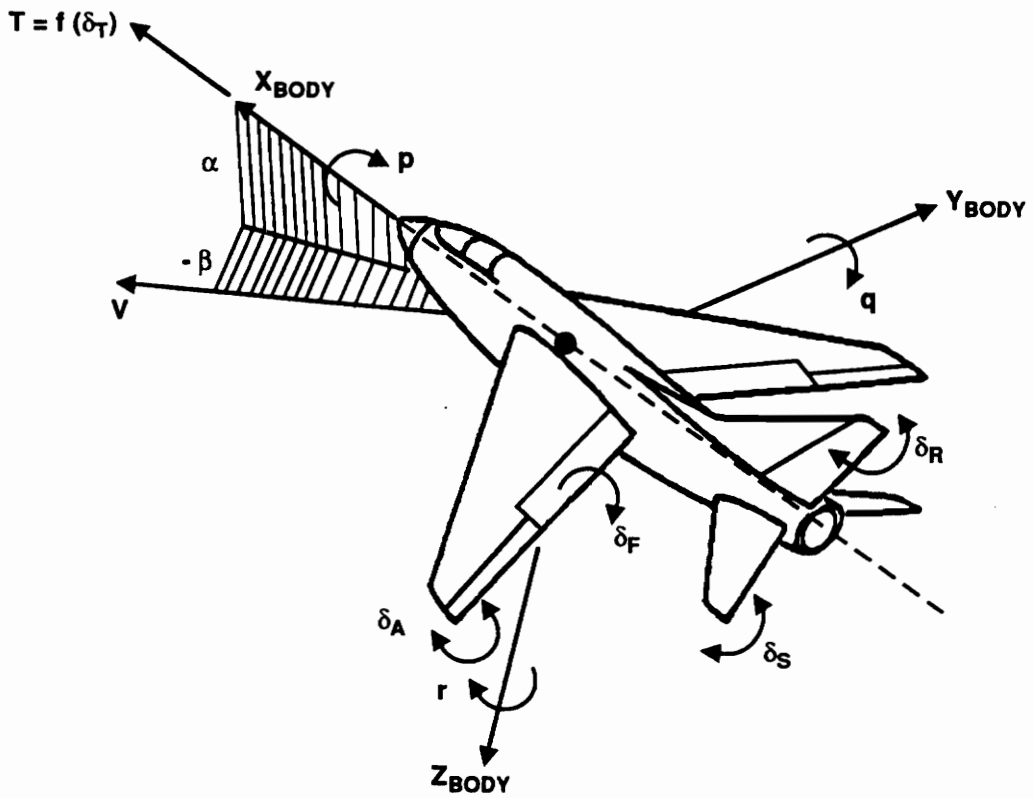

Rigid Body States		Rigid Body Controls	
Position Coordinates	*x,y,h*	Throttle Position	δ_T
Speed	*V*	Aileron Angle	δ_A
Flight Path Angle	γ	Stabilator Angle	δ_S
Heading Angle	χ	Rudder Angle	δ_R
Body Roll-Rate	*p*	Flap Angle	δ_F
Body Pitch-Rate	*q*		
Body Yaw-Rate	*r*		
Angle-of-Attack	α		
Side-Slip Angle	β		
Velocity Bank Angle	μ		

Figure 3.1. Typical Rigid-Body Dynamics Model

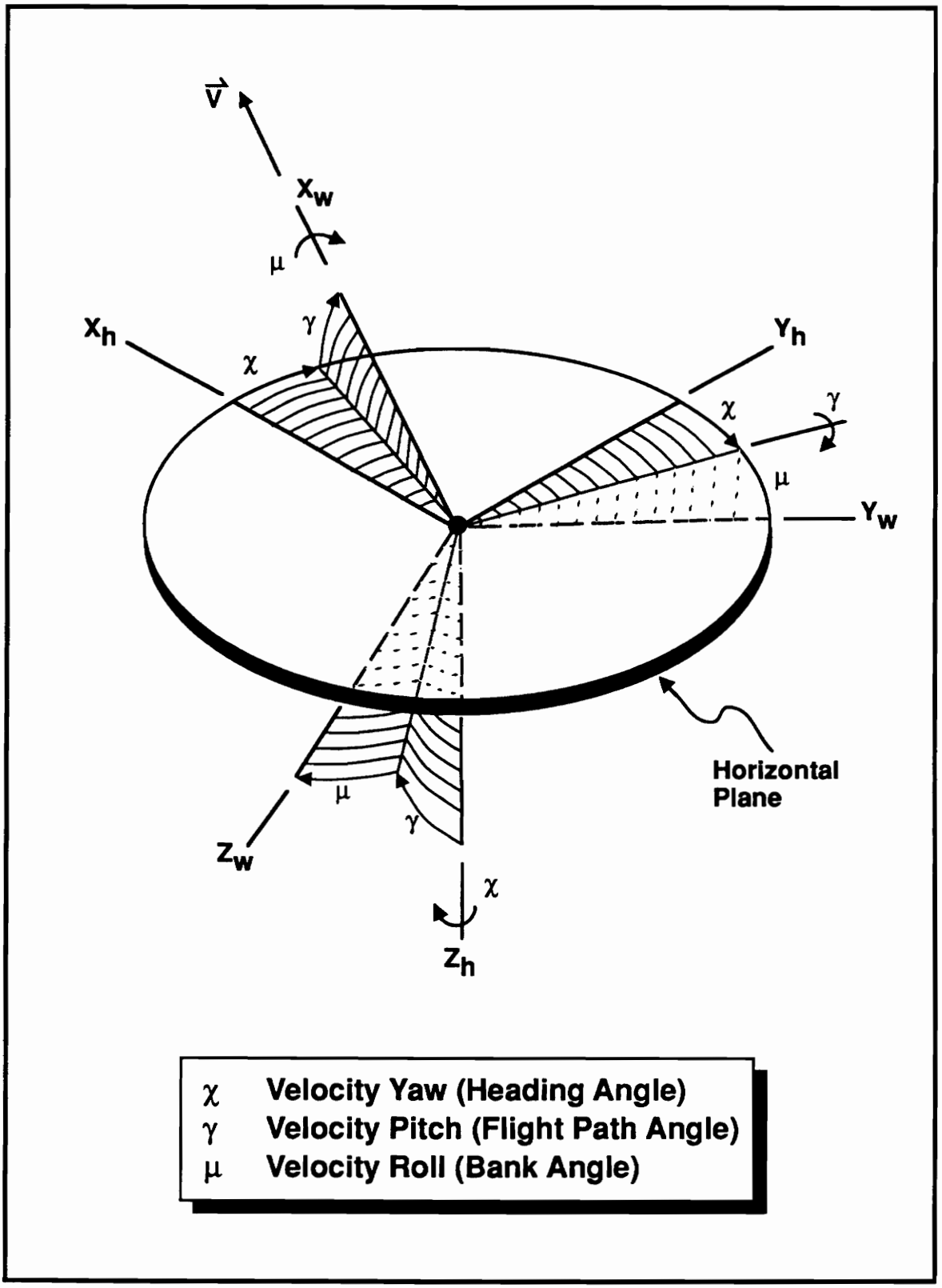

Figure 3.2. Velocity Euler Angle Definitions

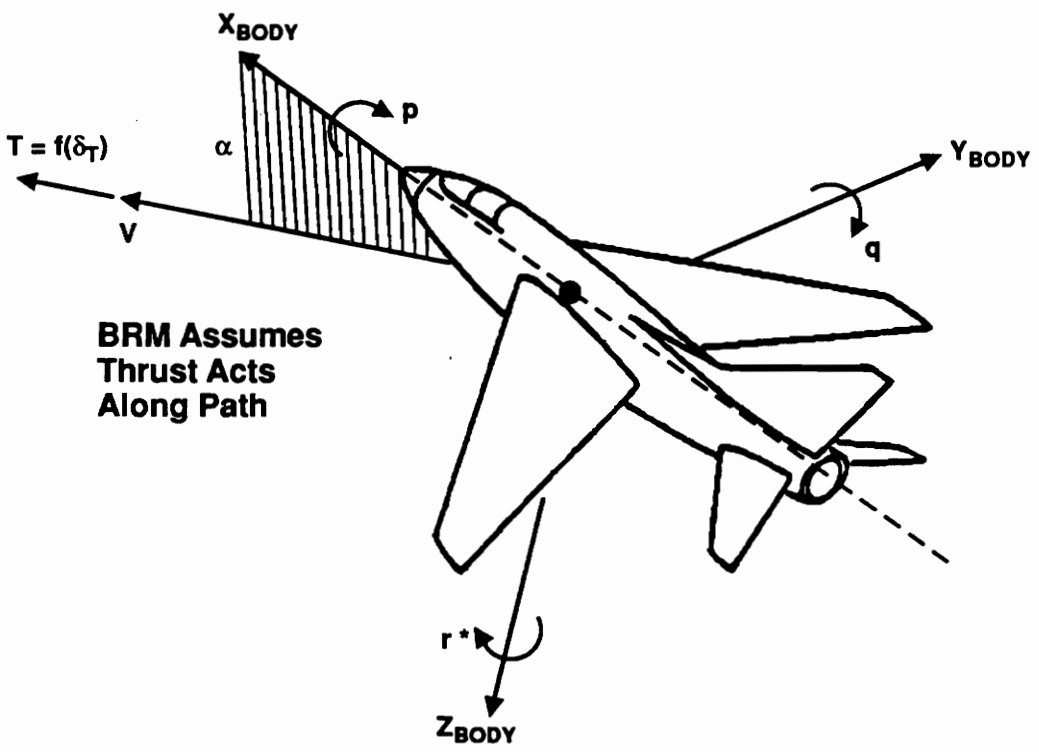

BRM States		BRM Controls	
Position Coordinates	*x,y,h*	Thrust Rate	$\dot{T}$
Speed	*V*	Body Roll Rate	*p*
Flight Path Angle	γ	Body Pitch Rate	*q*
Heading Angle	χ	Body Yaw Rate *	*r=f(p,S)*
Angle-of-Attack	α		
Velocity Bank Angle	μ		
Side-Slip Angle	$\beta = 0$		

* Body Yaw Rate Not Free Control Due To $\beta = 0$ Simplification

Figure 3.3. The Body-Rate Dynamics Model (BRM)

CHAPTER 4
INSTANTANEOUS AGILITY

4.1: Deriving Agility Sets

As noted in Section 3.2, the moment equilibrium conditions, in conjunction with physical bounds on the aerodynamic control surfaces, induce bounds on the possible equilibrium body-rates as dictated by equations 3.12. The body-rate bounds, in combination with thrust-rate bounds, may be used to determine a set of limiting agility vectors. We have previously described the locus formed by this set of vectors as the ***instantaneous aircraft agility set***. Each flight condition will produce a unique agility set. The purpose of the current section is to document the process by which agility sets may be constructed. In the following section we will present numerical results for several flight conditions.

In the present study we consider the analysis of agility sets subject to the following hypotheses:

- Zero sideslip angle, β
- Only primary aerodynamic flight controls (aileron, stabilator and rudder) considered
- Each control effects only a single moment
- Control effectiveness independent of body-rates

Given the hypotheses above, it is possible to determine an analytic solution to the three equilibrium equations (3.12) thereby providing an algebraic relation between the aircraft control surface deflection angles, which are known beforehand, and the limiting body-rates which we are seeking. We begin by writing the roll, pitch and yaw equilibrium equations respectively as:

(4.1) $$(I_z - I_y)qr = L = C_l \bar{q} S b$$

(4.2) $$(I_x - I_z)pr = M = C_m \bar{q} S \bar{c}$$

(4.3) $(I_y - I_x)qp = N = C_n \bar{q} S b$

where the moment coefficients are computed as:

(4.4) $C_l = C_{l_{\delta_a}} \delta_a + C_{l_p} \frac{pb}{2V}$

(4.5) $C_m = C_{m_0} + C_{m_{\delta_e}} \delta_e + C_{m_q} \frac{q\bar{c}}{2V}$

(4.6) $C_n = C_{n_{\delta_r}} \delta_r + C_{n_r} \frac{rb}{2V}$

Recall from Chapter 3 that the requirement of identically zero sideslip ($\beta \equiv 0$) implies that:

(4.7) $r = p \tan \alpha + (g/V) \frac{\sin \mu \cos \gamma}{\cos \alpha}$

Combining equations 4.4 and 4.7 with the roll channel constraint 4.1 yields a relationship of the following form:

(4.8) $0 = A_l \cdot p + B_l \cdot pq + C_l \cdot q + D_l$

We may solve the pitch and yaw equilibrium equations in a similar manner to obtain relations of the form:

(4.9) $0 = A_m \cdot p^2 + B_m \cdot p + C_m \cdot q + D_m$

(4.10) $0 = A_n \cdot p + pq + D_n$

In each of equations (4.8)-(4.10) the physical control appears in the D_x term and no place else. In the interest of completeness, the coefficients for these equations are provided in Appendix C.

Since the limits on the physical controls are known, and the other coefficients of these equations are merely functions of the flight state (which is provided) the only unknowns are the body-rates p and q. Our goal is to determine the bounding limits for all possible (p,q) control-pairs subject to the constraints imposed by equations (4.8)-(4.10). We may visualize the solution to this problem for a typical flight condition by solving the constraint equations for parameterized (p,q) pairs and overlaying the resulting curves to reveal the admissible body-rate set. This process is depicted in Figures 4.1-4.4 where we have plotted the pitch, roll, yaw and composite solutions, respectively, for a nominal flight condition of straight and level flight at sea-level and Mach 0.3. It is clear from these plots that there exists a distinct region of admissible body-rates which are dictated by the control deflection limits. Taking a closer look at this region in Figure 4.5, we see that the admissible body-rate set for a given flight condition is clearly dictated by constraints on the physical controls. Figure 4.6 shows the resulting simultaneous (at the boundary points) control deflections required to produce the limiting body-rate set depicted in Figure 4.5. Note that one or more of the controls is at an extreme limit at all times and that each of the controls progresses from one extreme to another as the pitch-rate goes from a minimum to a maximum.

Now that a procedure has been established for determining the admissible body-rates, the only remaining task required before we may begin to compute agility sets is to define the limiting thrust-rates. Figure 4.7 shows typical engine response histories [7] for a modern fighter for the cases of throttle-slam and throttle-chop. Since the engine response is primarily linear, except for short initial and final transients, it is reasonable to simplify the analysis by assuming that the thrust-rates are constant. This assumption results in a maximum and minimum thrust-rate capability as depicted in Figure 4.8 where we have assumed, for the purposes of the present analysis, that the thrust-rates are constant with time and invariant with flight condition. We have now demonstrated methods for obtaining bounds for all of the *BRM* controls, at this point we are ready to compute agility sets.

Figure 4.9 depicts a sample 3-dimensional agility set which has been produced from the body-rate set and thrust-rate limits shown in Figures 4.5 and 4.8, respectively, by substituting these limiting rates into the agility component equations (3.20)-(3.22). The nominal flight condition for this particular agility set is straight and level unaccelerated flight at sea-level altitude and Mach 0.3. One may immediately observe that the agility set is almost 2-dimensional in nature, in fact the "thickness" of the figure is entirely attributable to the thrust-rate term which appears only in the axial agility component. For this flight condition, as well as all other conditions examined by

the author, thrust-rate is seen to have a nearly negligible effect on agility in comparison to the effect of the aerodynamic rates. For example, the absolute maximum thrust-rate for this aircraft is just over 0.5 g's/sec (throttle-chop), while the maximum values for $\dot{L}$, $\dot{D}$ and $p_w L$, even at this low dynamic pressure flight condition, are 30, 8 and 3 g's/sec, respectively. It should also be noted at this point that the other terms in the agility components, *ie* $q_w L$, $r_w(T_n - D)$ and $q_w(T_n - D)$, only contribute a minuscule portion (typically less than 0.1 g's/sec) to the total agility, in comparison to the other terms listed above, and may therefore be neglected in most cases. Returning to Figure 4.9, we notice another interesting feature, namely that the agility displayed along the normal axis is significantly greater than that displayed along either the axial or lateral axes. The difference in axial and normal agility may be confusing at first since each of these components are a direct function of the pitch-rate, however, upon closer examination of the aerodynamic rate terms $\dot{L}$ and $\dot{D}$ (see equation 3.14) one will notice that $\dot{L}$ is driven by the lift-curve slope, C_{L_α}, while $\dot{D}$ is driven by the drag-curve slope C_{D_α}. The fact that the slope of the lift-curve is significantly steeper, at most low-to-moderate α flight conditions, than that of the drag-curve (see Appendix B) accounts for the difference in maximum magnitude of the axial and normal agility components. On the other hand, the difference in the maximum magnitude of the normal and lateral agility components is primarily due to the fact that the roll-rate simply gets multiplied by the lift-force in the lateral agility equation (see equations 2.19 and 3.17), while the pitch-rate is multiplied by the dynamic pressure and the reference area in the normal agility equation (see equations 2.20, 3.8 and 3.14). Another contributing factor here is that the maximum pitch-rate exceeds the maximum roll-rate by close to a factor of two as indicated in Figure 4.5. With these observations in-hand we now proceed to the next section where we will examine the effect of flight condition on the shape and orientation of the agility set.

4.2: Numerical Results

As noted in the Introduction, it may be of interest to compare the agility sets of one aircraft to another at one or more flight conditions to determine regions in which one aircraft is superior to the other. In the present study we will not attempt to analyze the performance characteristics of competing aircraft, instead we will present data for a single aircraft, operating at various flight conditions, in order to provide some insight into the expected variations in agility characteristics over the flight regime and to aid the reader in the visualization of our theory. In so

doing, methodologies are presented by which analysts or designers may employ our theory to assess and/or compare aircraft agility. The numerical results which we provide in this study are representative of the capabilities of a state-of-the-art fighter aircraft. All modeling data required to produce these results are provided in Appendix B.

One way to characterize aircraft agility at a particular flight condition is to plot the extreme values of each agility component together on a single plot vs. pitch-rate as shown in Figure 4.10. From this plot one may quickly determine maximum aircraft agility along each axis during pure-pitch, pure-roll or combined pitch-roll maneuvers. By overlaying the agility characteristics of another aircraft onto this plot, a direct performance comparison may be made at the given flight condition. It is also at this point that a designer who has received specifications to build an aircraft that is capable of specific levels of agility could relate the physical control authority to the predicted agility. If the agility predicted in Figure 4.10 is not adequate then the designer could return to the equilibrium control deflection and body-rate set plots (Figures 4.5 and 4.6) and identify the deficient control.

Although performance comparisons at a single flight condition are interesting, such a comparison in itself is generally not sufficient for choosing one design over another or for rating one aircraft as better than another. In order to be thorough it is necessary to compute data throughout the flight regime. Accordingly, we now provide data which examines the effect of flight condition (*ie* aircraft state) on the agility set. In particular, Figures 4.11 and 4.12 examine the effect of variations in Mach number during straight and level flight on the body-rate set, and the agility set, respectively. Similarly, Figures 4.13 and 4.14 examine the effect of load-factor during flight in the vertical plane and Figures 4.15 and 4.16 examine the effect of bank angle during flight in the horizontal plane. It should be emphasized that Mach number (velocity), load-factor (angle-of-attack) and bank-angle are states in the body-rate model. Recall that since thrust-rate primarily provides thickness to the agility set, plots were generated for a single thrust-rate (throttle-slam) only and the focus is placed on analyzing changes in the shape and orientation of the agility set.

Analysis of the effects of Mach number on agility for a nominal straight, level and unaccelerated flight condition reveal, not surprisingly, that increased Mach number, and thus increased dynamic pressure, significantly enhance the aircraft's capability to generate higher roll and pitch-rates (Figure 4.11). However, the effect that increased Mach number has on the agility

set itself is not so intuitive. Upon examining Figure 4.12 one will notice that one interesting effect of Mach number on the agility set is a rotation of the set within the X-Z plane. This rotation is due to the change in C_{D_α} as the angle-of-attack required to maintain level 1-g flight decreases with increasing Mach number (C_{D_α} is plotted versus angle-of-attack in Figure B.5). The other primary effect of increasing Mach number is to drastically enhance the potential agility along each of the axes, this holds especially true for normal agility which has an absolute maximum value of less than 30 g's/sec at Mach 0.3 and increases to an absolute maximum of nearly 350 g's/sec at Mach 0.7 (note the different axes scales in Figure 4.12). This effect is due almost entirely to the increase in dynamic pressure from Mach 0.3 flight to Mach 0.7 flight.

Turning to Figures 4.13 and 4.14 one will notice that changing load-factor (*ie* changing α), while holding speed constant at Mach 0.5, does not result in nearly so drastic of changes in the agility set as does changing the Mach number while holding g-level constant. The primary effect here is once again a rotation of the agility set within the X-Z plane. Although the change in angle-of-attack is significant for this example, the rotation is not as pronounced as in the previous example since the angle-of-attack is increasing which results in smaller changes in C_{D_α}. Another interesting point to make about this example is that the lateral and axial agility are much closer in magnitude to the normal agility. Note that it is even possible to plot them on the same scale while retaining clarity. The reduction in difference in axial and normal maximum agility is due to the C_{D_α} effect, while the reduction in difference in lateral and normal maximum agility is due to the fact that Lift is increasing with g-level, *ie* $A_y \propto (L \cdot p_w)$, while dynamic pressure remains constant in this example, *ie* $A_z \propto (\dot{\alpha} \cdot C_{L_\alpha} \cdot \bar{q}S)$.

Next we examine the effect of turning flight in the horizontal plane on the agility set. Here we have simply parameterized bank angle while maintaining sufficient angle-of-attack to achieve level flight, Mach number is constant at 0.5. From Figure 4.15 one will notice that bank angle has a negligible effect on the shape and size of the admissible body-rate set. The primary effect here is a skewing of the rate bounds at non-zero bank angle, this results in a non-symmetric figure about the zero roll-rate axis, whereas the figure is symmetric for all cases of zero bank angle. In terms of the agility set itself, (see Figure 4.16), we see that the set is once again rotated in the X-Z plane. The same reasoning holds true here as for the previous examples since angle-of-attack must increase as bank angle increases in order to maintain level flight in the horizontal plane. Other than this effect, we notice that the maximum normal agility is almost an order-of-magnitude greater than the maximum axial and lateral agility, the increase in difference between this case

and the previous example is primarily due to the effect of non-zero bank angle on wind-axes rate (see equations (3.17)-(3.19)), which directly affect the agility state-constant coefficients listed in equations (3.23)-(3.28).

In the preceding examples we have characterized the behavior of the agility set for different flight conditions and maneuvers at a constant altitude. Another way to assess aircraft agility is to look at the extreme limits of the admissible rates and the resulting extreme values of the agility components at different points in the flight envelope. In fact, this method is likely to be more useful to the designer or analyst than examining isolated agility sets since more data can be assessed on a single plot. Such an analysis is presented in Figures 4.17-4.20 for our aircraft and the case of straight, level and unaccelerated flight condition. Figure 4.17 examines the change in maximum and minimum pitch-rate and maximum roll-rate (min=-max) as a function of Mach number and altitude, while figures 4.18-4-20 examine the resulting extreme values of axial, lateral and normal agility, respectively, at those flight conditions. Starting with Figure 4.17 we note that there are no real surprises in the admissible rates, *ie* performance falls off with increasing altitude and decreasing Mach number (note that this particular aircraft cannot maintain 1-g flight at Mach 0.3 and 30000 ft, thus the truncation of data on the 30 kft curves). Moving on to Figure 4.18 one will notice an interesting feature in that the maximum axial agility crosses over as Mach number increases, once again this is due to the C_{D_α} effect as angle-of-attack changes to meet the 1-g lift requirement. In Figures 4.19 and 4.20 there are no unique features as performance once again is best at low altitudes and high speeds. As with the agility sets themselves, data such as that displayed in Figures 4.17-4.20 may provide a useful means for designers or analysts in comparing aircraft instantaneous agility performance.

4.3: Thoughts on the Body-Rate Bounds

Two additional features of the body-rate sets require examination before we proceed to the following chapter where we apply our agility theory towards the solution of an optimal control problem in integral agility. Looking back at Figures 4.11, 4.13 and 4.15, one may notice the following:

- the maximum achievable pitch-rates are extraordinarily high
- the body-rate sets are highly irregular in shape

The high rates are due to the fact that the *BRM* ignores the transient pitch-rate dynamics which take place in the higher-order rigid-body model where q is a state and therefore $\dot{q} \neq 0$ initially. In reality, an aircraft would be limited by either maximum lift, $(C_{L_\alpha} = 0)$, or maximum g-load before it could achieve the pitch-rates displayed in the *BRM* figures. The actual maximum steady-state pitch-rate capability would therefore be significantly less than that indicated in the preceding analysis. The fact that the body-rate sets are irregular in shape does not impair the analysis of instantaneous agility, however the irregularity of the control set can present difficulties in the solution of an optimal control problem where the set of possible state-rates must be convex to guarantee the existence of a solution [10,20]. In the absence of convexity an optimal control may want to "chatter"; that is rapidly switch between two bounds on the control set. Since our controls are body-rates this implies a train of impulses for the moments. Such an optimal control would stretch the credibility of the model too much.

In the following chapter we will require a body-rate control set that is more suitable for solving optimal control problems. Accordingly, we now present an alternative approach for determining the bounds to the body-rate set (p,q) whereby more realistic rate limits are achieved and the irregular body-rate bounds are ultimately replaced by a convex approximation. To achieve more realistic rate limits we return to considerations of a rigid-body model and consider the following two maneuvers for characterizing absolute limits on pitch and roll-rate respectively:

- Pure pull-up at maximum stabilator deflection
- Unloaded roll at maximum aileron deflection

Three state-rate equations are required for the first maneuver, they are:

$$\dot{q} = \frac{M(\alpha, \delta s)}{I_y}$$

$$\dot{\alpha} = q + \frac{g}{V}\left[\cos\gamma - n(\alpha)\right]$$

$$\dot{\gamma} = \frac{g}{V}\left[n(\alpha) - \cos\gamma\right]$$

where the pitching moment, $M(\alpha, \delta s)$, was previously defined in equations (4.2) and (4.5). For a step-input of maximum stabilator deflection, δs, one may expect pitch-rate responses such as those displayed in Figure 4.21. Note that the maximum pitch-rates here are far less than those predicted by the body-rate model for the same flight conditions (see Figure 4.11). This is due to the fact that the *BRM* achieves instant pitch-rates and therefore is not subjected to the transient angle-of-attack constraints that affect the rigid-body model.

For the second rigid-body maneuver we require only the bank-angle and roll-rate equations since we may assume that angle-of-attack and path-angle are zero during the unloaded roll, we therefore have:

$$\dot{p} = \frac{L(0, \delta A)}{Ix}$$

$$\dot{\mu} = p$$

where the rolling moment, $L(0, \delta A)$ was previously defined in equations (4.1) and (4.4) and the zero in the first entry refers to α. For a step-input of maximum aileron deflection, δA, one may expect roll-rate responses such as those displayed in Figure 4.22. Note that the maximum steady-state rates displayed here do *not* differ greatly from those displayed in Figure 4.11.

Finally, we may obtain a convex body-rate set at each flight condition by approximating the relation between maximum pitch-rate, q_{max}, and maximum roll-rate, p_{max}, (from Figures 4.21 and 4.22, respectively) as an ellipse, this implies that the controls (*p,q*) are limited as follows:

$$\text{(4.11)} \quad \left(\frac{p}{p_{max}}\right)^2 + \left(\frac{q}{q_{max}}\right)^2 \leq 1$$

For comparison purposes the elliptical body-rate bounds have been superimposed over the original bounds in Figure 4.23. Since the mapping from body-rates to agility components is affine, the agility set corresponding to the elliptical body-rate bound, equation (4.11), will also be elliptical in shape. Although we require these *approximated* elliptical body-rate bounds to solve our optimal integral agility flight problem in the following chapter, it is noted that the agility sets derived from

the original irregular body-rate bounds remain a valid means for evaluating instantaneous aircraft agility *within the context of the reduced-order BRM.*

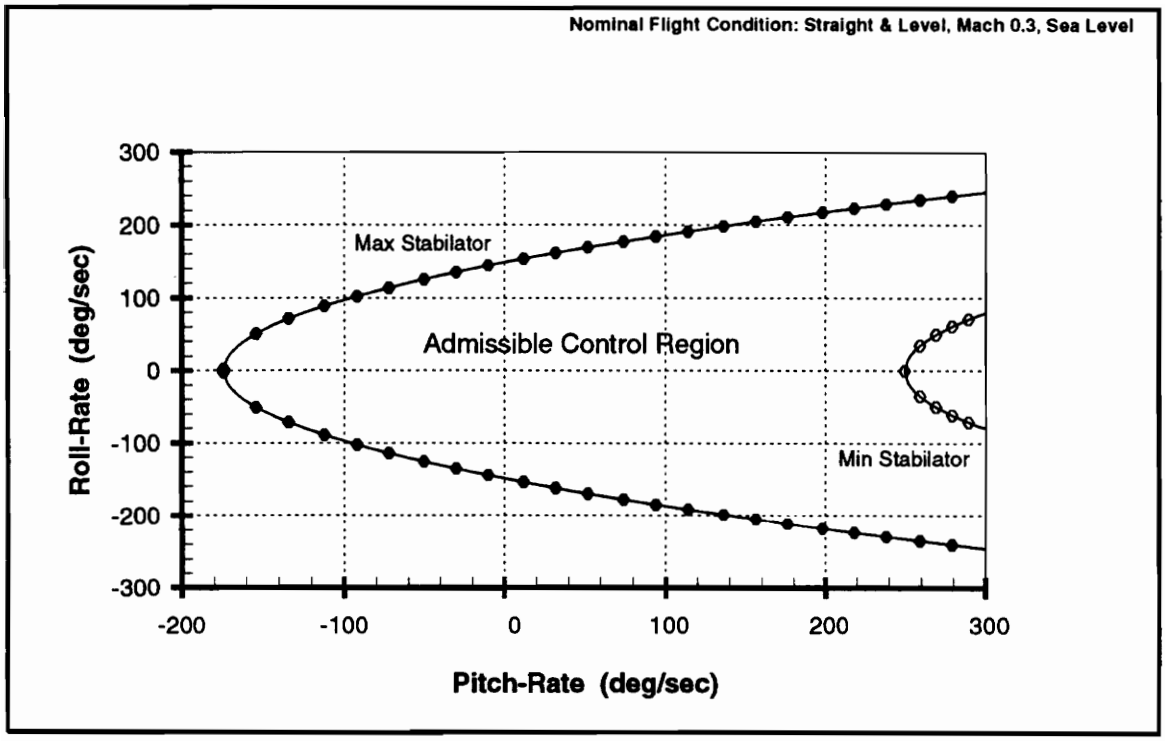

Figure 4.1. Pitch Equilibrium

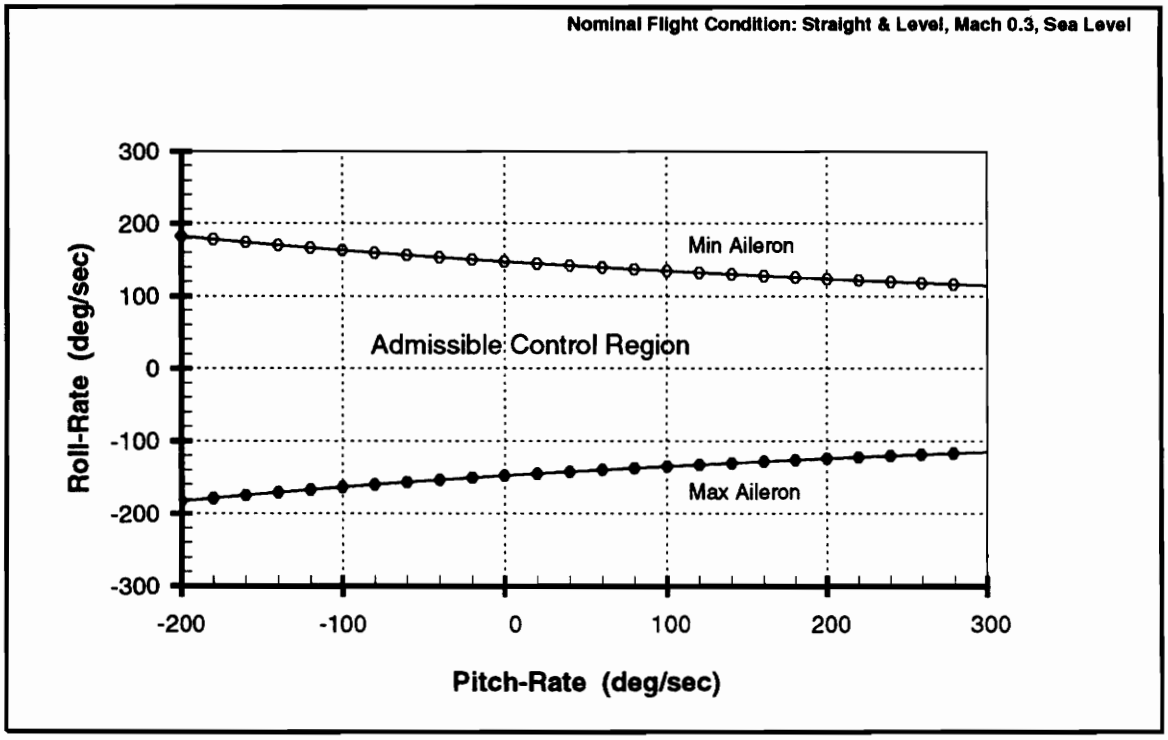

Figure 4.2. Roll Equilibrium

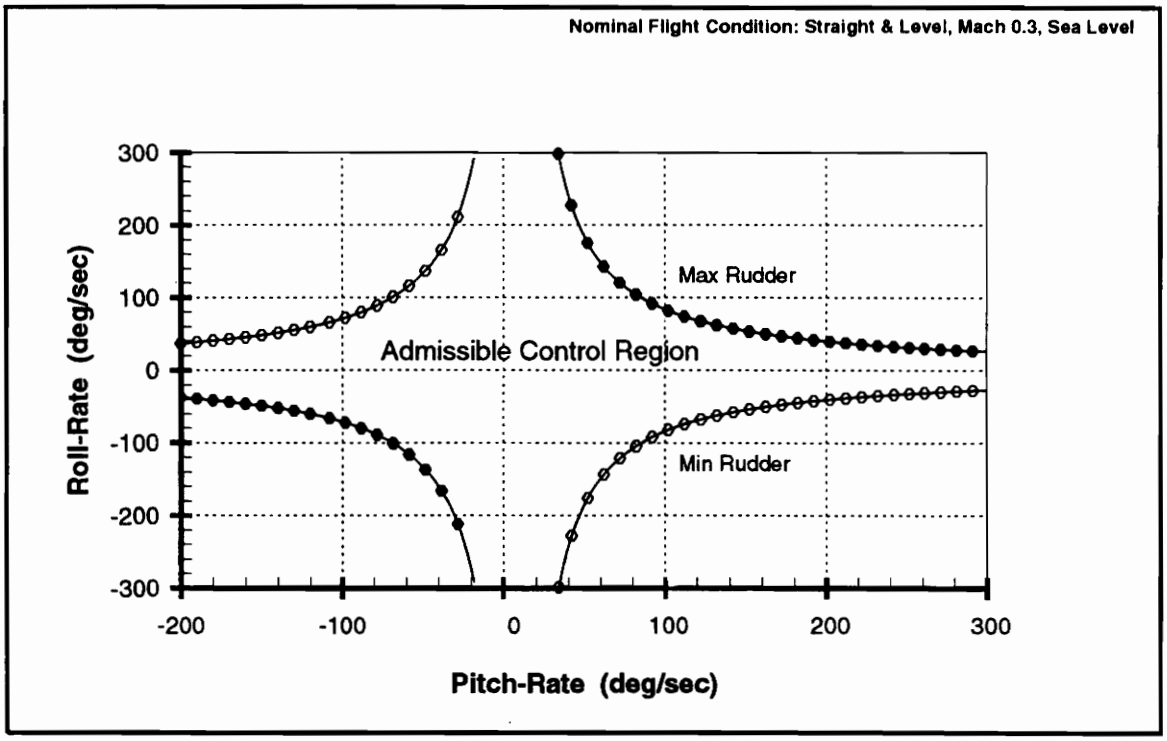

Figure 4.3. Yaw Equilibrium

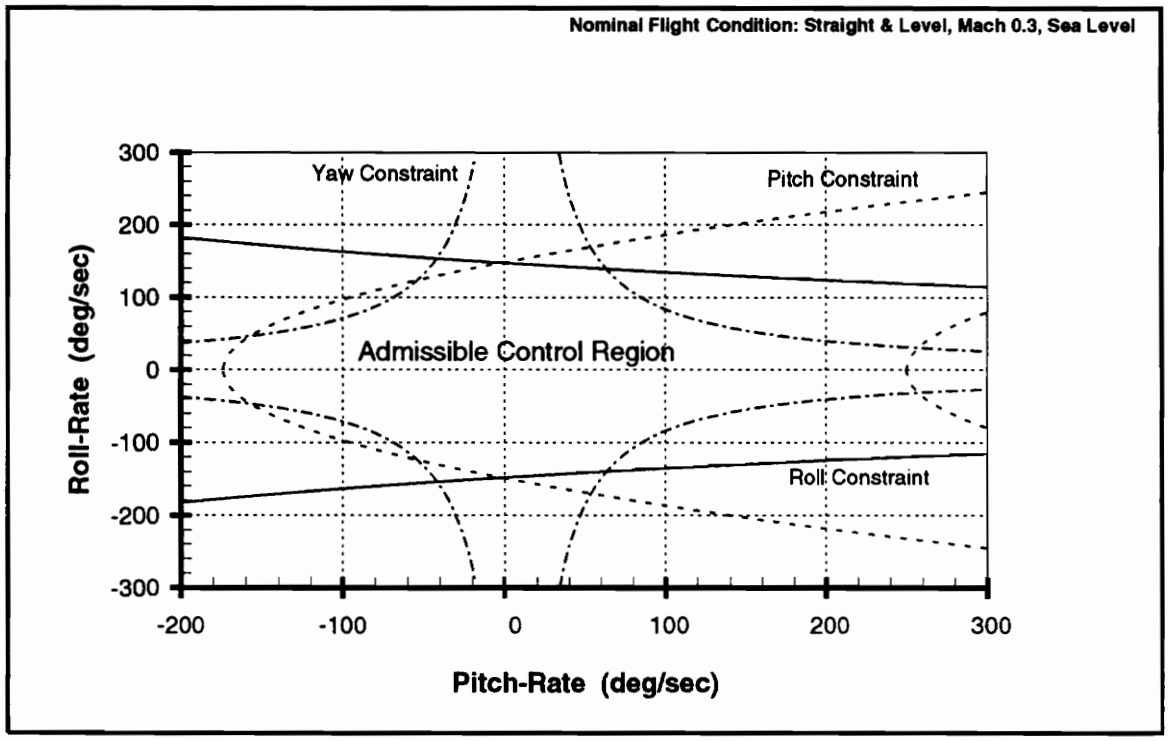

Figure 4.4. Composite Equilibrium Condition

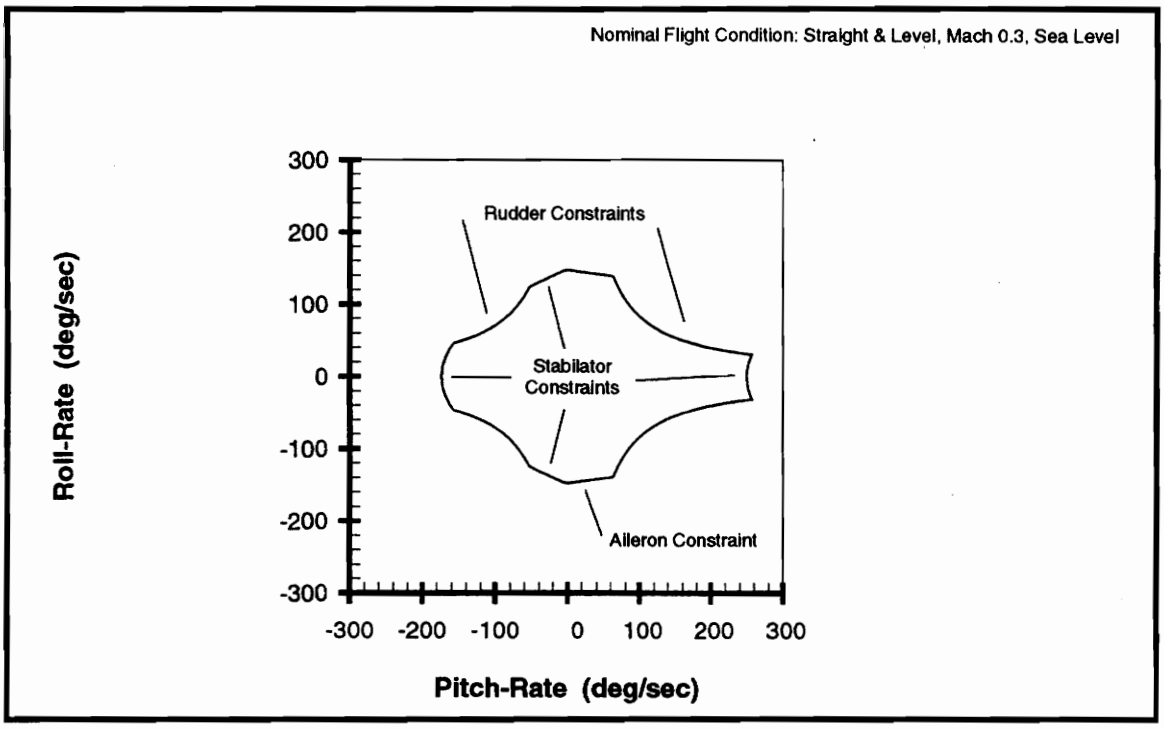

Figure 4.5. Admissible Body-Rate Set

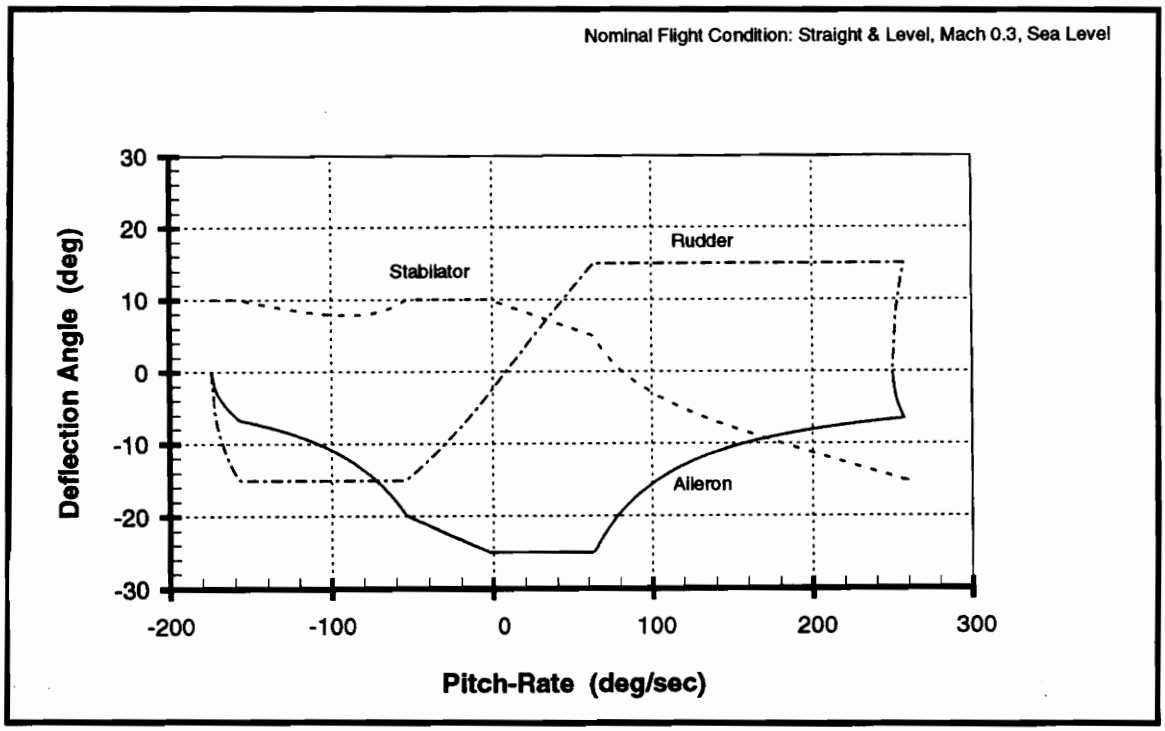

Figure 4.6. Equilibrium Control Deflections

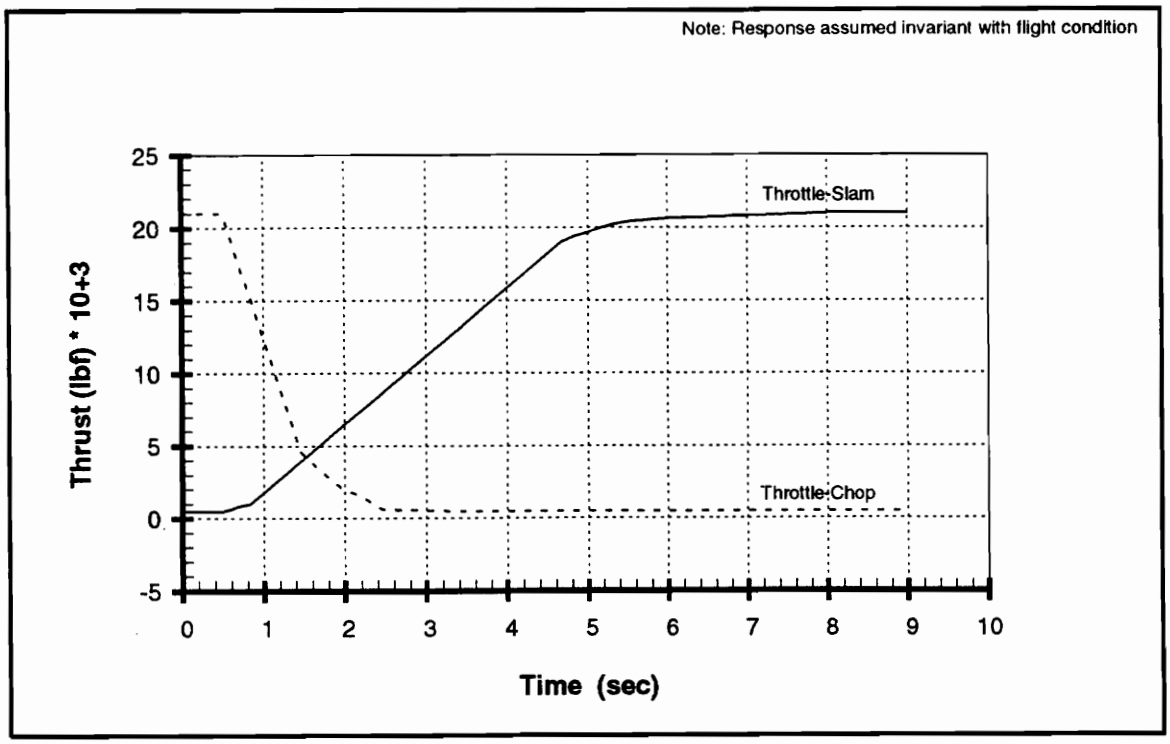

Figure 4.7. Engine Response Histories

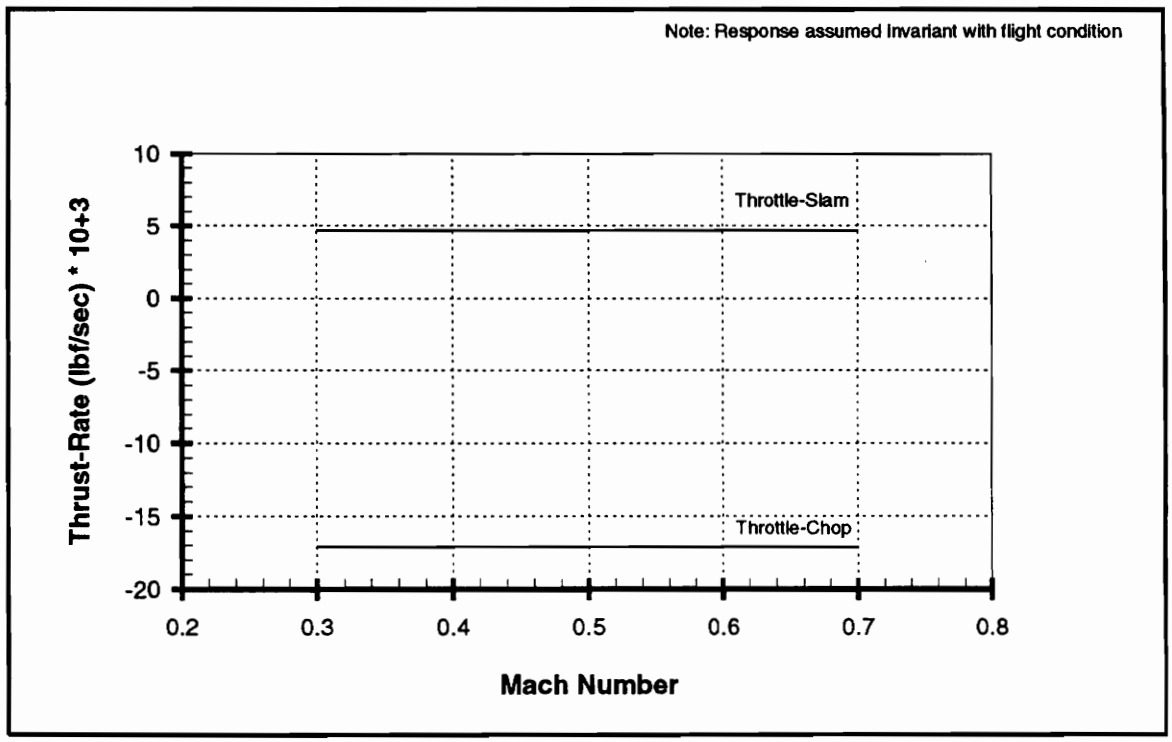

Figure 4.8. Admissible Thrust Rates

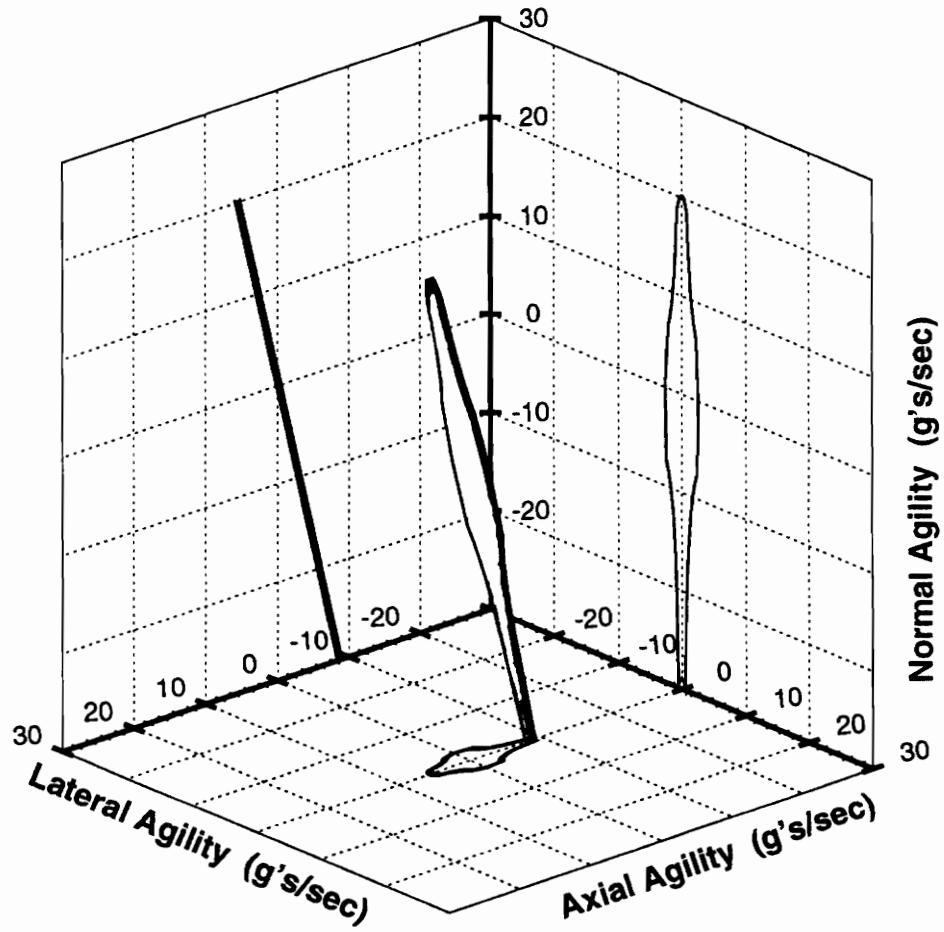

Flight Condition: Straight & Level, Mach 0.3, Sea Level

Figure 4.9. Agility Set: 3-D View

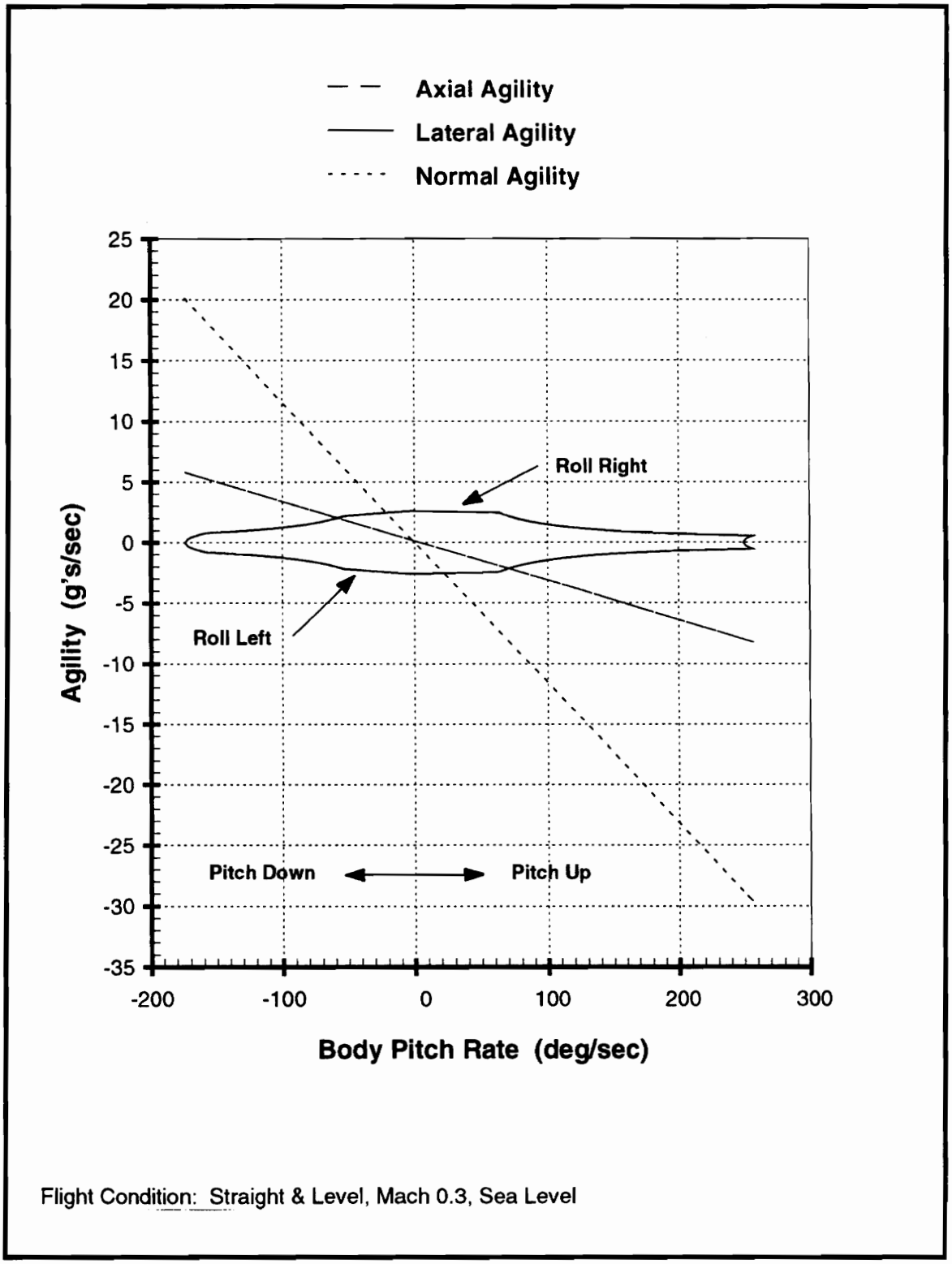

Flight Condition: Straight & Level, Mach 0.3, Sea Level

Figure 4.10. Extremal Agility: Pitch-Rate Dependence

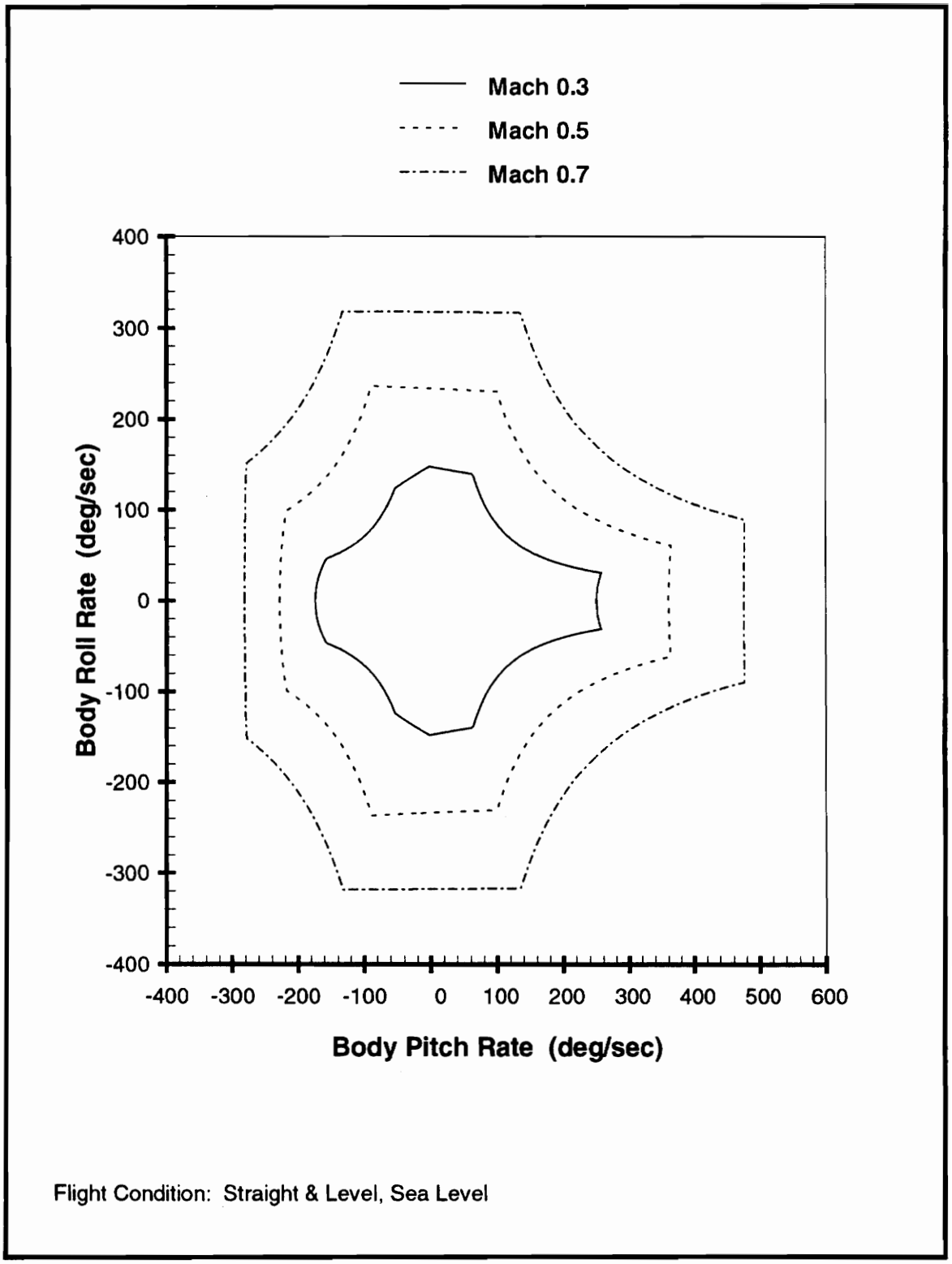

Figure 4.11. Body-Rate Sets: Mach Dependence

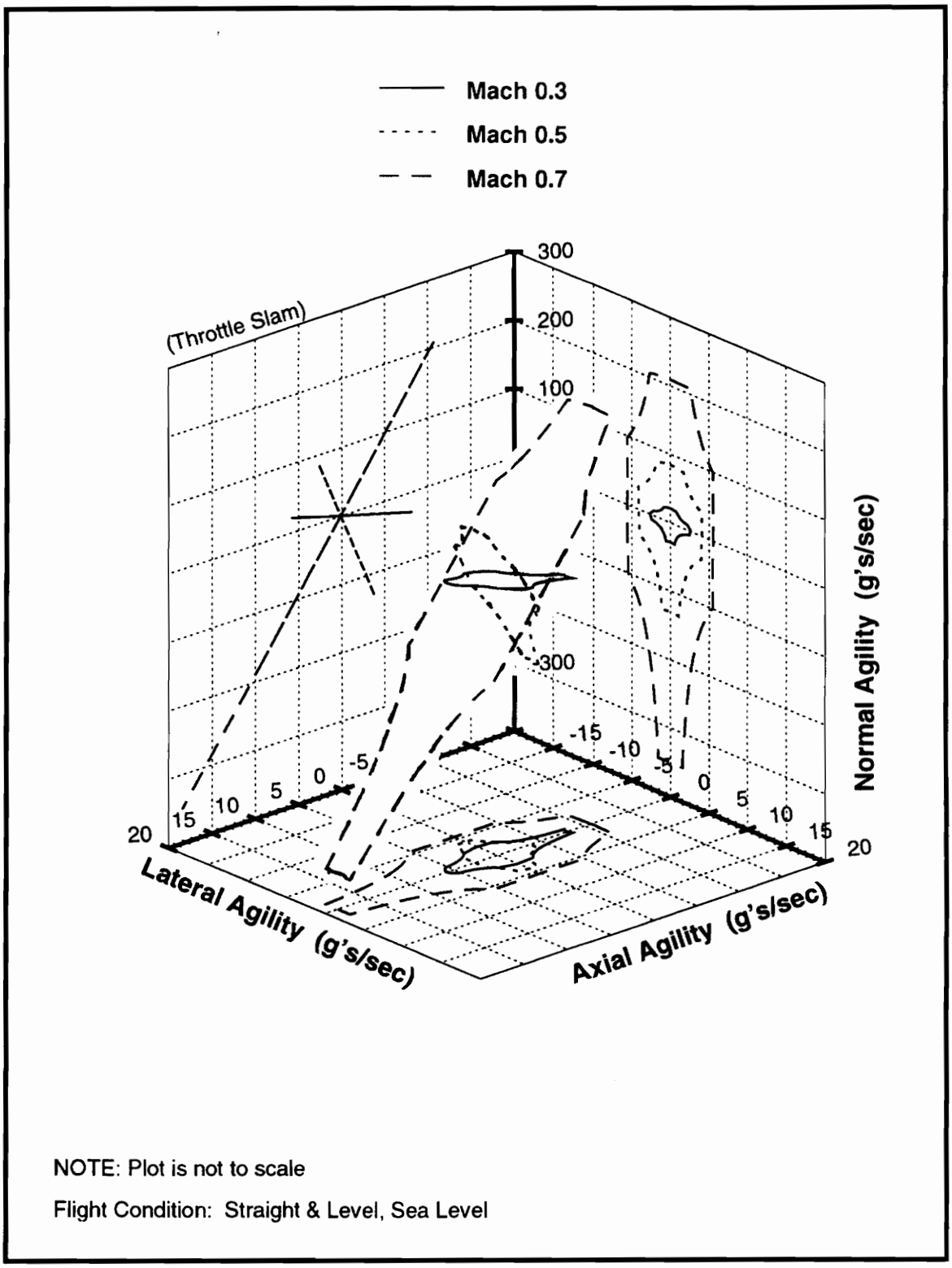

NOTE: Plot is not to scale

Flight Condition: Straight & Level, Sea Level

Figure 4.12. Agility Sets: Mach Dependence

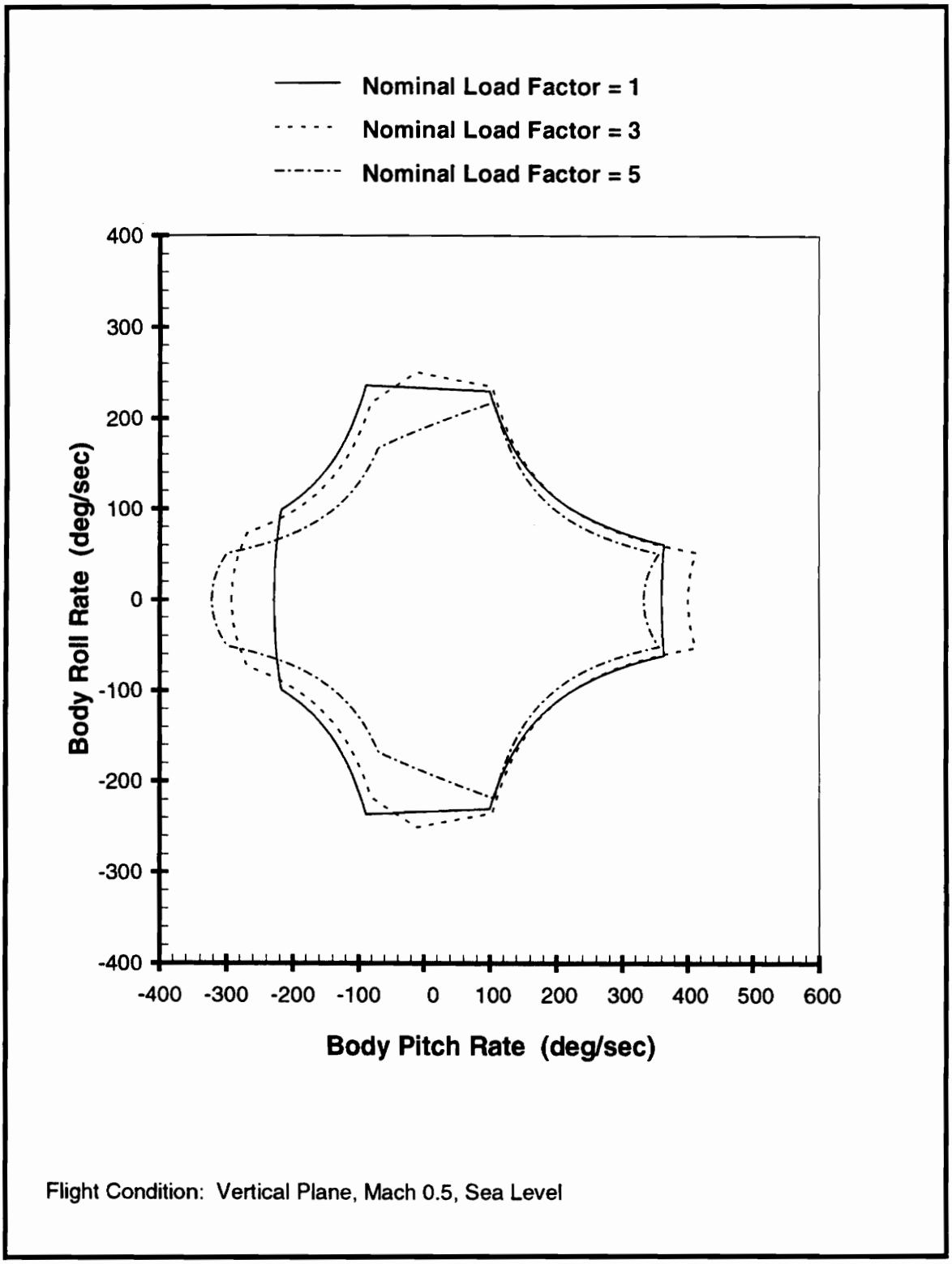

Figure 4.13. Body-Rate Sets: Load Dependence

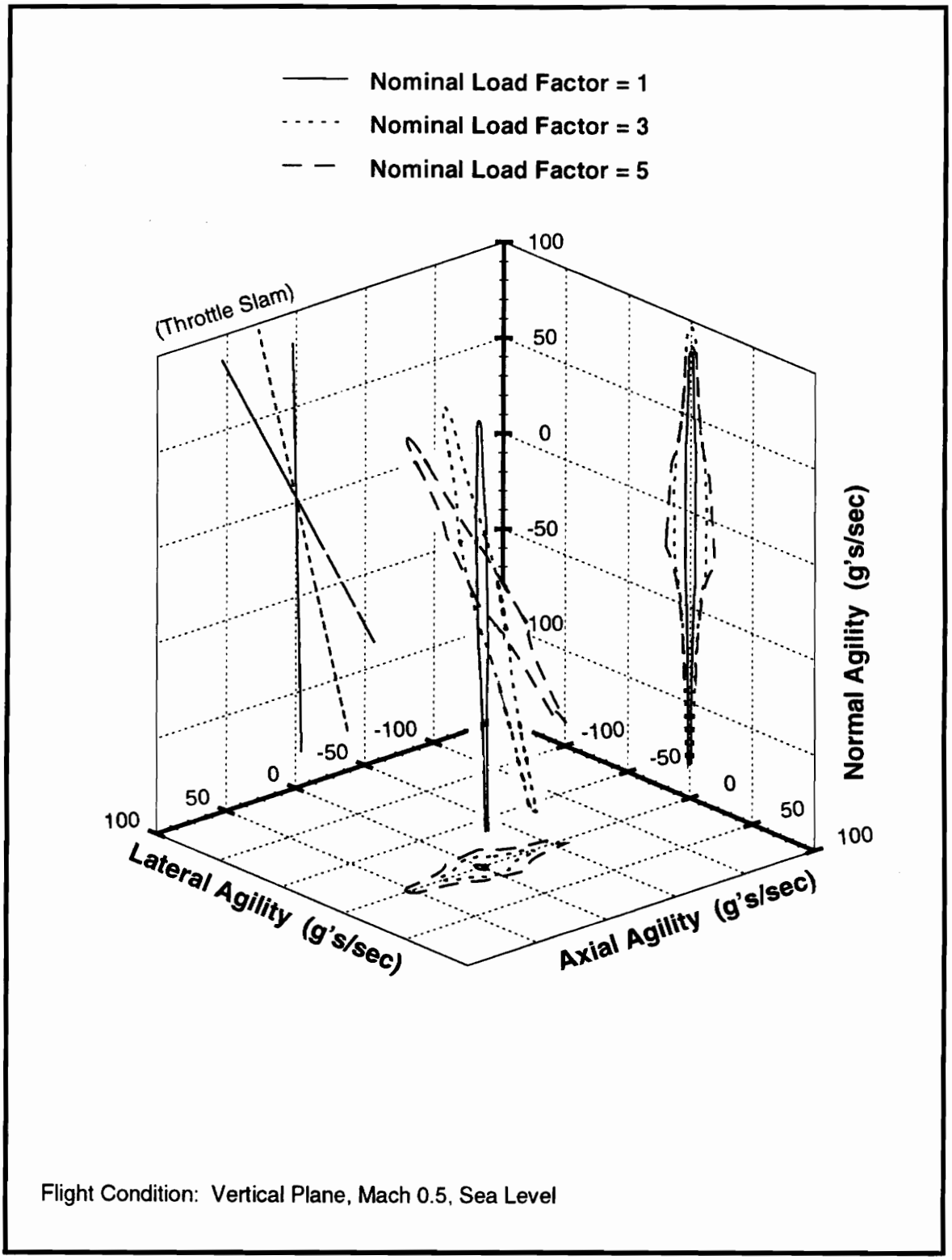

Figure 4.14. Agility Sets: Load Dependence

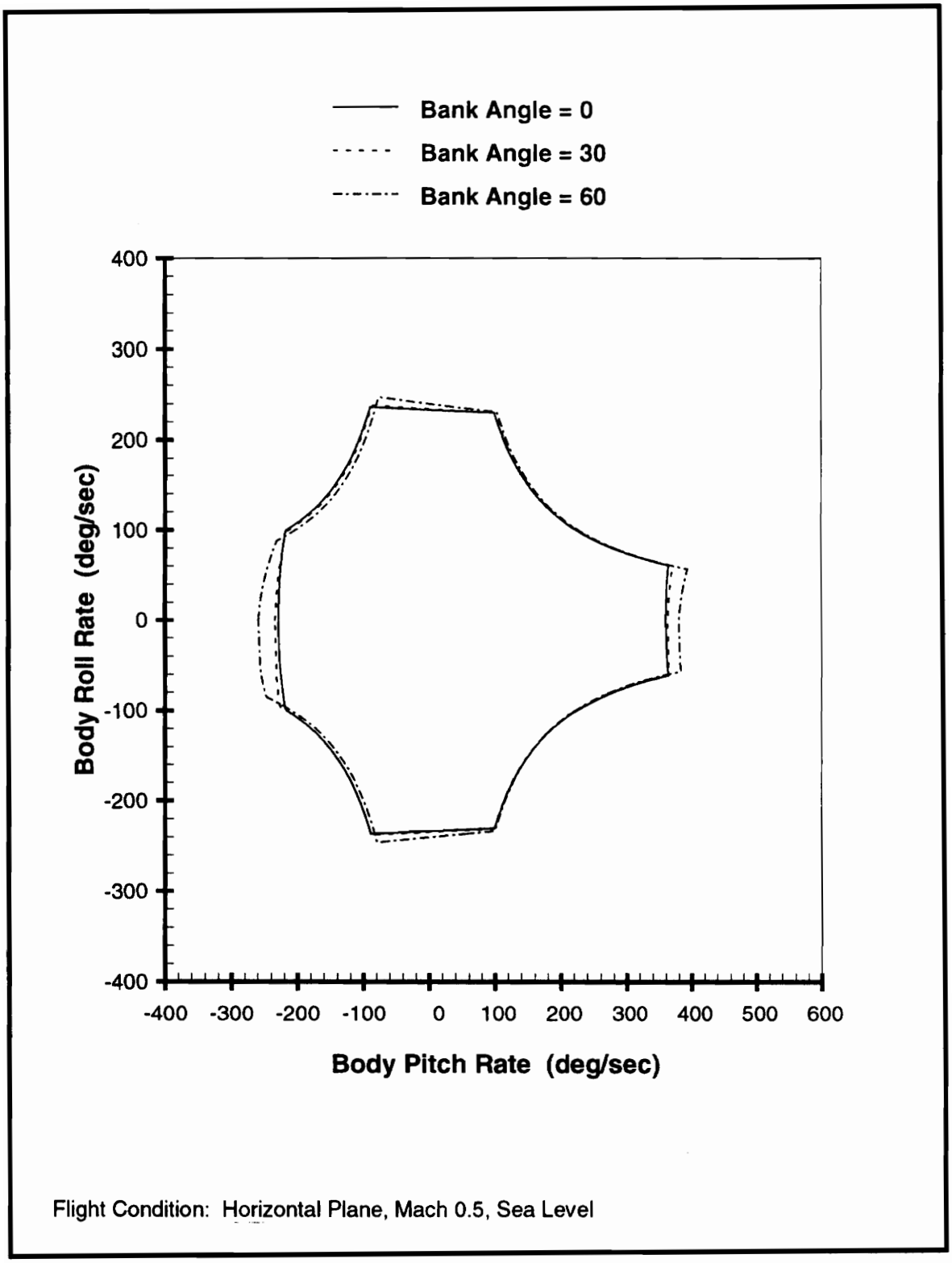

Flight Condition: Horizontal Plane, Mach 0.5, Sea Level

Figure 4.15. Body-Rate Sets: Bank-Angle Dependence

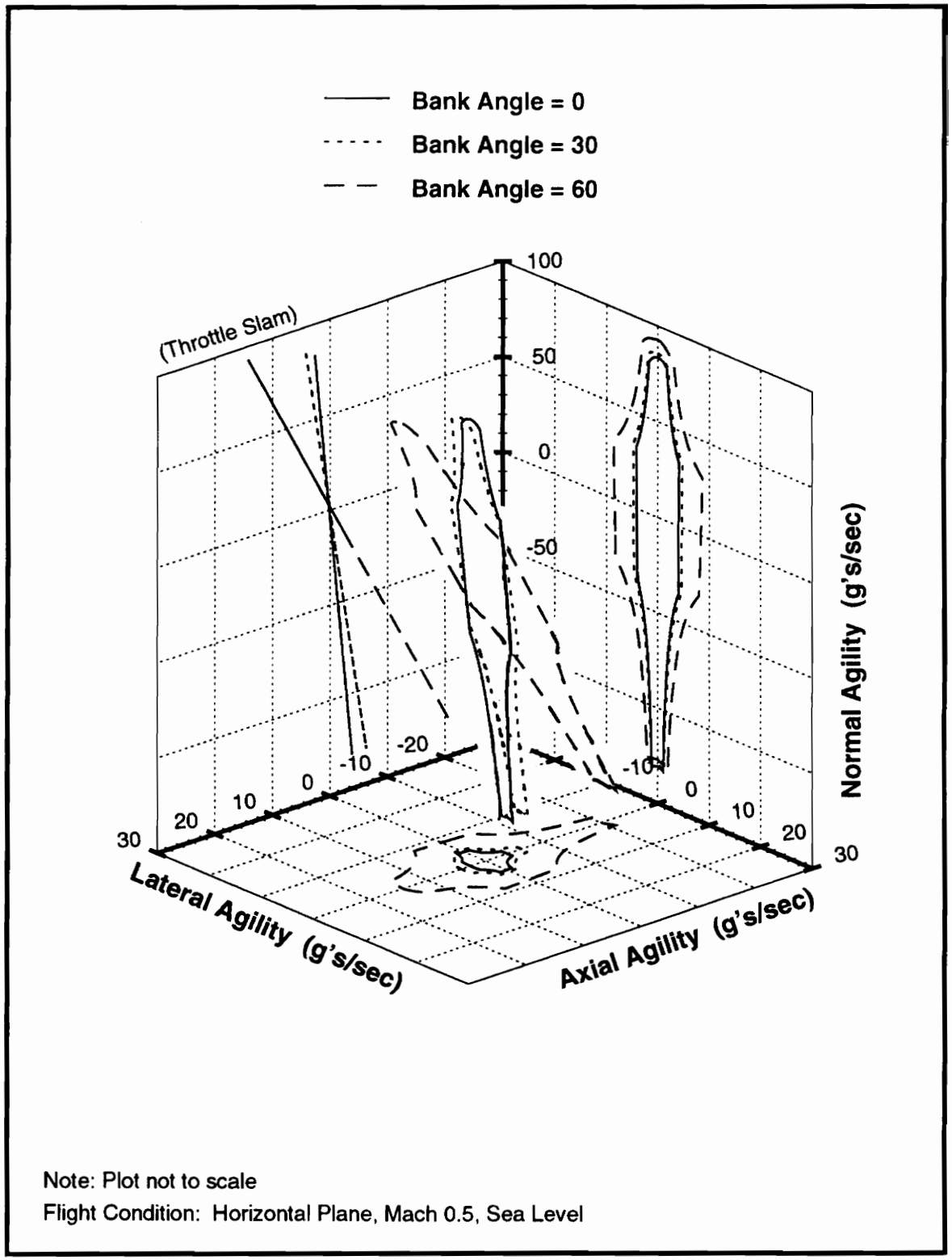

Note: Plot not to scale

Flight Condition: Horizontal Plane, Mach 0.5, Sea Level

Figure 4.16. Agility Sets: Bank-Angle Dependence

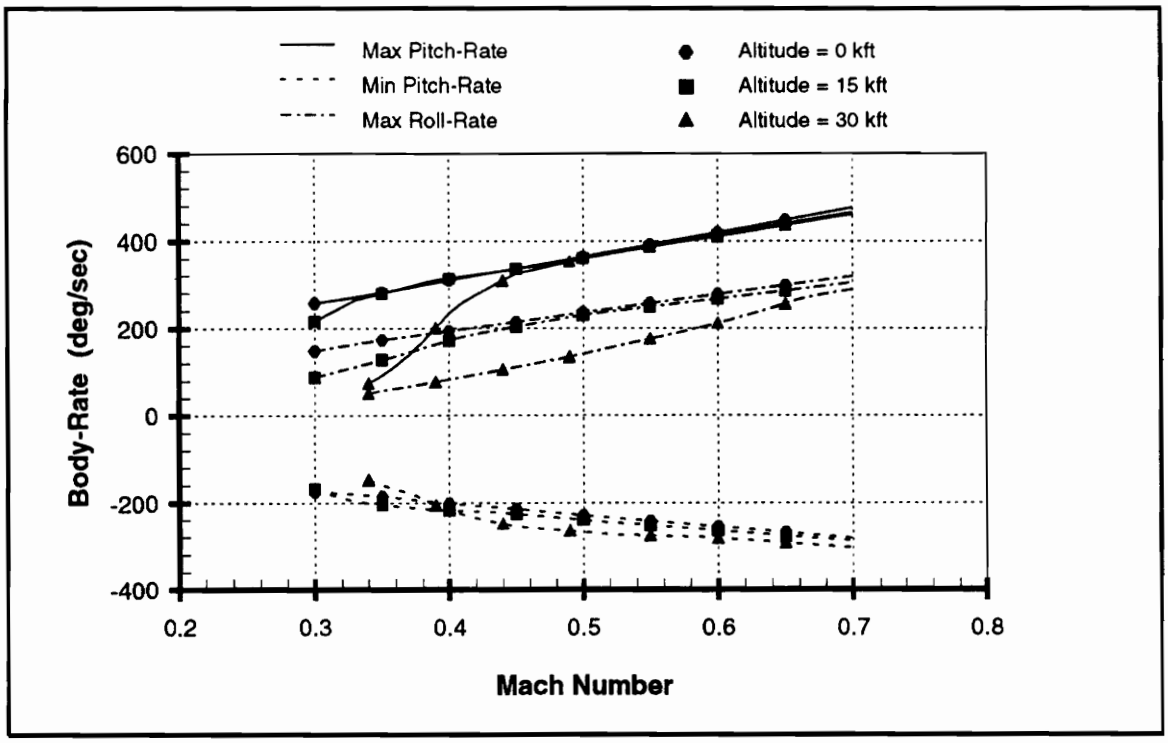

Figure 4.17. Limiting Body-Rates: Straight & Level Flight

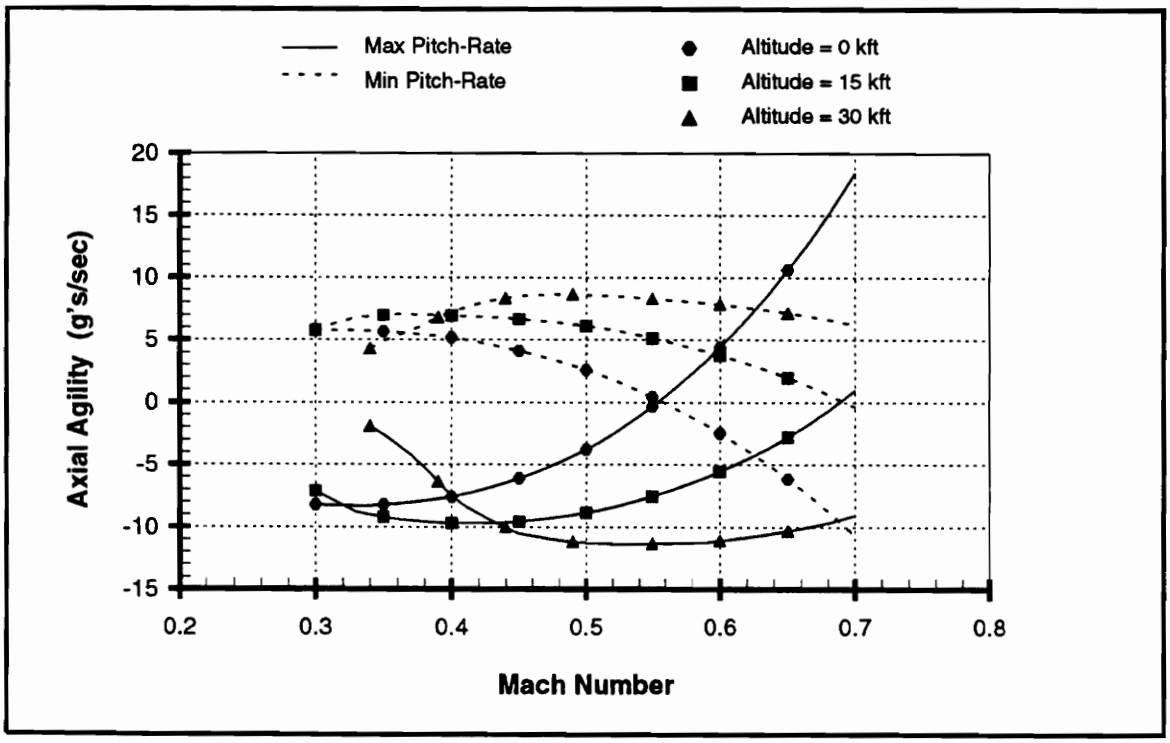

Figure 4.18. Axial Agility Limits: Straight & Level Flight

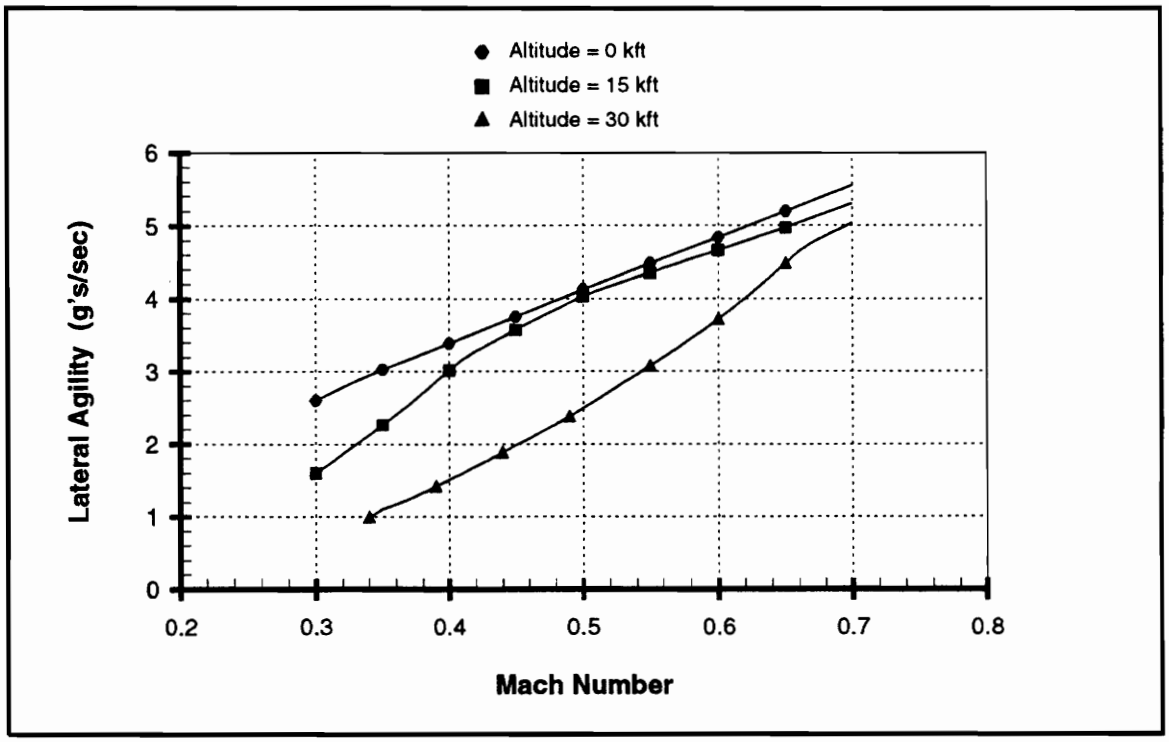

Figure 4.19. Lateral Agility Limits: Straight & Level Flight

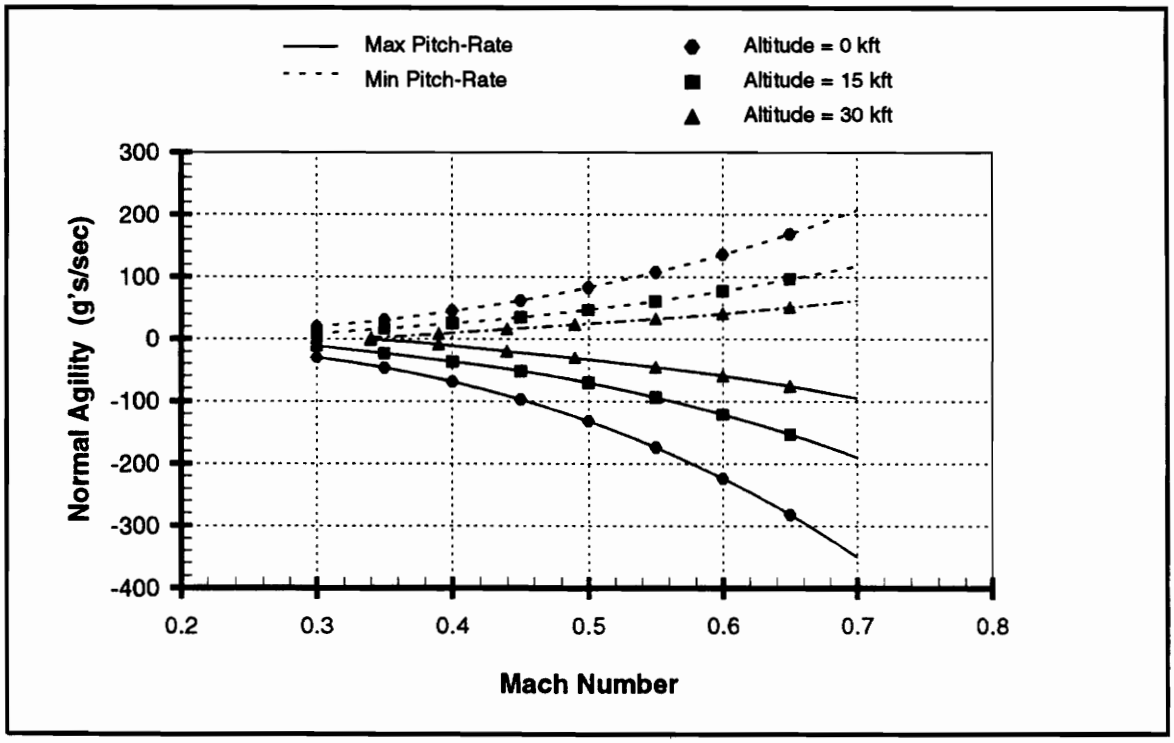

Figure 4.20. Normal Agility Limits: Straight & Level Flight

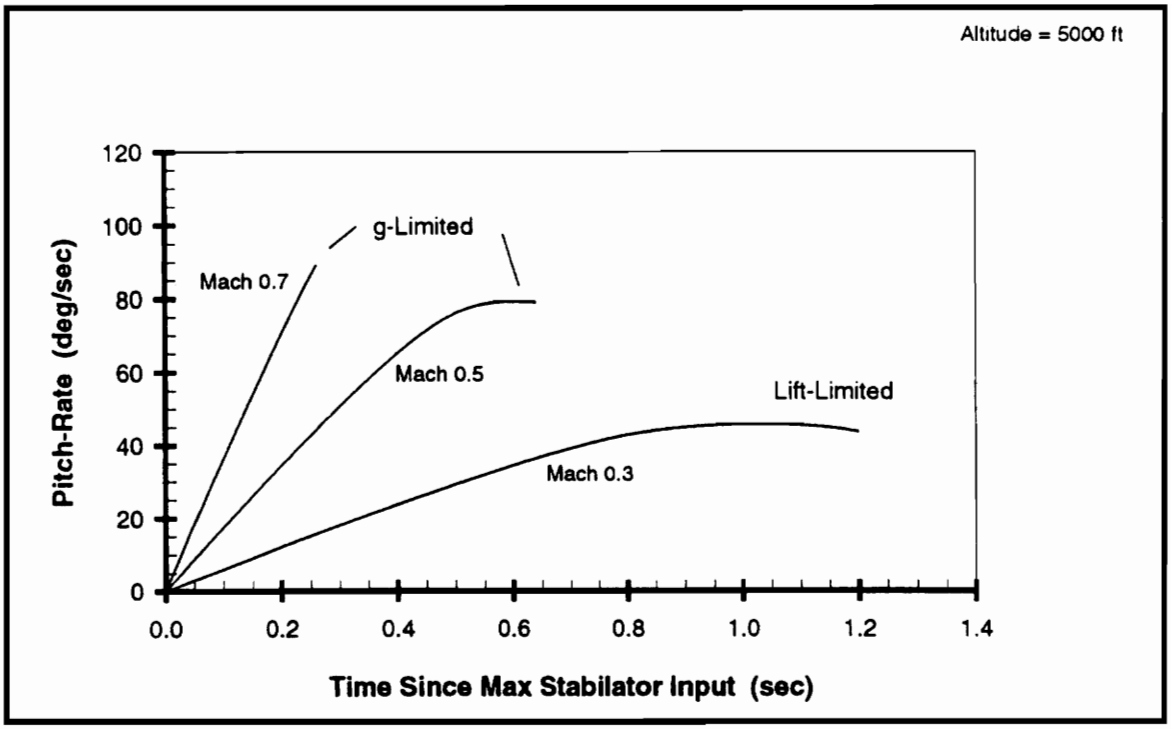

Figure 4.21. Rigid-Body Pitch-Rate Response

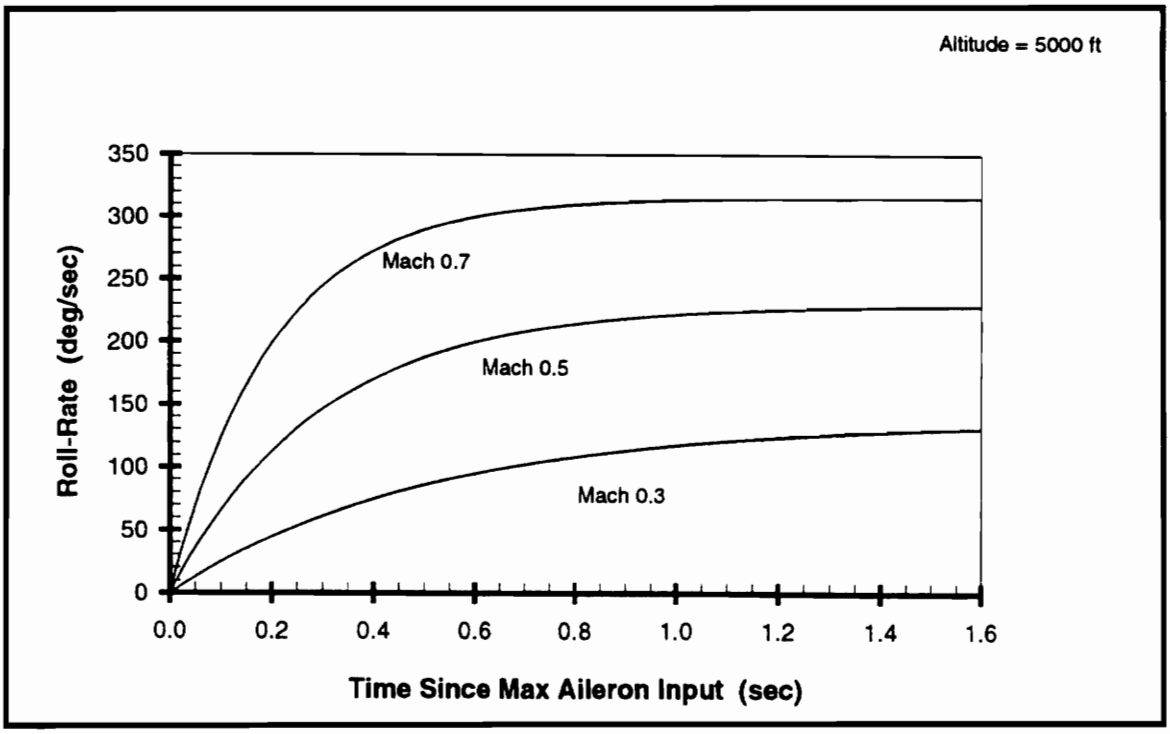

Figure 4.22. Rigid-Body Roll-Rate Response

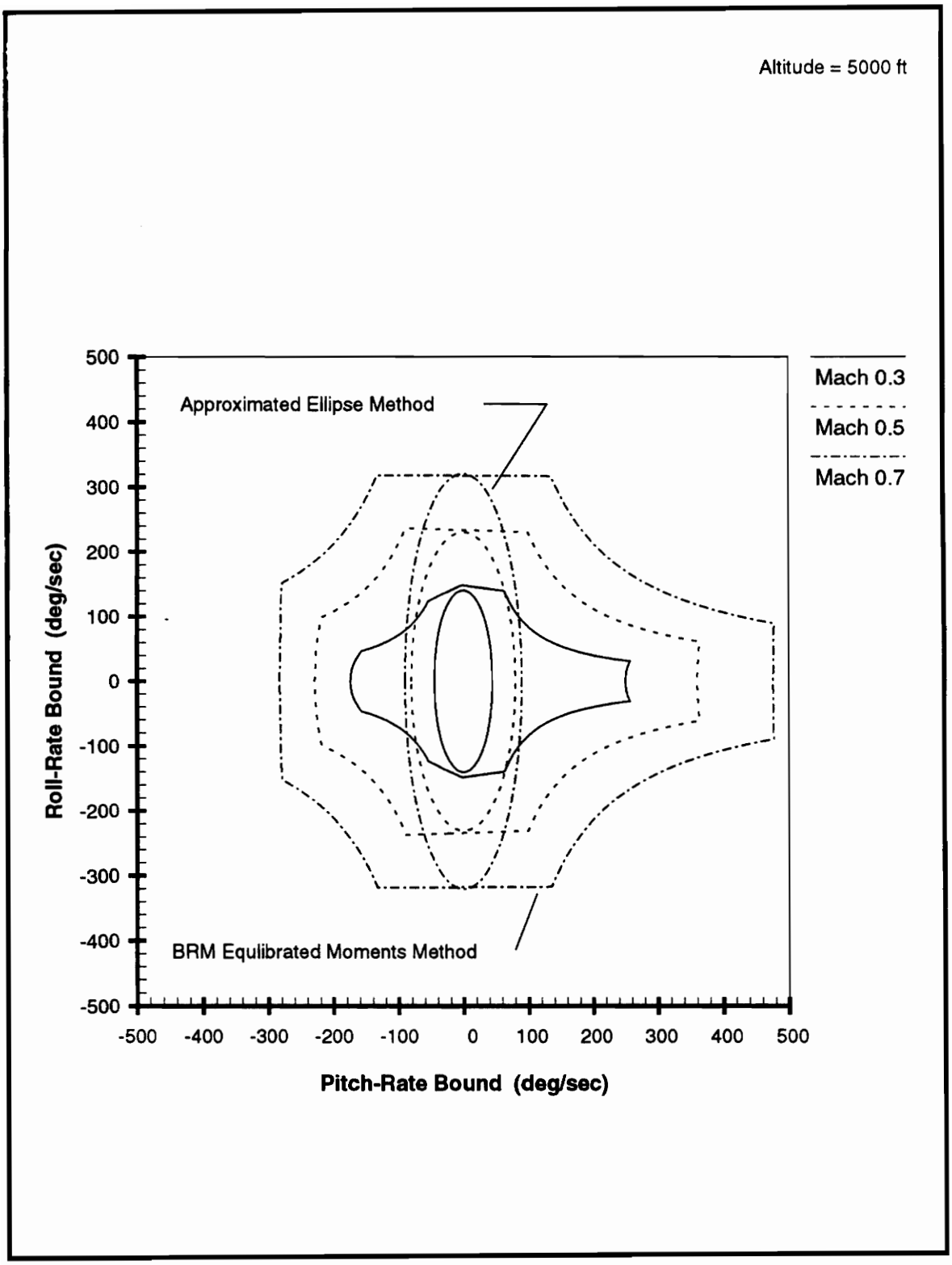

Figure 4.23. Alternative Body-Rate Sets

CHAPTER 5
INTEGRAL AGILITY

5.1: The Optimal Control Problem

In this chapter we will formulate an integral performance flight problem and solve that problem via the usual methods of optimal control theory [6,19,20,21]. The body-rate model which was developed in Chapter 3 will be employed to model the aircraft dynamics. The particular problem that we have chosen is a simple one, yet it has been suggested by Kalviste's roll reversal agility parameter Y^nT [17]. Related optimal maneuvers have been studied by Cannon [8].

Our flight problem is depicted in Figure 5.1. Consider an aircraft in straight and level (1-g) flight with an initial heading angle of $\chi_0 = 0$. At time t_0 the vehicle is to begin a rapid turn to the right and continue that turn up to a fixed final-time, t_f. The maneuver is to be flown in such a way so as to maximize the final heading angle, χ_f. The dynamics of interest for such a problem will occur over a brief time-span; accordingly, we may reasonably make the following assumptions:

- Aircraft speed is constant during the maneuver [neglect speed dynamics (3.5)]
- Atmospheric properties $\rho(h)$ and $a(h)$ are constant [neglect altitude dynamics (3.4)]

In addition to these assumptions, we will retain the previous simplifications to the body-rate model, *ie* symmetric flight $\left(\beta = \dot{\beta} = 0\right)$ and thrust along the path. Consideration of the constraints listed above, and elimination of the ignorable states, *x* and *y*, reduces the list of *BRM* state equations (see equations 3.2-3.10) which must be considered for this problem to the following:

$$\dot{\gamma} = \frac{g}{V}\left[n(\alpha)\cos\mu - \cos\gamma\right] \tag{5.1}$$

(5.2) $$\dot{\chi} = n(\alpha)\frac{g}{V}\frac{\sin\mu}{\cos\gamma}$$

(5.3) $$\dot{\alpha} = q + \frac{g}{V}\left[\cos\gamma\cos\mu - n(\alpha)\right]$$

(5.4) $$\dot{\mu} = \frac{p}{\cos\alpha} + \frac{g}{V}\sin\mu\left[n(\alpha)\tan\gamma + \cos\gamma\tan\alpha\right]$$

where the normal load-factor, $n(\alpha)$, is defined as:

(5.5) $$n(\alpha) = \frac{L(\alpha)}{W} = \frac{\bar{q}\,S\,C_L(\alpha)}{W}$$

and the function $C_L(\alpha)$ is the primary aerodynamic data required for our problem. Note that no thrust data is required for the problem since we have assumed that the velocity remains constant. During the maneuver the aircraft is to be limited to angles-of-attack such that neither a pre-defined load-factor limit ($n(\alpha) \le n_{max}$) nor an aerodynamic stall limit ($\alpha \le \alpha_{stall}$) are exceeded. These limits are depicted graphically in Figure 5.2.

Returning momentarily to modeling considerations, one may notice that in a point-mass approximation the angle-of-attack, α, and bank-angle, μ, act as controls and may therefore be changed instantly. In this case, at time t_0^+ the aircraft will already have achieved a non-zero turn-rate (see equation 5.2). For a rigid-body model, the control surfaces (elevator, rudder, aileron) would discontinuously change at t_0 but the body-rates, and therefore the body attitude, would not. The body-rate model is intermediate and permits instantaneous changes in the body-rate controls, *p* and *q*, but the body attitude is continuous. For the *BRM* the velocity-heading angle *and* its rate are still zero at time t_0^+. Our model will therefore produce a transient maneuver while the body pitches, rolls and yaws. We may consider the magnitude of this transient lag as a measure of integral agility. Longer lags mean less agility. The point mass model displays no lag and hence may be considered as having "infinite" agility. With finite limits on the body-rates, the agility will also be finite. To separate the agility inherent in the aircraft from the effects of pilot technique, one should perform the maneuver in an ***optimal*** way. This is the motivation for our

problem.

Since we are attempting to maximize the value of a state variable, χ, at a specified final time, the optimal control problem that we will be solving may be conveniently formulated as a Mayer-type problem where the performance index is:

(5.6) $$J = \phi[x(t_f), t_f] = \chi(t_f)$$

Mathematically speaking, we are to find the control histories $p(t)$ and $q(t)$ which will drive the system from an initial prescribed state

(5.7) $$\gamma(t_0) = \chi(t_0) = \mu(t_0) = 0$$

(5.8) $$\alpha(t_0) = \alpha_0$$

to maximize $\chi(t_f)$ while satisfying both the state inequality constraint;

(5.9) $$S\alpha = [\alpha(t) - \alpha_{max}] \leq 0$$

and the prescribed bound on the controls [see equation (4.11)];

(5.10) $$\left(\frac{p}{p_{max}}\right)^2 + \left(\frac{q}{q_{max}}\right)^2 \leq 1$$

With the integral flight problem adequately described, we now proceed to describe the necessary conditions and arc structures associated with solving our problem.

5.2: Constructing Extremals

In order to solve the optimal control problem we shall apply the usual necessary conditions for optimality [6,19,20,21]. We will start this procedure by assuming that the state

inequality constraint (5.9) does not become active. Accordingly, we construct the variational-Hamiltonian as:

$$H = \lambda^T f = \begin{pmatrix} \lambda_\gamma & \lambda_\chi & \lambda_\alpha & \lambda_\mu \end{pmatrix} \bullet \begin{pmatrix} \dot{\gamma} \\ \dot{\chi} \\ \dot{\alpha} \\ \dot{\mu} \end{pmatrix}$$

where the λ_x terms have been described in the literature as adjoint variables, co-states, influence functions and Lagrangian multipliers. Expansion of the Hamiltonian yields the following;

$$(5.11)\quad H = \lambda_\gamma \cdot \left\{ \frac{g}{V} \left[n(\alpha) \cos\mu - \cos\gamma \right] \right\} + \lambda_\chi \cdot \left[n(\alpha) \frac{g}{V} \frac{\sin\mu}{\cos\gamma} \right] + \lambda_\alpha \cdot \left\{ q + \frac{g}{V} \left[\cos\gamma \cos\mu - n(\alpha) \right] \right\}$$
$$+ \lambda_\mu \cdot \left\{ \frac{p}{\cos\alpha} + \frac{g}{V} \sin\mu \left[n(\alpha) \tan\gamma + \cos\gamma \tan\alpha \right] \right\}$$

The co-state differential equations are then derived from the Hamiltonian in the usual manner, that is;

$$\dot{\lambda}_j = -\frac{\partial H}{\partial x_j}$$

which yields;

$$(5.12)\quad \dot{\lambda}_\gamma = -\frac{g}{V} \left[\sin\gamma \left(\lambda_\gamma + \lambda_\chi\, n(\alpha) \frac{\sin\mu}{\cos^2\gamma} - \lambda_\alpha \cos\mu - \lambda_\mu \sin\mu \tan\alpha \right) + \lambda_\mu\, n(\alpha) \frac{\sin\mu}{\cos^2\gamma} \right]$$

$$(5.13)\quad \dot{\lambda}_\chi = 0 \qquad (\therefore\ \lambda_\chi = \textit{constant})$$

(5.14)

$$\dot{\lambda}_\alpha = -\frac{g}{V}\left[n'(\alpha)\left(\lambda_\gamma \cos\mu + \lambda_\chi \frac{\sin\mu}{\cos\gamma} - \lambda_\alpha + \lambda_\mu \sin\mu \tan\gamma \right) + \lambda_\mu \left(p \frac{V}{g} \frac{\sin\alpha}{\cos^2\alpha} + \frac{\sin\mu\cos\gamma}{\cos^2\alpha} \right) \right]$$

(5.15)

$$\dot{\lambda}_\mu = -\frac{g}{V}\left\{ -\lambda_\gamma n(\alpha) \sin\mu + \lambda_\chi n(\alpha) \frac{\cos\mu}{\cos\gamma} - \lambda_\alpha \sin\mu\cos\gamma + \lambda_\mu \cos\mu \left[n(\alpha)\tan\gamma + \cos\gamma\tan\alpha \right] \right\}$$

where $n'(\alpha)$ is the derivative of the load-factor with respect to the angle-of-attack.

The first necessary condition of optimality is derived from Pontryagin's Minimum Principle, it requires that at each time along an optimal trajectory the control must minimize the variational-Hamiltonian, *ie*:

$$H\left[\lambda(t), x^*(t), u^*(t) \right] = \min_u H\left[\lambda(t), x^*(t), u \right]$$

Note that the control dependent terms of the Hamiltonian, H_{cp}, are the only terms that enter into the optimality condition, we obtain these terms from equation (5.11) as:

$$H_{cp} = \lambda_\alpha \cdot q + \frac{\lambda_\mu}{\cos\alpha} \cdot p = \left\langle \begin{pmatrix} \lambda_\mu/\cos\alpha \\ \lambda_\alpha \end{pmatrix}, \begin{pmatrix} p \\ q \end{pmatrix} \right\rangle$$

From the last expression we interpret H_{cp} as a dot-product of the vector $(p, q)^T$ with a vector whose value depends on λ_α, λ_μ and α. Since the controls are restricted to an ellipse in the (p,q) plane it is clear that *extremal* controls will occur on the boundary of the ellipse. This minimization process can be simplified even further if we transform the elliptical constraint on the control bounds (see Figure 5.3) into a circular constraint as shown in Figure 5.4. We may then write the original body-rate controls as;

$$\tilde{q} = \frac{q}{q_{max}} = r\cos\sigma \qquad \tilde{p} = \frac{p}{p_{max}} = r\sin\sigma$$

where r is the length of the vector $\vec{r}$ which locates the transformed control pair $(\tilde{p}, \tilde{q})$ and will always be unity so long as the controls are extremal. This transformation therefore effectively reduces the number of control variables from two to one and allows us to rewrite the control dependent Hamiltonian as:

$$H_{CD} = \lambda\alpha \cdot q_{max} \cos\sigma + \frac{\lambda\mu}{\cos\alpha} \cdot p_{max} \sin\sigma$$

differentiating this equation with respect to the new control, σ, gives;

$$\frac{\partial H_{CD}}{\partial \sigma} = H_u = -\lambda\alpha \cdot q_{max} \sin\sigma + \frac{\lambda\mu}{\cos\alpha} \cdot p_{max} \cos\sigma$$

from which the following expression for the optimal control may be obtained:

$$\sigma(t) = \tan^{-1}\left(\frac{p_{max}}{q_{max}} \frac{\dot{\lambda}\mu(t)}{\lambda\alpha(t)\cos\alpha(t)} \right) \tag{5.16}$$

The solution to equation (5.16) must cause the Hamiltonian to be minimized at all points along the unconstrained arc in order to satisfy the first-order necessary condition of optimality. Since the optimality condition involves a $\tan^{-1}$ term it is necessary to resolve the angle σ, at each point in time, such that the quadrant chosen results in the minimum value of the term H_{CD}.

The same results can be derived without this control transformation and since this will be useful later we briefly discuss the procedure here. The "natural" controls p and q are subject to the elliptical bound (5.10). To carry out the $\min - H$ operation with this bound we can adjoin the constraint to the variational-Hamiltonian

$$\hat{H} = \lambda^T f + \nu\left[\left(\frac{p}{p_{max}}\right)^2 + \left(\frac{q}{q_{max}}\right)^2 - 1\right]$$

The usual Lagrange multiplier rule asserts that if (p^*, q^*) minimizes H subject to the bound, then there is a value of ν so that (p^*, q^*) is a stationary point for $\hat{H}$. Since the constraint is an inequality, the Kuhn-Tucker conditions guarantee that $\nu \geq 0$ (see [6], Chapter 1). For this problem the conditions are;

$$\frac{\lambda_\mu}{\cos\alpha} + 2\nu\frac{p}{p^2_{max}} = 0 \qquad \text{and} \qquad \lambda_\alpha + 2\nu\frac{q}{q^2_{max}} = 0$$

and (5.10) as equality. This leads to the same p and q as found above and to;

$$\nu = \left[\left(\frac{p_{max}\lambda_\mu}{\cos\alpha}\right)^2 + (q_{max}\lambda_\alpha)^2\right]^{1/2}$$

Finally, we require boundary conditions for the states and co-states at the initial and final times. For our problem the boundary conditions are split, *ie* we know the states at time t_0, see equations (5.7) and (5.8), and the co-states are prescribed at the final time by the transversality condition;

$$\lambda_j(t_f) = \lambda_0\left(\frac{\partial\phi}{\partial x_j}\right)$$

Applying this condition to our performance index yields the following transversality conditions for the optimal control problem at time t_f:

(5.17) $\lambda_\gamma(t_f) = \lambda_\alpha(t_f) = \lambda_\mu(t_f) = 0$

(5.18) $\lambda_\chi(t_f) = \lambda_0 \geq 1$

Since $\dot{\lambda}_\chi = 0$, (5.18) tells us that λ_χ will maintain a constant value over the entire problem duration.

The conditions described above apply only over arcs where the aircraft is not constrained in any state variable and where the variational-Hamiltonian is *regular*. In the present case the Hamiltonian will be regular if $H_{uu} > 0$, and this requires that at least one of the co-states, λ_α and λ_μ, must be non-zero. If λ_α and λ_μ both vanish identically on an interval then, from (5.14) and (5.15), we have;

$$\begin{bmatrix} n' \cos\mu & n' \sin\mu/\cos\gamma \\ -\sin\mu & \cos\mu/\cos\gamma \end{bmatrix} \begin{bmatrix} \lambda_\gamma \\ \lambda_\chi \end{bmatrix} = \begin{bmatrix} 0 \\ 0 \end{bmatrix}$$

The homogeneous linear system will have a non-zero solution only if the determinant is zero. Since the value of the determinant $(n'/\cos\gamma)$ is generally non-zero, the only solution is $\lambda_\gamma = \lambda_\chi = 0$. In this case all four co-states would be zero and the Minimum Principle guarantees that this won't happen (*ie* that the adjoints don't all vanish simultaneously). Hence, we are assured that the Hamiltonian will be regular. For subsequent discussions we shall refer to the extremal structure given by conditions (5.12)-(5.18) as a type-A arc.

Preliminary studies with the control logic discussed above indicated that the angle-of-attack did increase and, if permitted, would exceed the bound (5.9). Note that α_{max} must be the smaller of the stall-angle, α_{stall}, and the α that yields $n(\alpha) = n_{max}$. From equation (5.5) it is clear that there is a value of the dynamic pressure such that

$$\frac{\bar{q}}{W/S} C_L(\alpha_{stall}) = n_{max}$$

This critical value of dynamic pressure implies a critical value of velocity - the so-called *corner velocity* which depends on altitude through the air density

$$\frac{1}{2}\rho(h)V_c^2 = \bar{q}_{critical}$$

For speeds in excess of the corner velocity, the angle-of-attack limit is imposed by the structural limit $(n(\alpha) \leq n_{max})$. At speeds below the corner velocity the angle-of-attack limit is imposed by the stall-angle $(\alpha \leq \alpha_{stall})$. Since speed is a fixed parameter in our problem, we can compute the appropriate limit in advance.

Since type-A arcs can lead to a violation of the constraint (5.9), it is necessary to explicitly impose this constraint. Thus we consider a type-B arc wherein (5.9) is satisfied as an equality. Following the procedure in (see [6], Chapter 3) we differentiate (5.9) with respect to time and find that the constraint on angle-of-attack is of first-order since the control q appears explicitly, *ie*;

$$\frac{dS\alpha}{dt} = \dot{\alpha} = q + \frac{g}{V}\left[\cos\gamma\cos\mu - n(\alpha_{max})\right]$$

To enforce the constraint over an interval $[t_1, t_2]$ it is sufficient to require that $S\left[\alpha(\hat{t})\right] = 0$ for some $t_1 \leq \hat{t} \leq t_2$ and that the pitch-rate control q be chosen to make $\dot{S}\alpha = 0$ over the interval. This state-control equality constraint is handled by adjoining it to the original variational-Hamiltonian as;

$$(5.19)\quad H_B = \lambda^T f + \theta\left[q + \frac{g}{V}\left(\cos\gamma\cos\mu - n(\alpha_{max})\right)\right] + \nu\left[\left(\frac{p}{p_{max}}\right)^2 + \left(\frac{q}{q_{max}}\right)^2 - 1\right]$$

where we have opted to use the natural control variables and to adjoin the elliptical constraint. Along the type-B arc we then have the following co-state equations;

$$(5.20)\quad \dot{\lambda}_\gamma = -\lambda^T\frac{\partial f}{\partial\gamma} + \theta\cdot\left(\frac{g}{V}\sin\gamma\cos\mu\right)$$

$$(5.21)\quad \dot{\lambda}_\chi = 0$$

(5.22) $$\dot{\lambda}_\alpha = -\lambda^T \frac{\partial f}{\partial \alpha} + \theta \cdot \frac{g}{V} n'$$

(5.23) $$\dot{\lambda}_\mu = -\lambda^T \frac{\partial f}{\partial \mu} + \theta \cdot \left(\frac{g}{V} \sin\mu \cos\gamma \right)$$

Due to the state constraint, we must also rethink our condition of optimality. Along the constrained arc the control dependent Hamiltonian takes the following form;

$$H_{Bco} = (\lambda_\alpha + \theta) \cdot q + \frac{\lambda_\mu}{\cos \alpha_{max}} \cdot p + \nu \left[\left(\frac{p}{p_{max}} \right)^2 + \left(\frac{q}{q_{max}} \right)^2 - 1 \right]$$

The $\min - H$ operation applied to this expression yields four conditions of stationarity along the type-B arc;

(5.24) $$\frac{\partial H_B}{\partial p} = \frac{\lambda_\mu}{\cos \alpha_{max}} + 2\nu \frac{p}{p^2_{max}} = 0$$

(5.25) $$\frac{\partial H_B}{\partial q} = (\lambda_\alpha + \theta) + 2\nu \frac{q}{q^2_{max}} = 0$$

(5.26) $$\dot{S}_\alpha = q + \frac{g}{V} \left[\cos\gamma \cos\mu - n(\alpha_{max}) \right] = 0$$

(5.27) $$\left(\frac{p}{p_{max}} \right)^2 + \left(\frac{q}{q_{max}} \right)^2 - 1 = 0$$

These equations are to be solved for p, q, ν, and θ for given λ_α, λ_μ, μ and γ (α_{max}, p_{max}, q_{max}, g and V are fixed parameters). From the structure of these equations it is clear that the pitch-rate is computed from (5.26) and the roll-rate (up to its sign) follows from (5.27).

From (5.24) and (5.25) we then find that;

$$v = -\frac{p^2{}_{max}\,\lambda_\mu}{2p\cos\alpha_{max}} \qquad \text{and} \qquad (\lambda_\alpha + \theta) = -\frac{2vq}{q^2{}_{max}} = \frac{\lambda_\mu}{\cos\alpha_{max}}\frac{p^2{}_{max}}{q^2{}_{max}}\frac{q}{p}$$

While the choice for q, dictated by (5.26) above, will ensure that $S\alpha$ is constant along the arc, we must also impose a "tangency" condition to be sure that the value of $S\alpha$ will be zero. This "interior point" condition

$$S\alpha\left[\alpha(t_1)\right] = \alpha(t_1) - \alpha_{max} = 0$$

leads to a "jump condition" for the co-states. The general jump conditions are given by (see [6], Chapter 3);

$$\lambda^T(t_1^-) = \lambda^T(t_1^+) + \pi\frac{\partial S\alpha}{\partial x(t_1)}$$

$$H(t_1^-) = H(t_1^+) - \pi\frac{\partial S\alpha}{\partial t_1}$$

If one carries out the operations in these equations, the results reveal that the only co-state which may experience a jump is λ_α, specifically we have;

(5.28) $\lambda_\gamma(t_1^-) = \lambda_\gamma(t_1^+)$

(5.29) $\lambda_\chi(t_1^-) = \lambda_\chi(t_1^+)$

(5.30) $\lambda_\alpha(t_1^-) = \lambda_\alpha(t_1^+) + \pi$

(5.31) $\lambda_\mu(t_1^-) = \lambda_\mu(t_1^+)$

(5.32) $H(t_1^-) = H(t_1^+)$

where t_1 is the time at which the constrained arc begins. Equations (5.20)-(5.32) are the necessary conditions which are required for a type-B arc to be optimizing.

As in the case of the type-A arc, we are required to examine the regularity of the Hamiltonian for the type-B arc. From the conditions (5.24)-(5.27) we note that if the elliptical control bound is inactive then we have $\nu = 0$ and hence

(5.33) $\lambda_\mu = 0$

(5.34) $(\lambda_\alpha + \theta) = 0$

are required conditions of stationarity, *ie* conditions which lead to $H_u = 0$. In this case the variational-Hamiltonian does not depend on either of the controls and the matrix H_{uu} is therefore singular. Accordingly, extremal arcs over which such a condition occurs are called *singular arcs* (see [6], Chapter 8). We shall refer to the singular arc in our problem as a type-C arc. In order to maintain the singular condition for a finite period of time we note that;

(5.35) $\dot{\lambda}_\mu(t) = 0$

With conditions (5.33)-(5.35) the co-state equation for λ_μ becomes a constant along this type-C arc. From equation (5.23) and the conditions listed above we have;

$$\lambda_\gamma \cos\gamma = \lambda_\chi \frac{\cos\mu}{\sin\mu}$$

This expression effectively amounts to a constraint on either the bank-angle or the path-angle. Physically, this corresponds to the case wherein the dynamics are represented by the point-mass model and the bank-angle is a control. In fact, the constraint above corresponds exactly with the optimal bank-angle control for the point-mass solution to our flight problem (see equation D.12). In a manner which is similar to the treatment of the state constraint on angle-of-attack, we may

now take time derivatives of the equation above to obtain an expression for the control p. The first time derivative yields;

$$-\dot{\lambda}_\gamma \cos\gamma + \dot{\gamma}\sin\gamma\,\lambda_\gamma = -\lambda_\chi \frac{\dot{\mu}}{\sin^2\mu}$$

Since $\dot{\mu} = f(p)$ we see that the singular arc is of first-order. Substitution of equations (5.1), (5.4) and (5.20) into this expression, along with conditions (5.33)-(5.35), results in the desired expression for the control p along the singular arc. Omitting the details of the algebraic manipulation, the final result is;

$$(5.36)\quad p(t) = -\frac{g}{V}\sin\mu(t)\cos\gamma(t)\sin\alpha_{max}$$

Note that the control q will continue to be specified by equation (5.26) along the type-C arc since the state constraint on angle-of-attack is still active. Equations (5.20)-(5.23), (5.26), (5.33), (5.34) and (5.36) constitute the required necessary conditions for the constrained-singular arc.

In summary we see that three distinctive arc-types exist for our optimal control problem when employing the body-rate dynamics model. Other types of models would of course yield different arc structures, for instance the point-mass model requires only a single unconstrained, non-singular arc (see Appendix D). As we shall see in the following section, the sequence of the arcs in the *BRM* problem is not fixed and instead depends on the corner-velocity condition discussed above.

5.3: Numerical Results

In this section we solve our flight problem for each of the cases of α_{stall}-limited and g-limited flight and examine the effect of the maximum available body-rates on the transient lag metrics which were first discussed in Section 5.1. For the numerical solutions to the optimal control problem we chose to fly our maneuver at 5000 feet altitude and to impose a g-limit of $n_{max} = 6$. The aircraft lift data for the problem is depicted in Figure 5.2 from which we obtain

$C_{L_{max}} = 1.673$ at $\alpha_{stall} = 35.4^{\circ}$. These conditions result in a corner-velocity of 540 ft/s (Mach 0.49) at the indicated altitude. The effect of Mach number on the function $n(\alpha)$, equation (5.5), at 5000 ft is depicted in Figure 5.5. From this data we may compute the maximum allowable angle-of-attack as a function of Mach number, the results of this computation are displayed in Figure 5.6.

The explicit arc structure for the situation where the aircraft is α_{stall}-limited (*ie* at Mach numbers less than 0.49) is shown in Figure 5.7. Note that in this case there is no type-B arc and the problem transitions directly from the type-A arc (unconstrained/non-singular) to the type-C arc (constrained/singular). For the numerical solution to this 2-arc Multi-Point Boundary Value Problem (MPBVP) a non-linear Newton problem was set-up wherein we performed the integration backwards and forwards from the start of the singular arc at switch-time, t_s. A 7th-8th order variable-step Runge-Kutta scheme was used to integrate the states and co-states. The unknowns (parameters) in this problem consisted of the state values at the switch-time, $\gamma(t_s), \alpha(t_s)$ and $\mu(t_s)$, the value of λ_α at the switch-time and the switch-time itself. The corresponding boundary conditions are:

1. $\gamma(t_0) = 0$ (specified by initial-time boundary conditions)
2. $\alpha(t_0) = \alpha_0$ (specified by initial-time boundary conditions)
3. $\mu(t_0) = 0$ (specified by initial-time boundary conditions)
4. $C_{L\alpha}(t_s) = 0$ (lift-curve slope zero at start of singular arc in α_{stall}-limited case)
5. $\lambda_\gamma(t_f) = 0$ (specified by transversality condition)

One may also note that in addition to these conditions the problem admits the first integral $H(t) =$ constant. We employed this integral as a check for numerical accuracy requiring that the Hamiltonian be constant to within 7 digits before accepting a solution as valid.

The problem described above was solved for a variety of flight conditions over a fixed time of 2.0 seconds. This flight duration proved to be amply sufficient to display all of the interesting dynamics in the problem while allowing us to reasonably maintain our simplifications of constant velocity and atmospheric properties. The optimal control history which was produced at an α_{stall}-limited, Mach 0.3 flight condition is shown in Figure 5.8. Note that the problem goes singular at approximately 0.9 seconds into the maneuver when the controls are no longer

extremal. One may also notice that the optimal control program increases pitch-rate to its maximum value while decreasing roll-rate. For this flight condition then, we see that pitch-rate capabilities play an important role in quickly changing the aircraft heading. In Figure 5.9 we have plotted the state histories which result from integrating the state-rate equations with the optimal control program shown in Figure 5.8. Note that the angle-of-attack reaches its stall-limit of 35.4° at the point where arc C begins. Similarly, the aircraft quickly achieves a bank-angle of over 90° by the beginning of the singular arc and ends the maneuver at $\mu = 90^{\circ}$. It is also interesting to note that the path-angle initially increases, due to the positive pitch-rate, and then goes slightly negative by the end of the problem, due to the large bank-angle. Finally, one will notice that the heading-angle does indeed vary smoothly with the *BRM* model. The co-state histories are plotted in Figure 5.10, note that all three multipliers end up at zero at the end of the maneuver (recall that $\lambda_{\chi} = 1$ throughout the maneuver) as required by the transversality conditions. One will also notice that not only λ_{μ}, but also λ_{α}, identically vanish at the start of the constrained, singular arc. While this was required for λ_{μ}, we only required that the sum $(\lambda_{\alpha} + \theta) = 0$. This result therefore indicates that both λ_{α} and θ go to zero at the same time at the entrance to the singular arc.

In Figure 5.11 we define two *integral agility metrics* based on the notions of the *BRM* transient lags which were discussed in Section 5.1. In this figure heading-lag is defined as the steady-state difference in the heading-angle achieved via a point-mass simulation and that achieved via the *BRM* simulation. Similarly, time-lag is defined as the difference in time taken to achieve a specific heading-angle. These measurements may be taken any time after the transient dynamics have settled. In Figures 5.12 and 5.13 we apply these agility metrics to the results of several optimal control problems wherein the maximum available pitch and roll-rate have been parameterized and the respective heading and time lags have been measured and displayed. As noted in the discussions on the optimal control for the sample problem above, we see that the results seem to indicate a stronger dependence on the pitch-rate bound, q_{max}, than on the roll-rate bound, p_{max}. Apparently at this flight condition the vehicle's agility is more limited by its ability to increase the load-factor than by its ability to re-direct the lift by rolling. Recall that because we have solved an optimal control problem, we are coordinating the two motions in such a way as to produce the fastest possible heading change. The results shown in Figures 5.12-5.13 show, not surprisingly, that agility increases as maximum available body-rate is increased, however, the effect is not linear and we see that the marginal effectiveness of increasing either pitch-rate or roll-rate does decrease with increasing rates. This type of information could prove

useful to aircraft designers who are attempting to meet agility requirements, subject to control effectiveness constraints, since it may identify the point at which the agility payoff is not worth the cost of increased control effectiveness.

The explicit arc structure for the situation where the aircraft is g-limited (*ie* at Mach numbers greater than 0.49) is shown in Figure 5.14. In this case we see that all three of the arc-types discussed in Section 5.2 appear. We solved this 3-arc problem in a manner similar to the previous one except that here the direction of integration is direct from t_0 to t_f. The unknowns (parameters) in the problem are the initial values of the multipliers, $[\lambda_\gamma(t_0), \lambda_\alpha(t_0), \lambda_\mu(t_0)]$, and the switch times corresponding to the start of arcs B and C, t_c and t_s respectively. The boundary conditions are:

1. $\alpha(t_c) = \alpha_{max}$ (start of state-constrained arc)
2. $H(t_c^-) = H(t_c^+)$ (Hamiltonian must be continuous)
3. $\lambda_\mu(t_s) = 0$ (start of singular arc)
4. $\dot{\lambda}_\mu(t_s) = 0$ (λ_μ must smoothly go to zero at start of singular arc)
5. $\lambda_\gamma(t_f) = 0$ (specified by transversality condition)

As was the case in the 2-arc problem, we also required that the Hamiltonian be constant, over all times, to within 7 digits in the 3-arc problem before accepting a solution as valid.

The optimal control history which was produced at a g-limited, Mach 0.7 flight condition is shown in Figure 5.15, note that the first two arcs are extremely short for this flight condition and the problem has decayed to the point-mass approximation at only 0.325 seconds into the maneuver. Results for the entire 2.0 second problem duration are not shown here since the interesting dynamics are displayed over the first two arcs. This quick arc sequence is due to the fact that the dynamic pressure is extremely high thereby allowing the aircraft to achieve a correspondingly high load-factor. As in the previous example, the optimal control initially increases the pitch-rate to close to its maximum value while decreasing roll-rate. However, this effect is not nearly so pronounced here since the aircraft can achieve a much higher load-factor at this flight condition. In fact, the control program reverses direction on the rate-trends shortly into the maneuver and ultimately calls for maximum roll-rate. The state histories for this problem

are plotted in Figure 5.16. Note that the angle-of-attack reaches its limit in only 0.2 seconds at which point arc B begins. Similarly, it only takes 0.325 seconds for the aircraft to achieve a bank-angle of approximately 90° at which point the singular arc begins. Once again, the path-angle initially increases, due to the initial positive pitch-rate, and then goes slightly negative by the end of the problem. The co-state histories are plotted in Figure 5.17, note that all three non-constant multipliers end up at zero at the end of the maneuver as required by the final-time boundary conditions. One will also notice in Figure 5.17 that λ_{μ} smoothly transitions to zero at the beginning of the singular arc (as required by the interior boundary conditions listed above), while the jump in λ_{α} is very evident at the start of the constrained, non-singular arc.

We have plotted the heading and time-lag metrics corresponding to this flight condition in Figures 5.18 and 5.19 respectively. Note that the transient lags here are significantly less than those for the low dynamic pressure case as one might expect. This is primarily due to the increase in maximum available body-rates at the higher mach number.

This concludes our presentation of results describing the utilization of the body-rate model for the assessment of aircraft agility performance characteristics. In the final chapter we will make some conclusions about our model and recommend topics for future development of the theory.

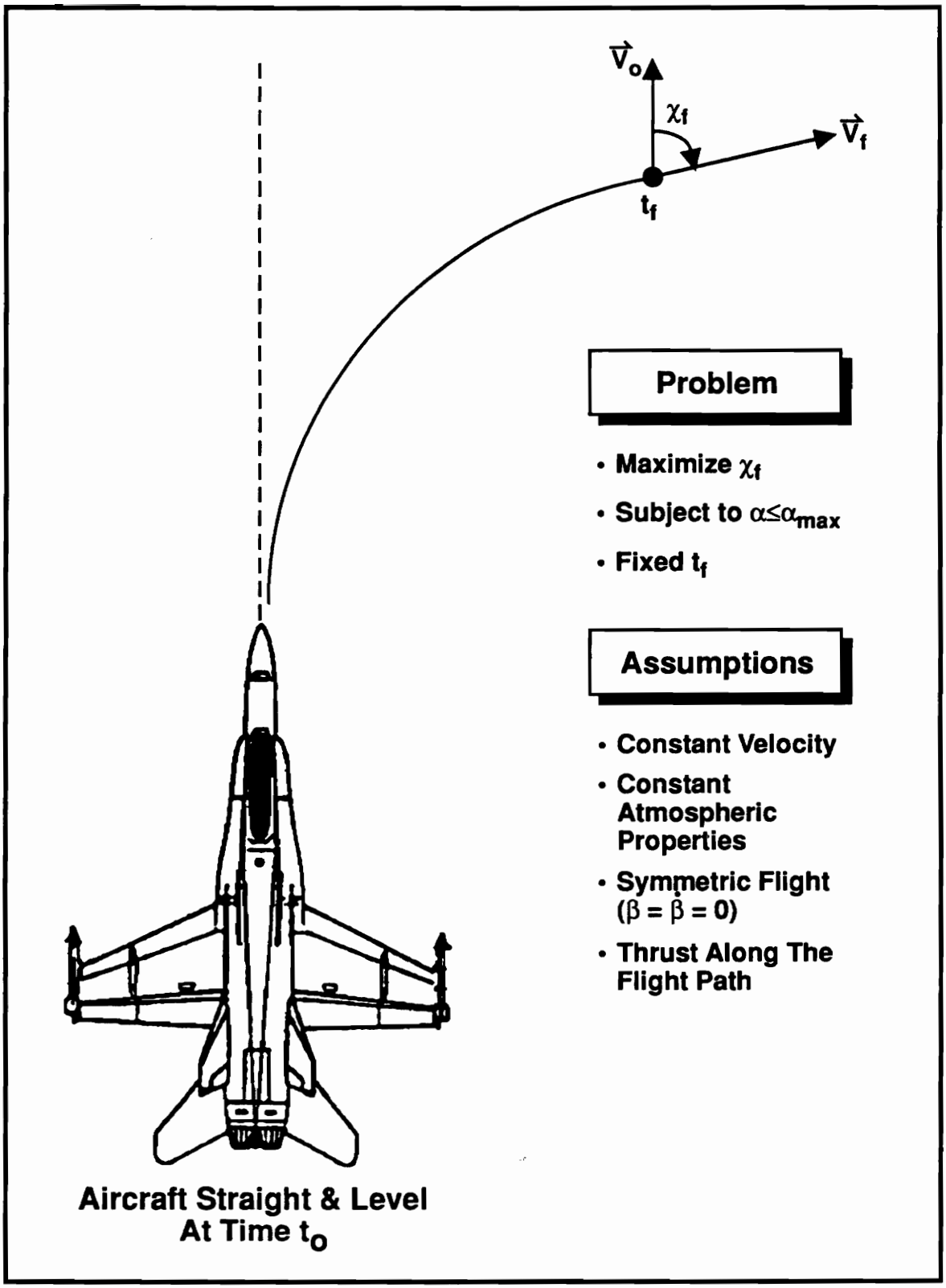

Figure 5.1 The Optimal Control Problem

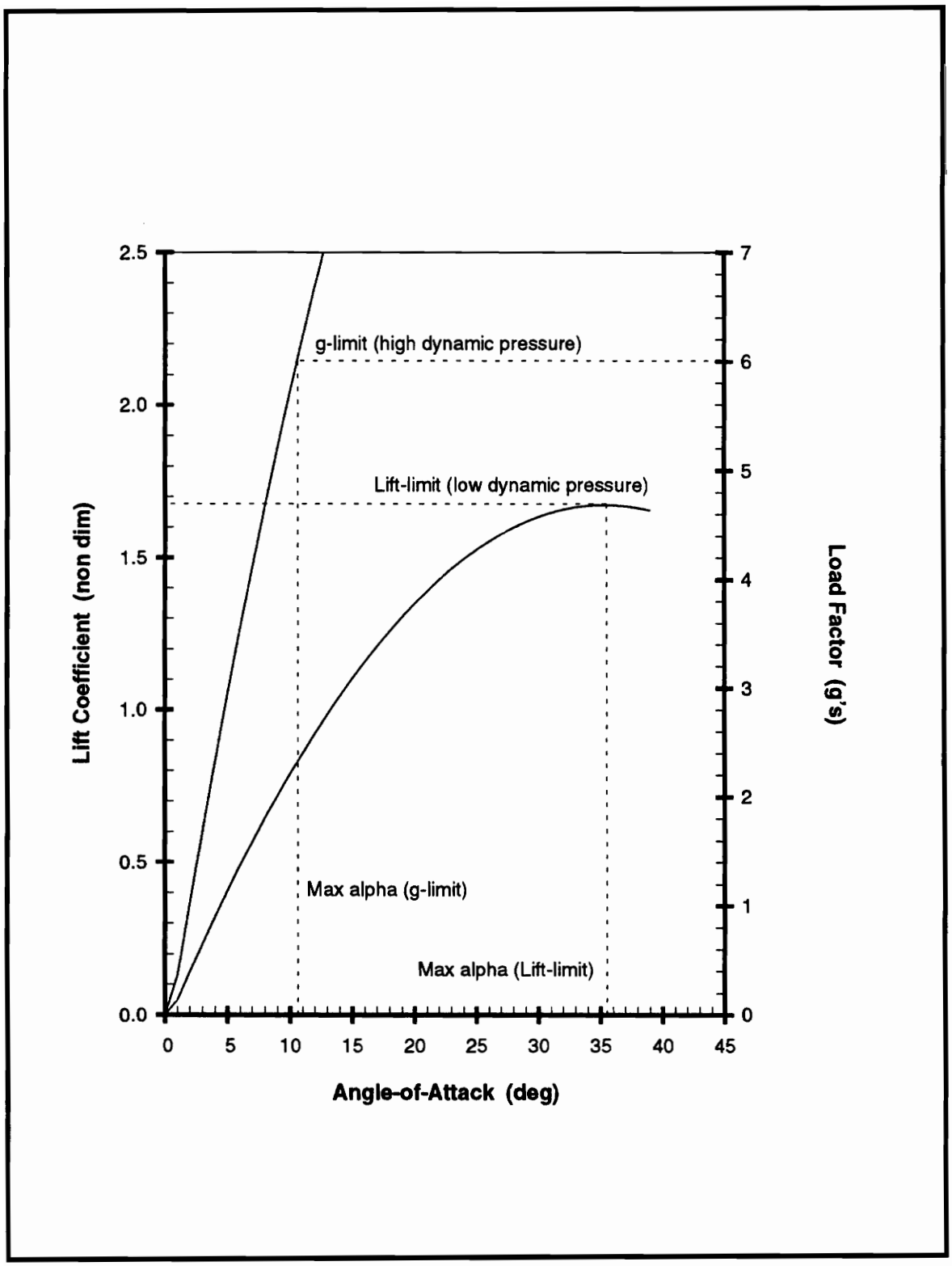

Figure 5.2. Aircraft Maneuver Limits

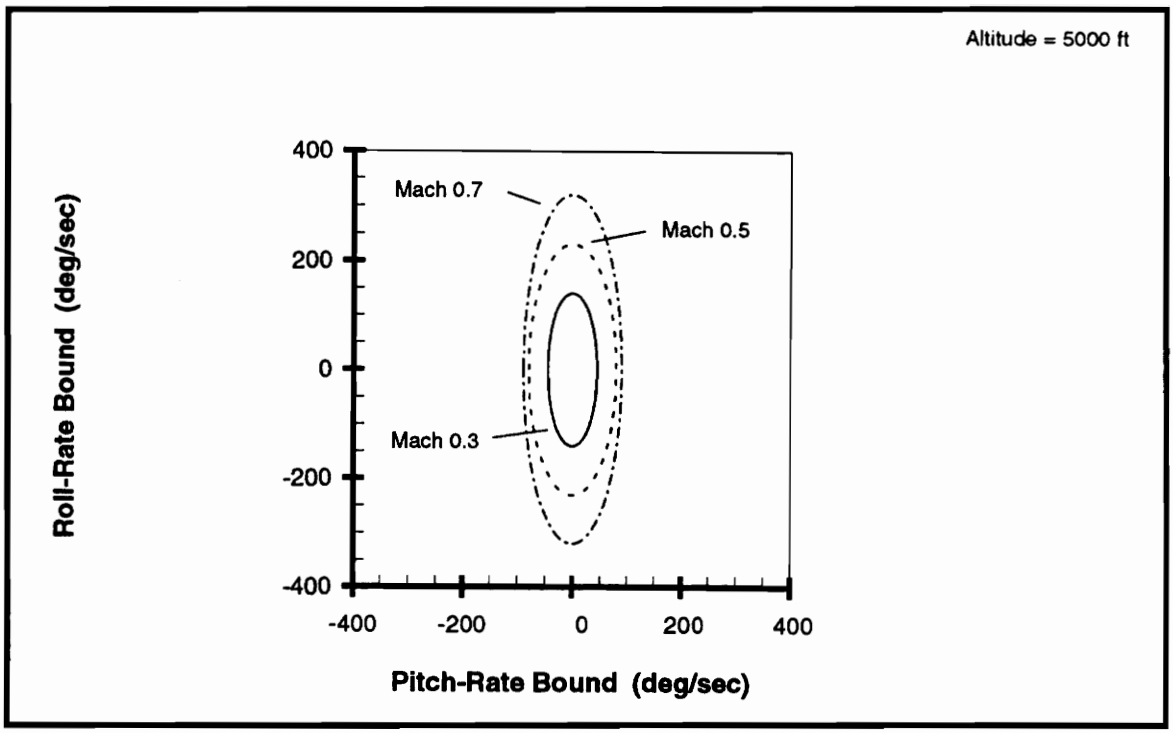

Figure 5.3. Convex Body-Rate Bounds

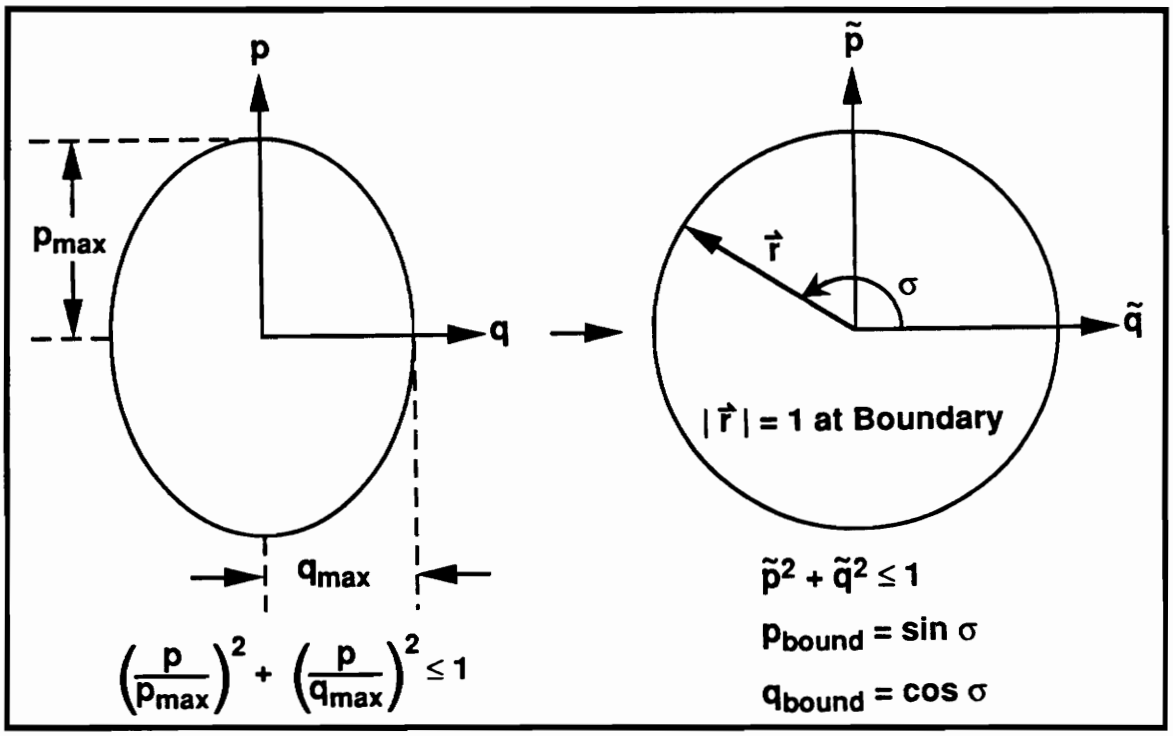

Figure 5.4. Circular Control Bounds

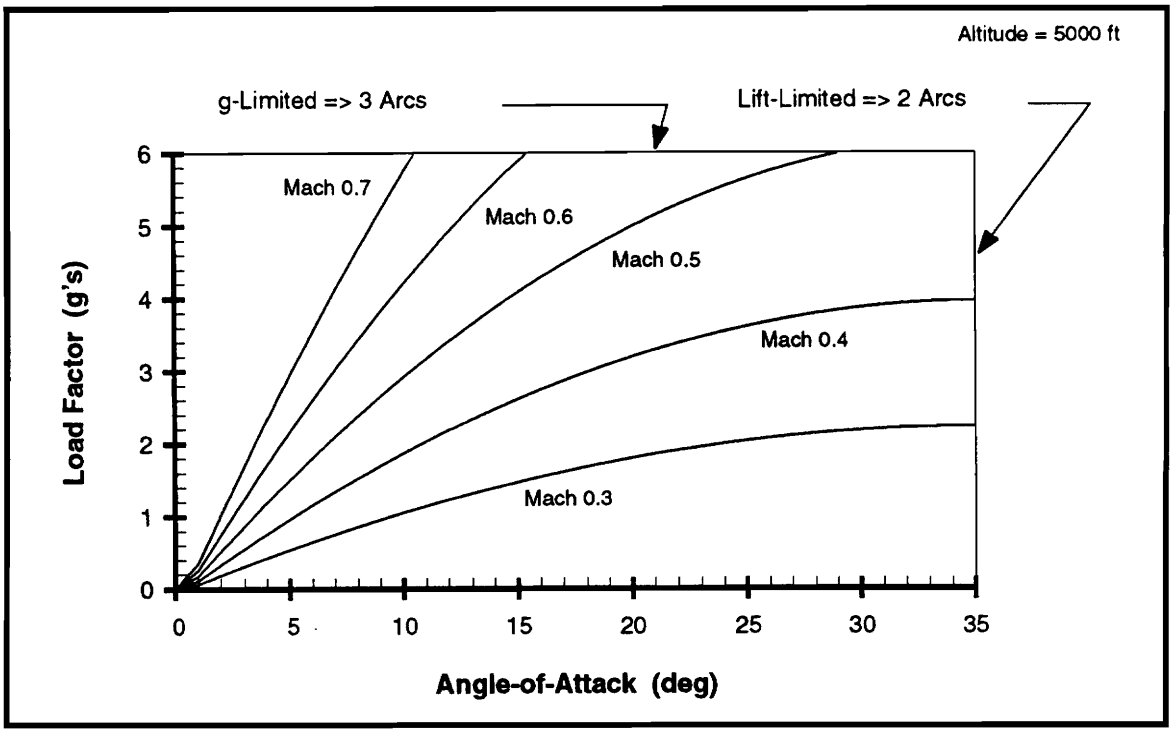

Figure 5.5. Corner-Velocity Considerations

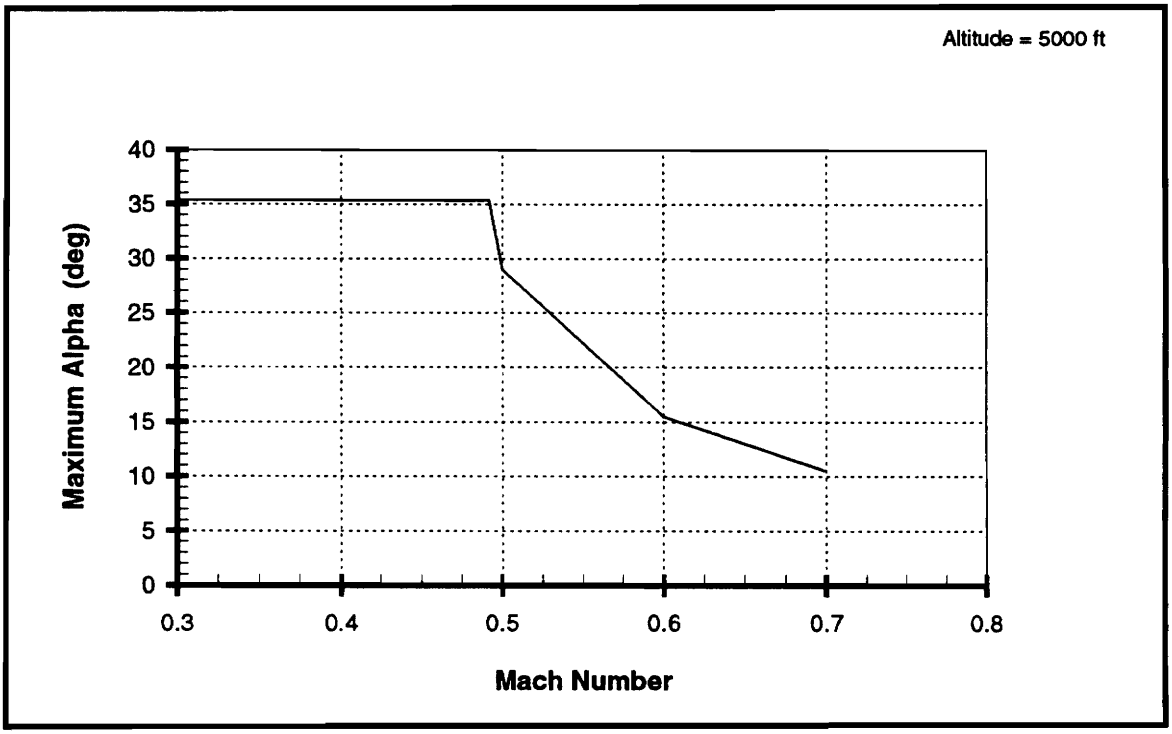

Figure 5.6. Maximum Alpha vs Mach Number

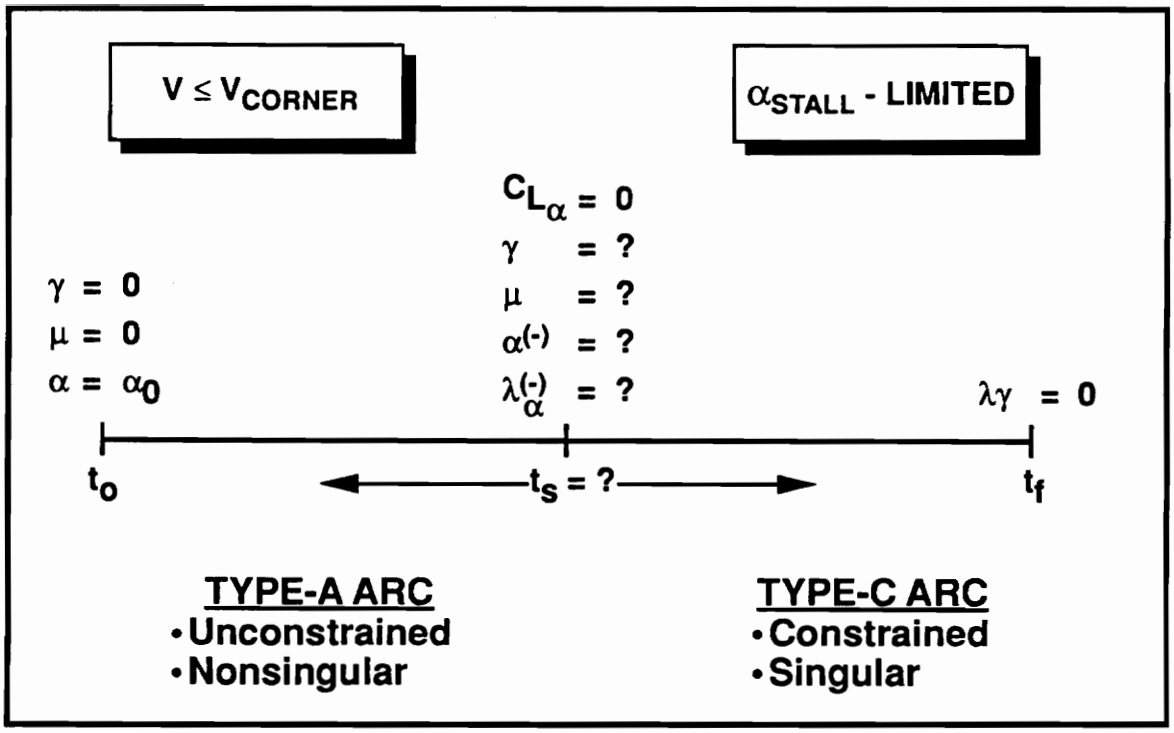

Figure 5.7. Problem Structure: 2-Arcs

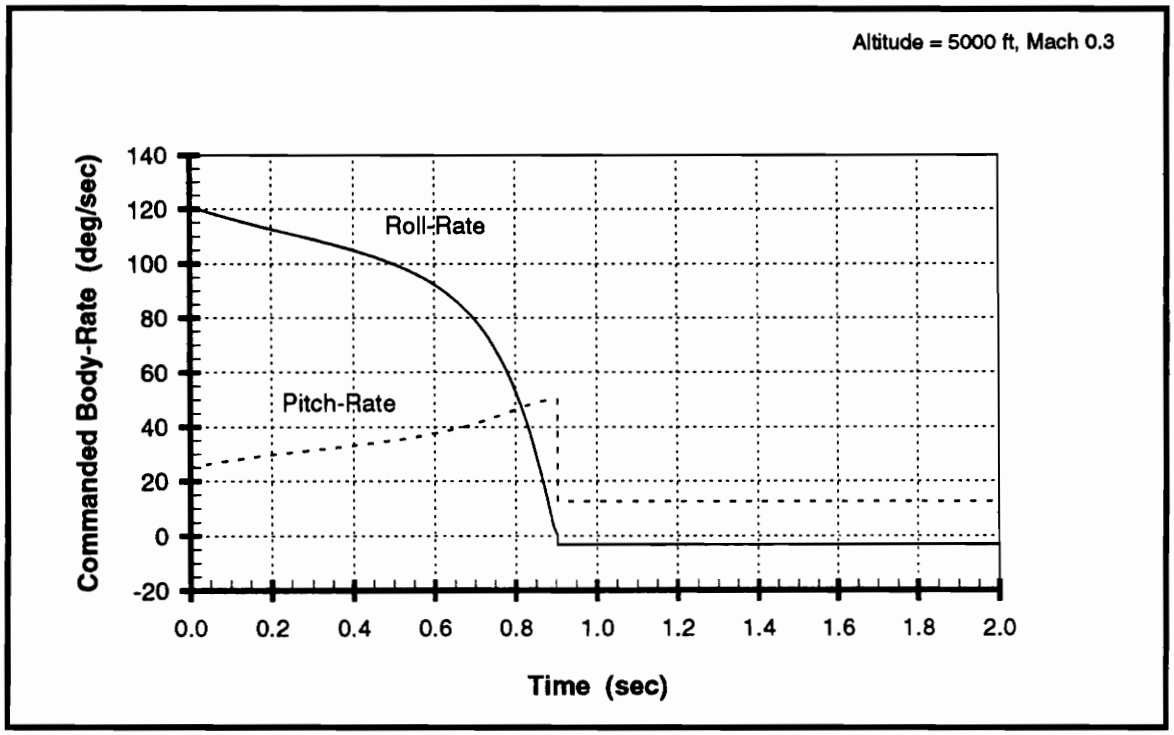

Figure 5.8. Optimal Control History: 2-Arc Example

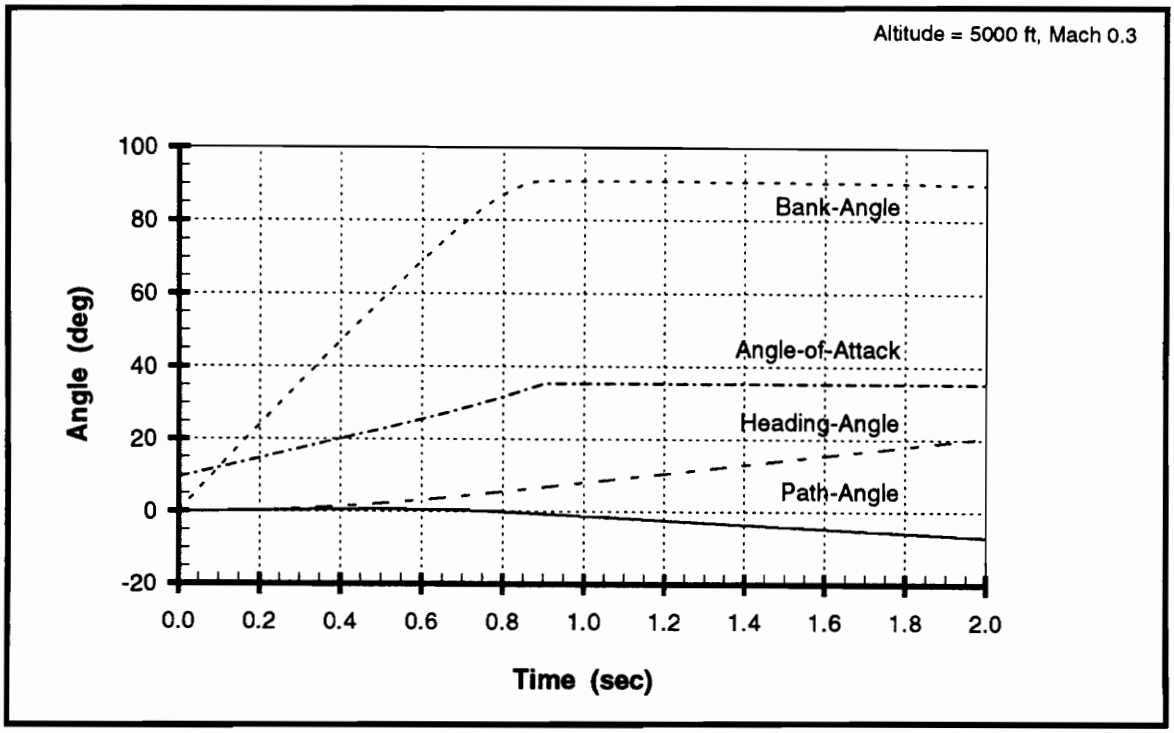

Figure 5.9. State History: 2-Arc Example

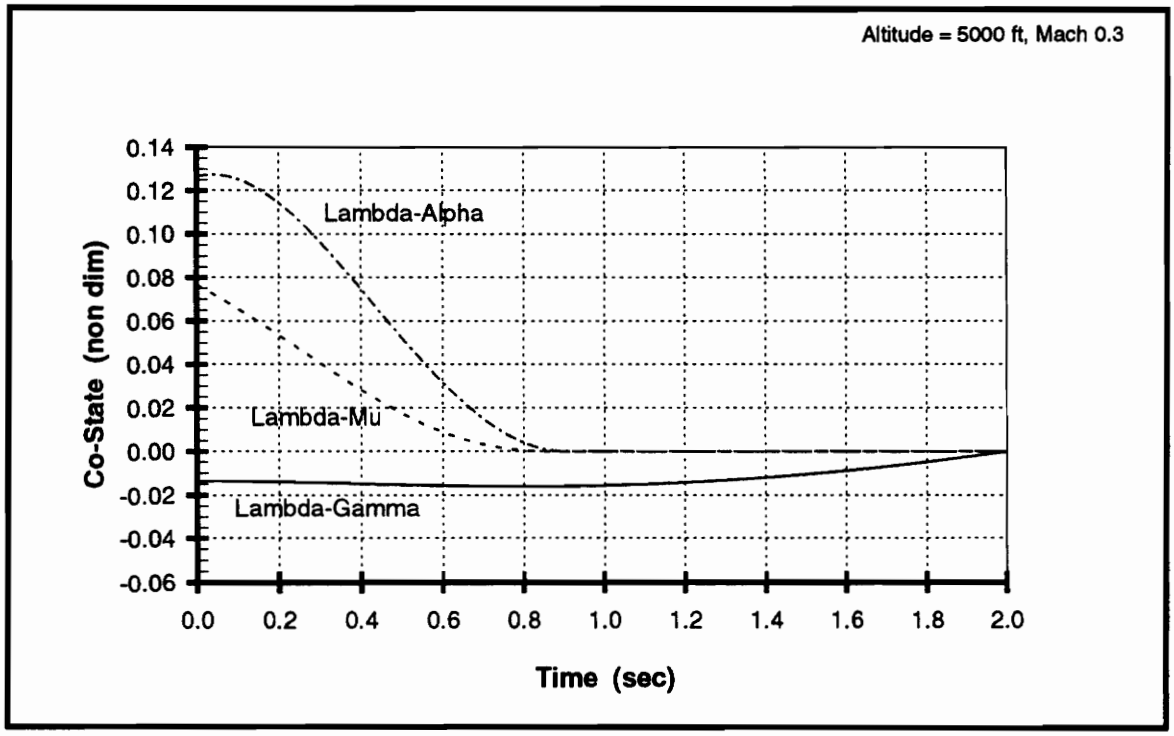

Figure 5.10. Co-State History: 2-Arc Example

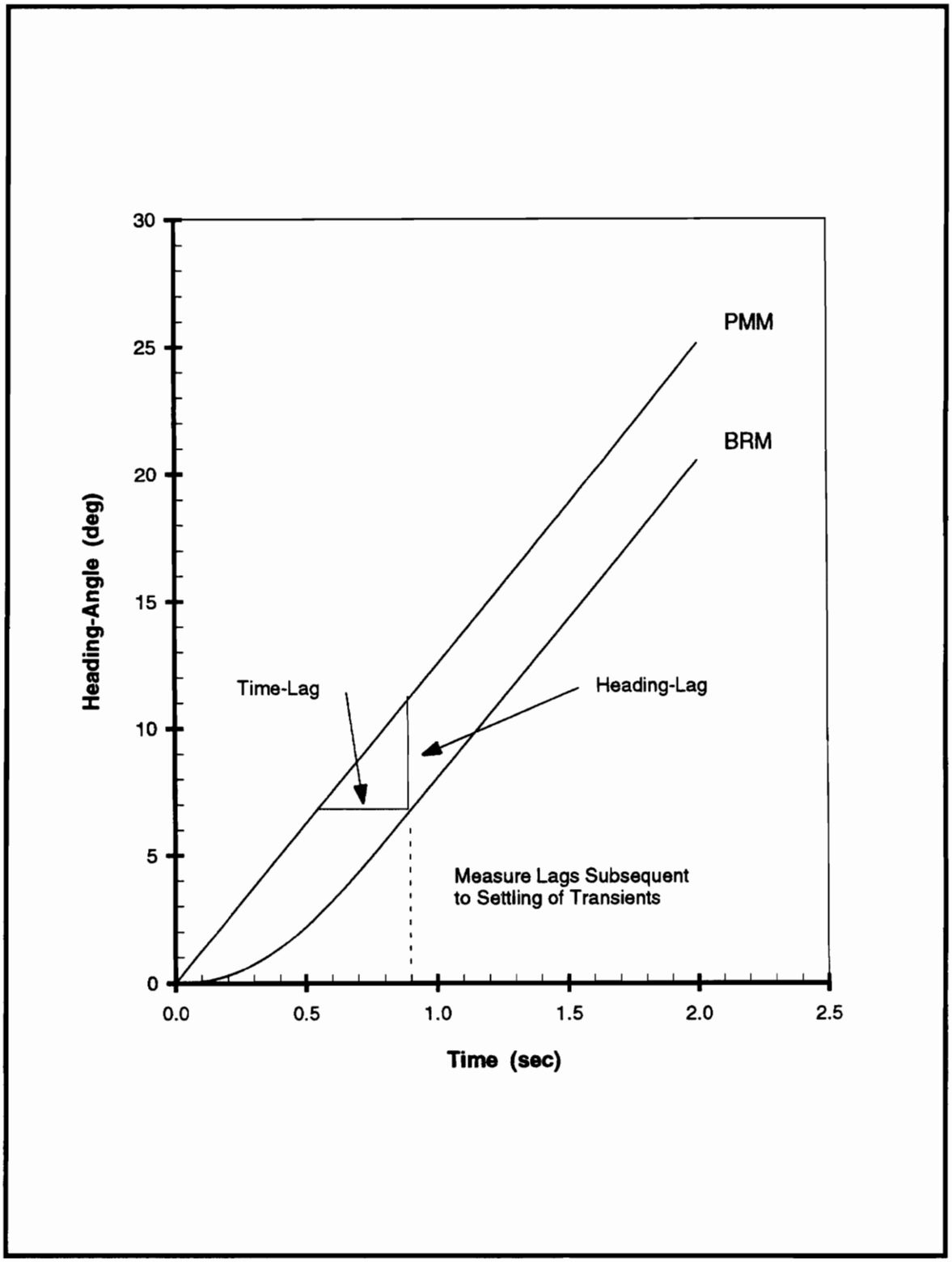

Figure 5.11. Body-Rate Model Dynamic Transients

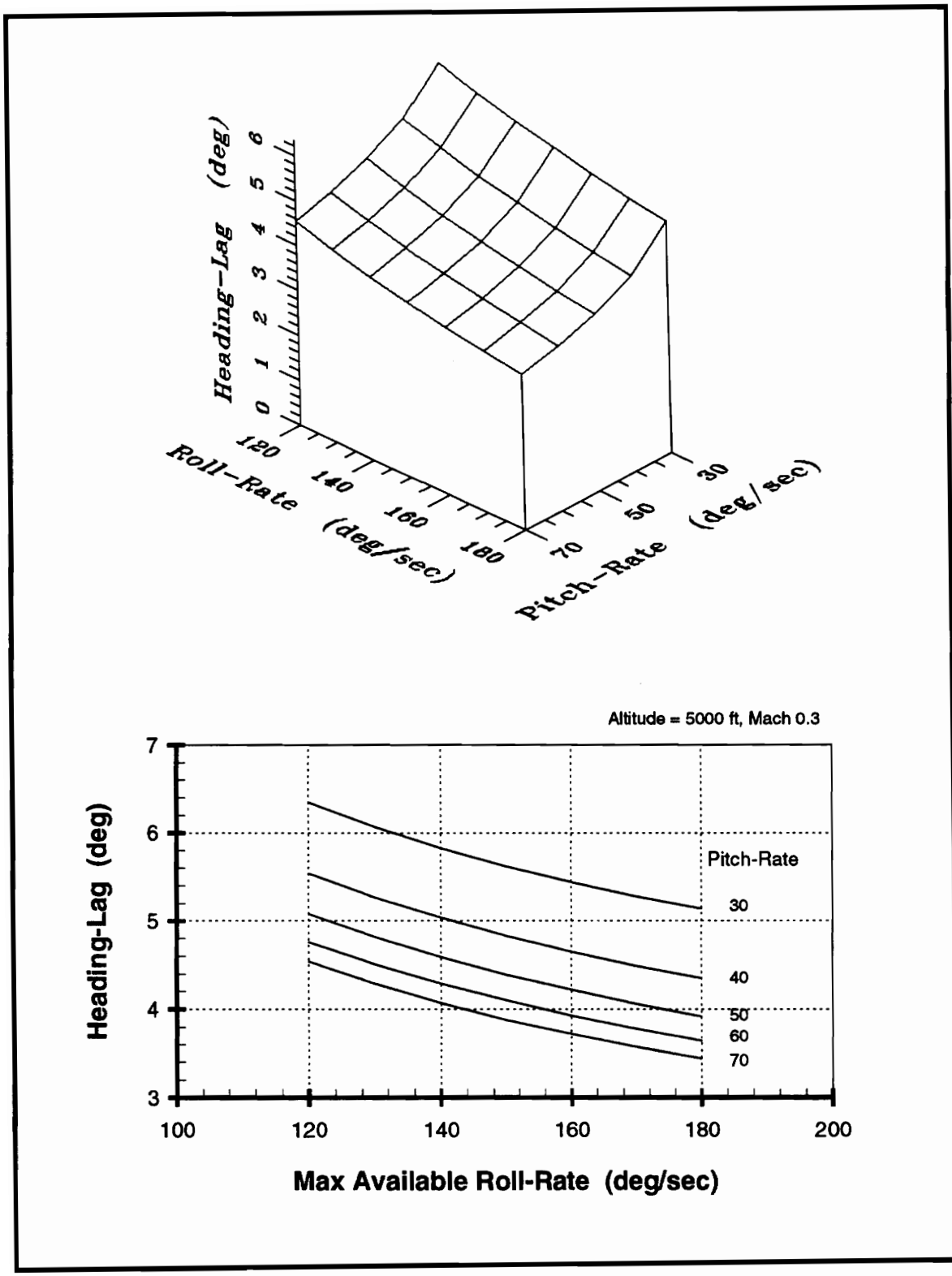

Figure 5.12. Heading Lags: 2-Arc Problem

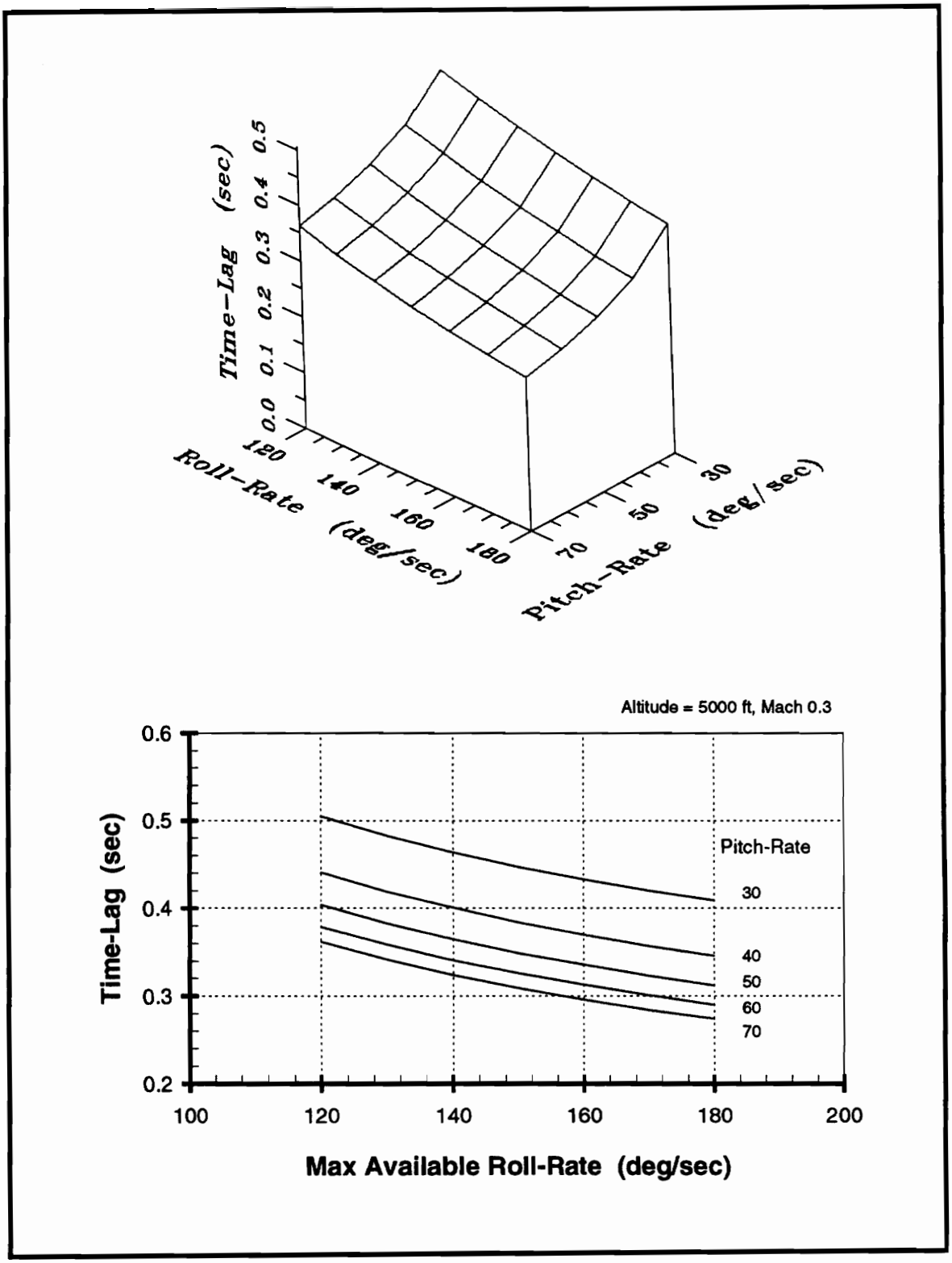

Figure 5.13. Time Lags: 2-Arc Problem

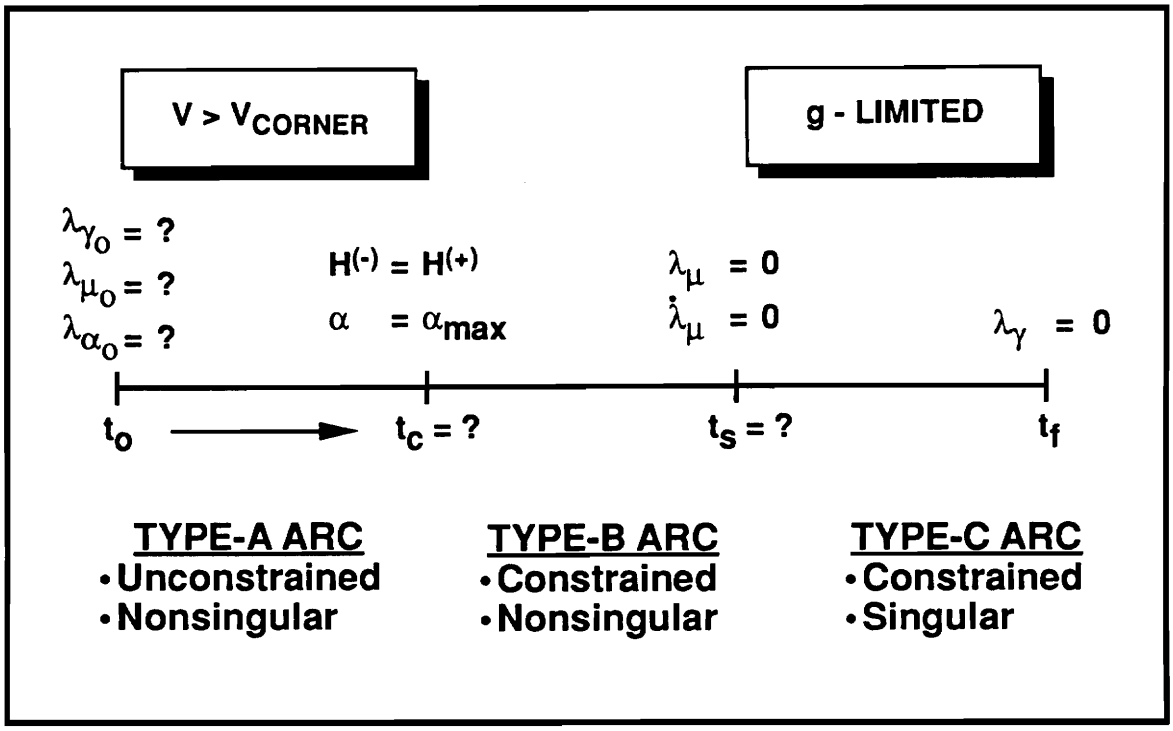

Figure 5.14. Problem Structure: 3-Arcs

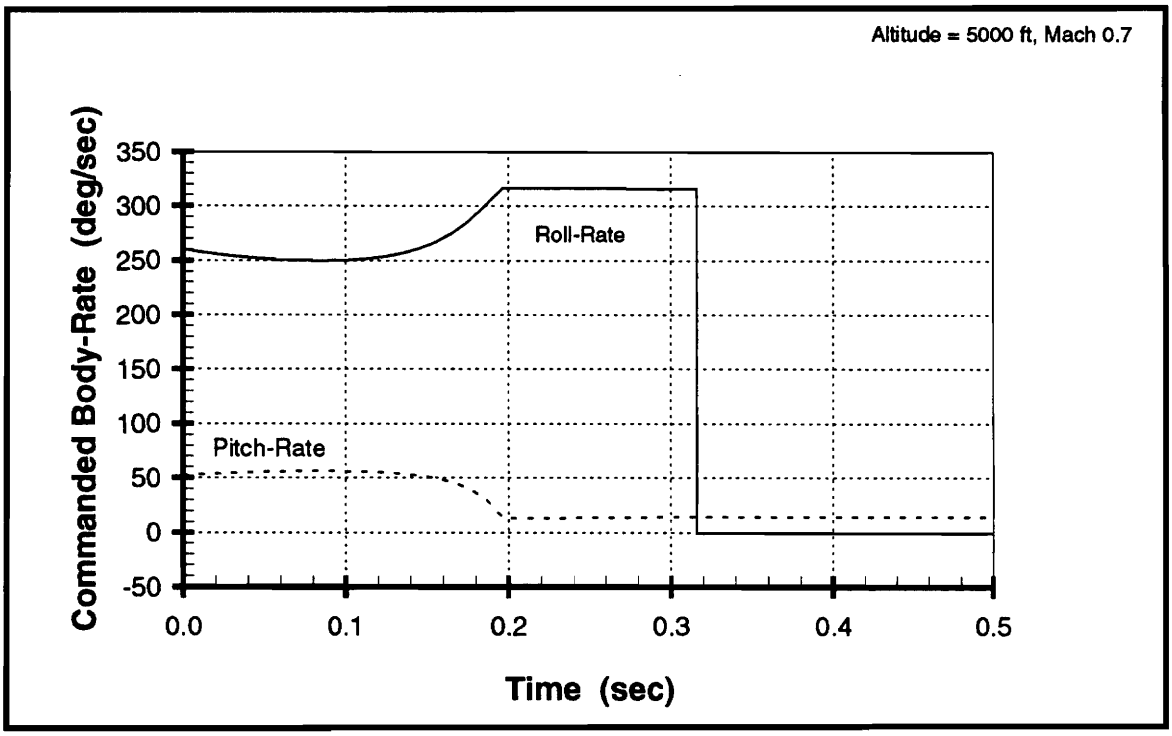

Figure 5.15. Optimal Control History: 3-Arc Example

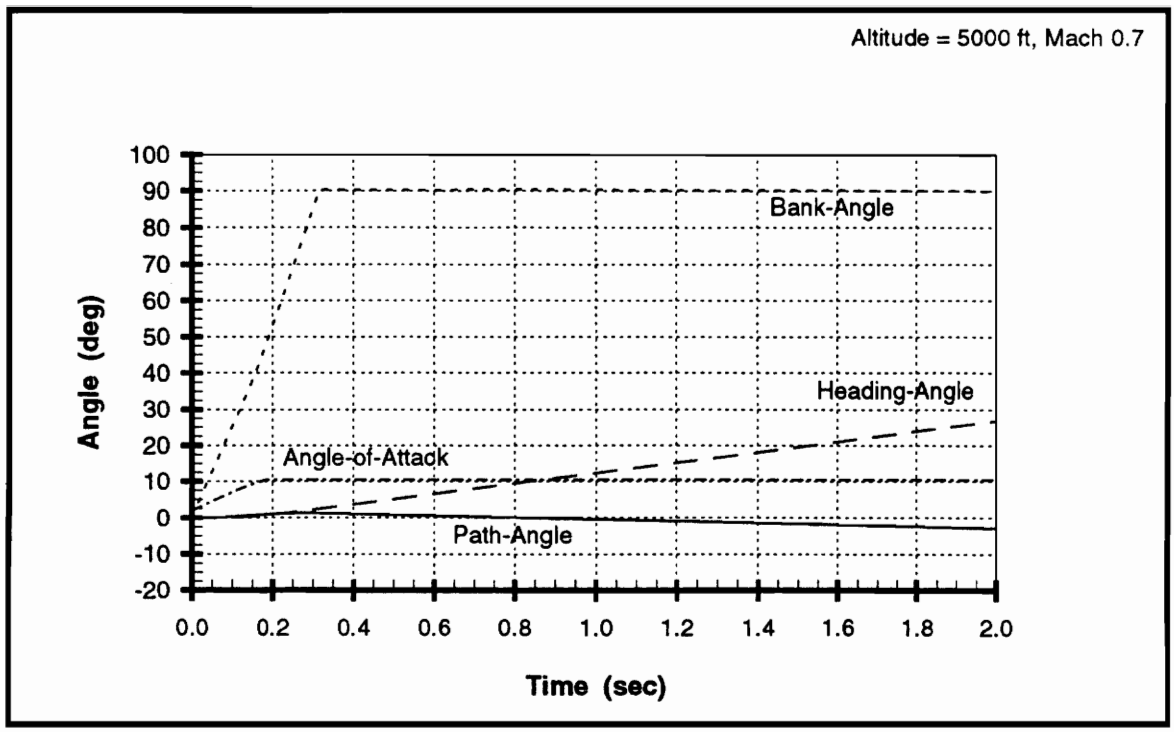

Figure 5.16. State History: 3-Arc Example

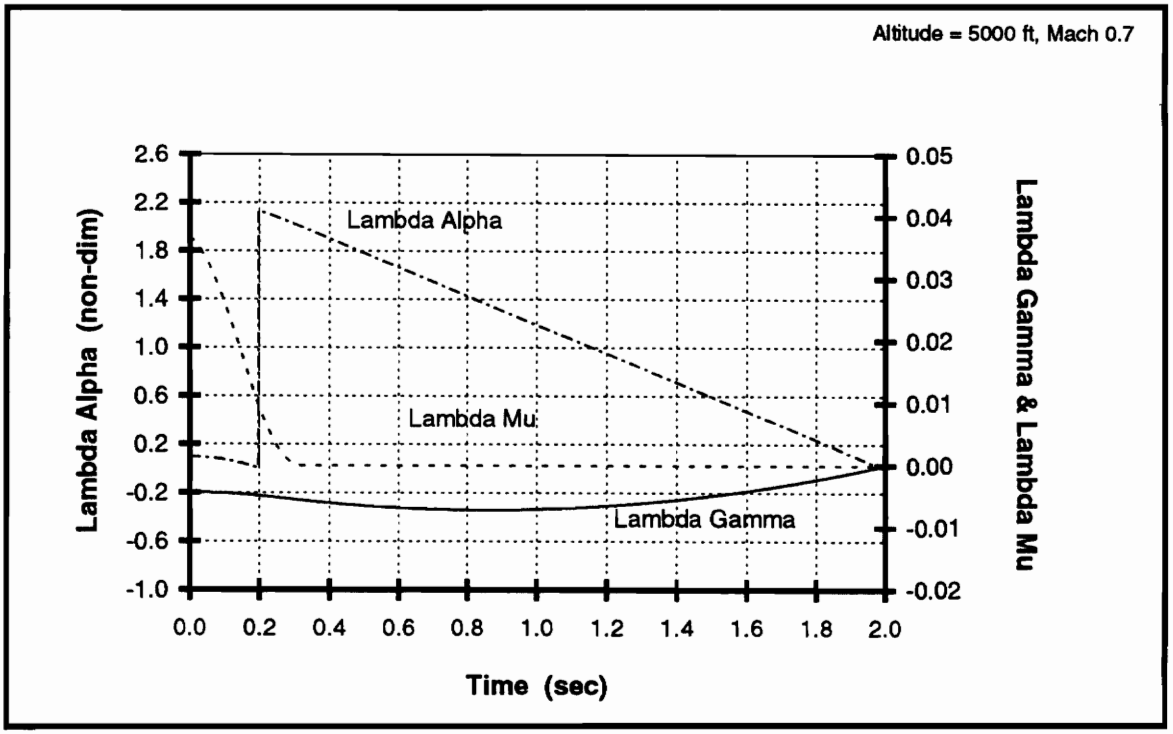

Figure 5.17. Co-State History: 3-Arc Example

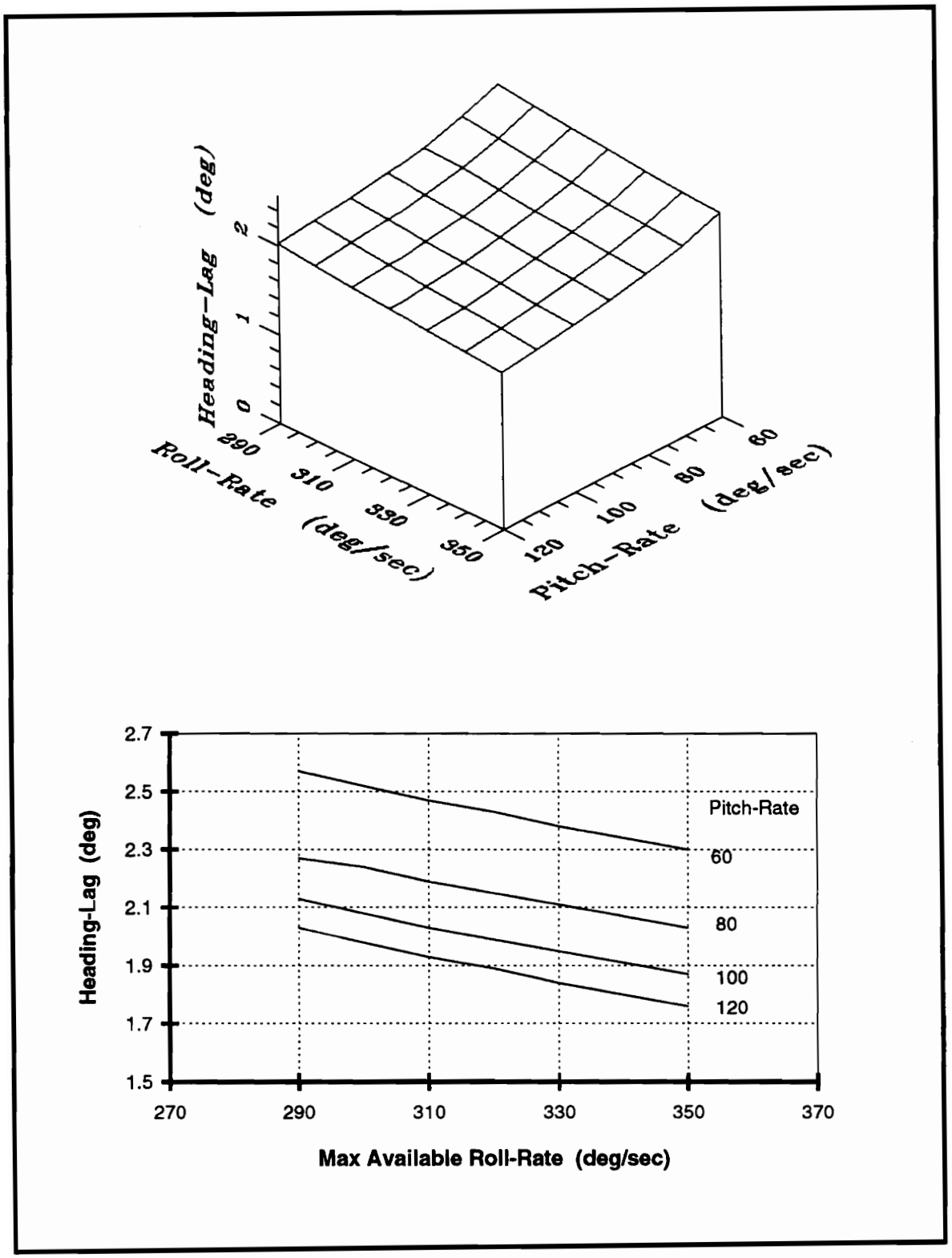

Figure 5.18. Heading Lags: 3-Arc Problem

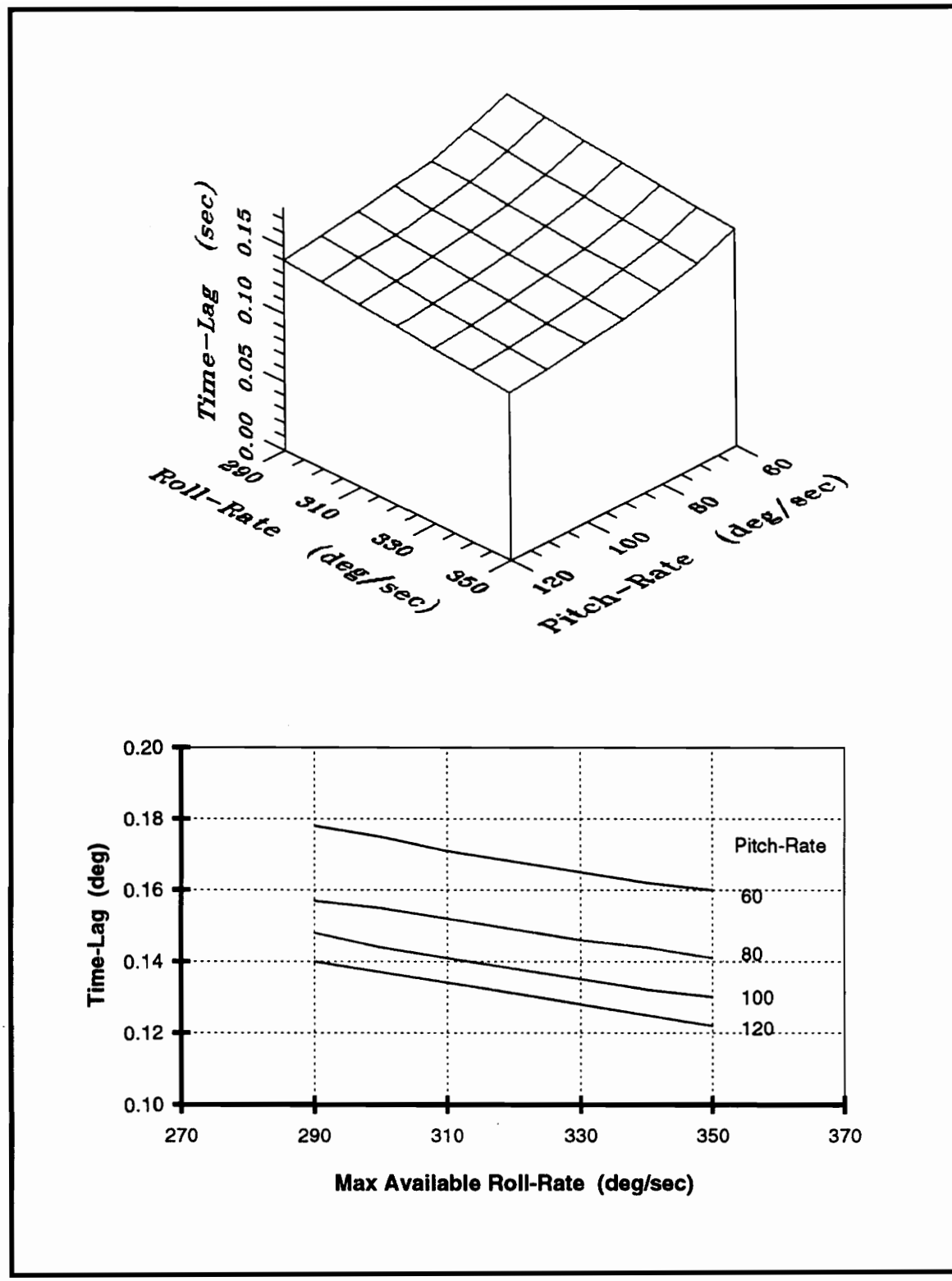

Figure 5.19. Time Lags: 3-Arc Problem

CHAPTER 6
CONCLUSIONS AND RECOMMENDATIONS

6.1: Conclusions

An agility vector has been defined as the time rate-of-change of the applied forces acting on an aircraft. Represented in wind-axes this leads to notions of axial, lateral and normal agility components. A new dynamics model, the body-rate model (*BRM*), was formulated to aid in the study of certain aspects of instantaneous and integral agile flight performance. The *BRM* employs body-rates as controls and may therefore be characterized as intermediate to the point-mass and rigid-body dynamics models. The *BRM* was utilized in the development of procedures wherein the locus of achievable agility vectors may be computed as a function of flight condition. This locus of potential agility values has been defined as an *agility set* and may be used to characterize aircraft instantaneous agility performance. It was demonstrated that the shape and orientation of agility sets depend on the aircraft aerodynamic and propulsive properties and that the bounds of these sets are directly correlated to the available aircraft control power.

An integral turning-flight problem was proposed and solved via optimal control theory. The *BRM* was utilized to model the dynamics of the problem and figures-of-merit based on the transient dynamic behavior of the *BRM* relative to the point-mass model dynamics were suggested as appropriate *agility metrics*. The extremal solutions of the flight problem were found to consist of two distinct arc structures, one for speeds above the corner-velocity and one for speeds below the corner-velocity. In both cases the problem collapses to the point-mass case along the final constrained-singular arc. It may therefore be concluded that *agility* is displayed along only the arcs preceding the singular arc. It is also of interest to note that the natural duration of the initial arcs depends on the problem data (*ie* α_0, α_{max}, $n(\alpha)$, p_{max}, q_{max}, t_f) and may therefore provide some insight into an appropriate duration for agility flight-test maneuvers. Finally, we noted that in some cases the pitch-bound is the important limitation (see Figures 5.12 and 5.13) while in others the roll-bound limits performance (see Figures 5.18 and 5.19). Different problems and different flight conditions may lead to other scenarios.

5.2: Suggestions for Future Research

An extension of the agility theory to include the effects of secondary aerodynamic controls and thrust vectoring would be of interest in terms of enhanced dynamics modeling. Continued studies of varying integral flight problems, with either the current model or an extended one, would also be of use in furthering the understanding and development of a unified theory of aircraft agility.

REFERENCES

1. Ardema, M.D., "Singular Perturbations in Flight Mechanics", NASA TM X-62,380, 1977.

2. Bilimoria, K.D., Cliff, E.M., and Kelley, H.J., "Classical and Neo-Classical Cruise-Dash", Journal of Aircraft, Volume 22, 1985, pp 555-560.

3. Bitten, R., "Qualitative and Quantitative Comparisons of Government and Industry Agility Metrics", Proceedings of AIAA Atmospheric Flight Mechanics Conference, Boston, MA, August 1989, paper AIAA-89-3389.

4. Boyd, J.N., Christie, T.P., and Gibson, J.E., "Energy Maneuverability", Armament Laboratory Reports, Volumes I and II, Eglin AFB, FL, 1966.

5. Bryson, A.E., Desai, M.N., and Hoffman, K., "Energy-State Approximation in Performance Optimization of Supersonic Aircraft", Journal of Aircraft, Volume 6, 1969, pp 481-488.

6. Bryson, A.E., Ho, Y.C., Applied Optimal Control, Revised printing, Hemisphere Publishing Corp., Washington D.C., 1975.

7. Bundick, W.T., et al, "HARV Thrust-Vectored Engine and Mixer/Predictor Simulation", NASA internal note, 27 April 1990.

8. Cannon, J., "Predicting the Victor", Proceedings of AIAA Aerospace Sciences Meeting, Reno, NV, January 1991, paper AIAA-91-0418.

9. Cliff, E.M., and Kelley, H.J., "Thrust-Vectored Energy Turns", Automatica, Volume 18, 1982, pp 559-564.

10. Contensou, P., "Conditions d'Optimalite pour les Domaines de Manoeverabilite a Frontiere Semi-affine", Lecture notes in Mathematics, Number 12, Springer-Verlag, 1970.

11. Cord, T.J., "A Standard Evaluation Maneuver Set for Agility and the Extended Flight Envelope - An Extension to HQDT", Proceedings of AIAA Guidance, Navigation & Control Conference, Boston, MA, August 1989, paper AIAA-89-3357-CP.

12. Dorn, M., "Aircraft Agility: The Science and the Opportunities", Proceedings of AIAA/AHS/ASEE Aircraft Design, Systems and Operations Conference, Seattle, WA, July 1989, paper AIAA 89-2015.

13. Etkin, B., Dynamics of Atmospheric Flight, Wiley & Sons, Inc., New York, 1972.

14. Herbst, W.B. and Kiefer, A., "Aircraft Agility", Messerschmitt-Bolkow-Blohm GMBH, Munich, Germany, Personal notes communicated to Dr. E.M. Cliff, Virginia Polytechnic Institute and State University, Blacksburg, VA, September 1989.

15. Hodgkinson J., Skow, A.M., et al, "Relationships Between Flying Qualities, Transient Agility and Operational Effectiveness of Fighter Aircraft", Proceedings of AIAA Atmospheric Flight Mechanics Conference, Minneapolis, MN, August 1988, paper AIAA-88-4329.

16. Kaiser, F., "Der Steigflug mit Strahlflugzeugen-Teil I, Bahngeschwindigkeit fur Besten Steigens", Versuchbericht 262-02-L44, Messerschmitt A.G., Augsburg, April 1944, Translated as British Ministry of Supply RPT/TIB, Translation GDC/15/148T.

17. Kalviste, J., "Measures of Merit for Aircraft Dynamic Maneuvering", Proceedings of SAE Aerospace Atlantic Meeting, Dayton, OH, April 1990, paper 901005.

18. Kelley, H.J., "Aircraft-Maneuver Optimization by Reduced-Order Approximation", in Control and Dynamic Systems, C.T. Leondes, editor, Academic Press, New York, NY, 1973.

19. Kirk, D.E., Optimal Control Theory, An Introduction, Prentice-Hall Inc., Englewood Cliffs, NJ, 1970.

20. Lee, E.B., and Markus, L., Foundations of Optimal Control Theory, reprint edition, Robert Kreiger Publishing Co., Malabar, FL, 1986.

21. Leitmann, G., The Calculus of Variations and Optimal Control, Plenum Press, New York, NY, 1981.

22. Liefer, R.K., Valasek, J., et al, "Assessment of Proposed Fighter Agility Metrics", Proceedings of AIAA Atmospheric Flight Mechanics Conference, Portland, OR, August 1990, paper AIAA-90-2807-CP.

23. Lush, K.J., "A Review of the Problem of Choosing a Climb Technique with Proposals for a New Climb Technique for High Performance Aircraft", Aeronautical Research Council Report, Memo 2557, 1951.

24. McAtee, T.P., "Agility - Its Nature and Need in the 1990s", 31st Symposium Proceedings of The Society of Experimental Test Pilots, Beverly Hills, CA, September 1987, pp 53-75.

25. Miele, A., Flight Mechanics, Volume 1, Theory of Flight Paths, Addison-Wesley Publishing Company, Inc, Reading, MA, 1962.

26. Riley, D.R., and Drajeske, M.H., "An Experimental Investigation of Torsional Agility in Air-to-Air Combat", Proceedings of AIAA Atmospheric Flight Mechanics Conference, Boston, MA, August 1989, paper AIAA-89-3388-CP.

27. Riley, D.R., and Drajeske, M.H., "Relationships Between Agility Metrics and Flying Qualities", Proceedings of SAE Aerospace Atlantic Meeting, Dayton, OH, April 1990, paper 901003.

28. Riley, D.R., and Drajeske, M.H., "An Experimental Investigation of Torsional Agility in Air-to-Air Combat", Proceedings of AIAA Atmospheric Flight Mechanics Conference, Portland, OR, August 1990, paper AIAA-90-2809-CP.

29. Rutowski, E.S., "Energy Approach to the General Aircraft Performance Problem", Journal of the Aeronautical Sciences, Volume 21 1954, pp 187-195.

30. Shankar, U.J., Cliff, E.M., and Kelley, H.J., "Aircraft Cruise-Dash Optimization: Periodic versus Steady-State Solutions", Proceedings of AIAA Guidance Navigation & Control Conference, Minneapolis, MN, August 1988, pp 917-927.

31. Skow, A.M., "Advanced Fighter Agility Metrics", Proceedings of AIAA Atmospheric Flight Mechanics Conference, Snowmass, CO, August 1985, paper AIAA-85-1779.

32. Skow, A.M., et al, "Transient Agility Enhancements for Tactical Aircraft, Volume III", Eidetics International Technical Report TR-89-001, prepared under USAF contract F33657-87-C-2045, January 1989.

33. Suwal, K.R., "Singular Arcs in Periodic Solutions to Aircraft Cruise-Dash Optimization", M.S. Thesis, Virginia Polytechnic Institute and State University, September, 1989.

34. Tamrat, B.F., "Fighter Aircraft Agility Assessment Concepts and Their Implication on Future Agile Aircraft Design", Proceedings of AIAA/AHS/ASEE Aircraft Design, Systems and Operations Meeting, Atlanta, GA, September 1988, paper AIAA-88-4400.

35. Walden, R., "Aircraft Trajectory Optimization by Curvature Control", University Paderborn, D-4790 Paderborn, Germany, 1987.

36. Wilson, D., et al, Briefing Charts, Standard Evaluation Maneuver Set Contract, Government Industry Review, Wright Laboratory, 24 July 1991.

APPENDIX A
EQUATIONS OF MOTION

Since a major portion of this study is concerned with the development of a new dynamics model for aircraft motion, *ie* the body-rate model (*BRM*), it is useful to provide the reader with the fully developed rigid-body equations of motion from which the *BRM* was derived. Accordingly, the full rigid-body, constant mass equations of motion for flight over a flat earth are presented below for the general case of thrust along the body x-axis. As mentioned in Chapter 3, there is more than one choice for state variables in a rigid-body model, for reasons described in that chapter we identified the following twelve states as best-serving the purposes of the present study of agility:

Rigid-Body States

x,y,h :	position coordinates	
V :	speed	
γ :	flight path elevation angle (velocity pitch)	
χ :	flight path heading angle (velocity yaw)	
p :	body-axis roll rate	
q :	body-axis pitch rate	(S)
r :	body-axis yaw rate	
α :	angle-of-attack	
β :	side-slip angle	
μ :	velocity bank angle (velocity roll)	

The position coordinates (x, y, h) are known as trajectory or kinematic states and the equations governing their evolution may be derived by differentiating the local horizon aircraft position vector and equating the result with the local horizon representation of the aircraft velocity vector (see Miele, p. 48). This procedure results in the following differential equations:

(A.1) $\dot{x} = V \cos\gamma \cos\chi$

(A.2) $\dot{y} = V \cos\gamma \sin\chi$

(A.3) $\dot{h} = V \sin\gamma$

which also appear exactly in this form in the *BRM*. The next three variables (V, γ, χ) are determined from the representation of the force equations (force equals time rate of change of linear momentum) on the wind-axes as described by Miele on pp. 49-50. If one solves Miele's equations for the state-rates the result is:

(A.4) $$\dot{V} = \frac{1}{m}(T \cos\alpha \cos\beta - D - mg \sin\gamma)$$

(A.5) $$\dot{\gamma} = \frac{1}{mV}\left[T(\sin\alpha \cos\mu - \cos\alpha \sin\beta \sin\mu) + L \cos\mu + Q \sin\mu - mg \cos\gamma\right]$$

(A.6)

$$\dot{\chi} = \frac{1}{mV \cos\mu \cos\gamma}\left[T\left(\cos\alpha \sin\beta + \sin\alpha \cos\mu \sin\mu - \cos\alpha \sin\beta \sin^2\mu\right) + L \cos\mu \sin\mu - Q \cos^2\mu\right]$$

For the more general case of arbitrary thrust direction, one may do as Miele has done and replace angle-of-attack and sideslip angle with the corresponding thrust attitude angles ε and ν respectively. Continuing with our list of states, we note that the state-rate equations for the body angular rates (p, q, r) are derived from the body-axis representation of the moment equations (torque equals time rate of change of angular momentum) as described in Chapter 5 of Etkin. Ignoring internal angular momentum and jet damping effects, and assuming that the body-axes are principal axes ($I_{xy} = I_{yz} = I_{xz} = 0$), leads one to the simplest form of the moment equations *ie*:

(A.7) $$\dot{p} = \frac{L + (I_y - I_z)qr}{I_x}$$

$$\dot{q} = \frac{M + (I_z - I_x)pr}{I_y} \tag{A.8}$$

$$\dot{r} = \frac{N + (I_x - I_y)pq}{I_z} \tag{A.9}$$

where L, M and N are the external aerodynamic moments, in roll, pitch and yaw respectively, and L is not to be confused with the external aerodyamic lift force. The external moments are defined in more detail in equations (4.1)-(4.6).

The final three states (α, β, μ) represent a somewhat unique choice for states in a rigid-body model. The state-rate equations for these variables will therefore be derived in greater detail than were those for the more common preceding states. In order to arrive at state-rate equations for these angles one must consider the relationships which exists among the angular velocity of the wind-axes frame (p_w, q_w, r_w), the angular velocity of the body-axes frame (p, q, r) and the velocity Euler angle-rates $(\dot{\gamma}, \dot{\chi}, \dot{\mu})$. Considering the first relationship, we note that the angular velocity of the body-axes is related to the angular velocity of the wind-axes in the following manner:

$$\vec{\omega}_b = \vec{\omega}_w + \vec{\omega}_{b/w}$$

where $\vec{\omega}_b$ is the angular velocity of the body, $\vec{\omega}_w$ is the angular velocity of the wind-axes and $\vec{\omega}_{b/w}$ is the angular velocity of the body with respect to the wind-axes. If these vectors are represented on the wind-axes one obtains the following:

$$\vec{\omega}_b = \begin{bmatrix} p\cos\alpha\cos\beta + q\sin\beta + r\sin\alpha\cos\beta \\ -p\cos\alpha\sin\beta + q\cos\beta - r\sin\alpha\sin\beta \\ -p\sin\alpha + r\cos\alpha \end{bmatrix}$$

$$\vec{\omega}_w = \begin{bmatrix} p_w \\ q_w \\ r_w \end{bmatrix} \qquad \vec{\omega}_{w/e} = \begin{bmatrix} \dot{\alpha} \sin \beta \\ \dot{\alpha} \cos \beta \\ -\dot{\beta} \end{bmatrix}$$

where we note that the quantities q_w and r_w are known for a given value of the state, since from the point-mass force equations written on the wind-axes (see Miele p. 49 eqns. 26) we have:

(A.10) $$q_w = \frac{1}{mV}(T \sin \alpha + L - mg \cos \mu \cos \gamma)$$

(A.11) $$r_w = \frac{1}{mV}(T \cos \alpha \sin \beta - Q + mg \sin \mu \cos \gamma)$$

We may therefore solve the equations $\vec{\omega}_b = \vec{\omega}_w + \vec{\omega}_{w/e}$ for the aerodynamic angular-rates $\dot{\alpha}$ and $\dot{\beta}$ and the wind-axes roll-rate p_w in terms of known values of the states. Carrying out this process yields the following equations:

(A.12) $$\dot{\alpha} = \frac{1}{\cos \beta}(-p \cos \alpha \sin \beta + q \cos \beta - r \sin \alpha \sin \beta - q_w)$$

(A.13) $$\dot{\beta} = p \sin \alpha - r \cos \alpha + r_w$$

(A.14) $$p_w = q_w \tan \beta + \frac{1}{\cos \beta}(p \cos \alpha + r \sin \alpha)$$

Finally, we derive the remaining state-rate, $\dot{\mu}$, by relating the velocity Euler angle-rates to the wind-axes angualr rates, as described by Miele on pp. 46-48 of his text, which results in the equation:

(A.15) $$\dot{\mu} = p_w + \dot{\chi} \sin \gamma$$

where $\dot{\chi}$ and p_w are provided in equations (A.6) and (A.14) respectively.

In summary, we see that the our rigid-body system is described by the twelve differential equations (A.1)-(A.9), (A.12), (A.13) and (A.15). It is these equations that form the basis of the body-rate model which is obtained by employing body-rates as controls rather than as states. The *BRM* is then further simplified in our study by the assumptions of symmetric flight ($Q = \sin\beta = 0, \cos\beta = 1$) and thrust-along-the-path. The latter of these assumptions results in the complete elimination of all terms containing either $T\sin\beta$ or $T\sin\alpha$ (independent of the symmetric flight assumption) since thrust now acts along the x-wind axis.

APPENDIX B
THE AIRCRAFT MODEL

B.1: Aerodynamic Data

The aircraft aerodynamic data used in producing the results in Chapters 4 and 5 of this study are representative of data for a current generation tactical fighter aircraft. Thanks are due to NASA Langley Research Center for providing the original data. The specific aerodynamic data which was used to solve the *BRM* moment equilibrium equations (see equations (4.1)-(4.10) and Appendix C) and subsequently produce the agility sets described in Chapter 4 are provided in Figures B.1 to B.13. The lift data used in solving the optimal control problem presented in Chapter 5 is displayed in Figure 5.2. Note that the data required to produce agility sets was not required to be smooth since the solution process here was analytic and corresponded to a single flight state. However, the lift data required for solution of the optimal control problem has been fit with piece-wise cubic functions to avoid convergence problems which are sometimes encountered in optimization problems when non-smooth data are present.

B.2: Propulsive Data

The propulsive data used in this study was also originally obtained from NASA Langley. The important data here are the aircraft thrust-rate capability, which was presented in Figures 4.7 and 4.8, and the maximum net thrust vs Mach number and altitude which is displayed in Figure B.14. In producing the agility sets described in Chapter 4, it was always assumed that the instantaneous thrust was equal to the minimum of the drag force and the maximum thrust. Since variations in velocity were neglected in the solution of the optimal control problem, thrust did not enter into that problem (see the state equations (5.1)-(5.4)) and hence no propulsive data was required.

B.3: Aircraft Physical Characteristics

The aircraft geometric and mass properties are characteristic of a current generation tactical fighter aircraft with aerodynamic and thrust properties similar to those discussed above. Data used in this study are:

$$\bar{c} = 11.52\,ft, \qquad b = 37.42\,ft, \qquad S = 400.0\,ft^2$$

$$I_x = 23000\ sl\text{-}ft^2, \qquad I_y = 151293\ sl\text{-}ft^2, \qquad I_z = 169945\ sl\text{-}ft^2$$

$$W = 33310\ lbf, \qquad m = 1035.31\ slugs \qquad \left(g_\circ = 32.174\ ft/s^2\right)$$

B.4: Atmospheric Data

As in most problems in Flight Mechanics, the solution of our agility sets require data for atmospheric density and sonic speed as a function of altitude. Data for these variables are depicted in Figure B.15. However, we also require the derivatives of these variables with respect to altitude in order to completely specify the aerodynamic force-rates, see equations (3.14)-(3.16). Data for these derivatives are accordingly supplied in Figure B.16.

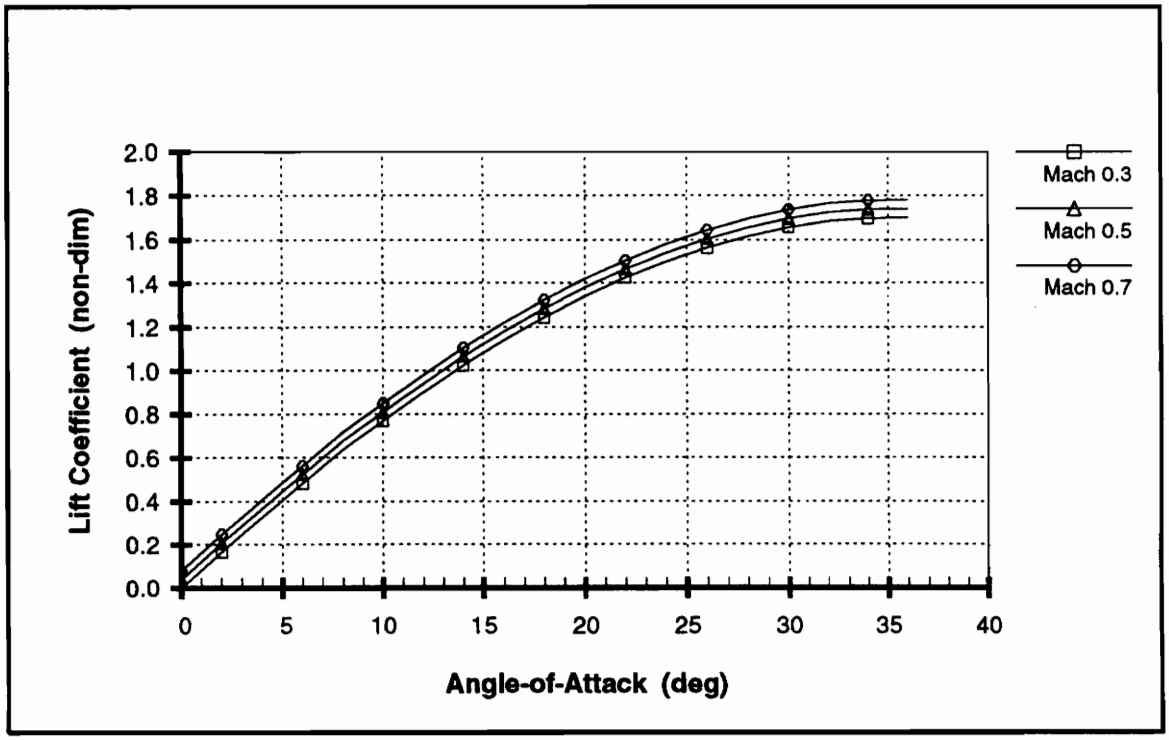

Figure B.1 Lift Coefficient vs Mach and Alpha

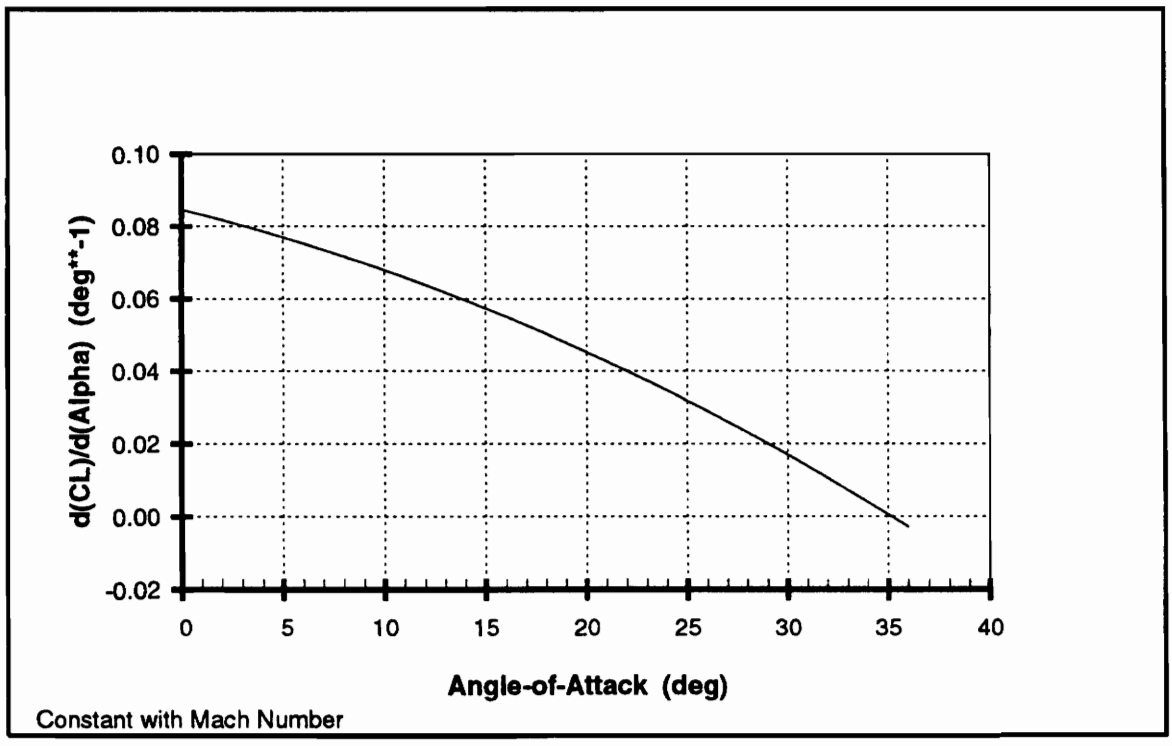

Figure B.2 Lift-Alpha Derivative vs Alpha

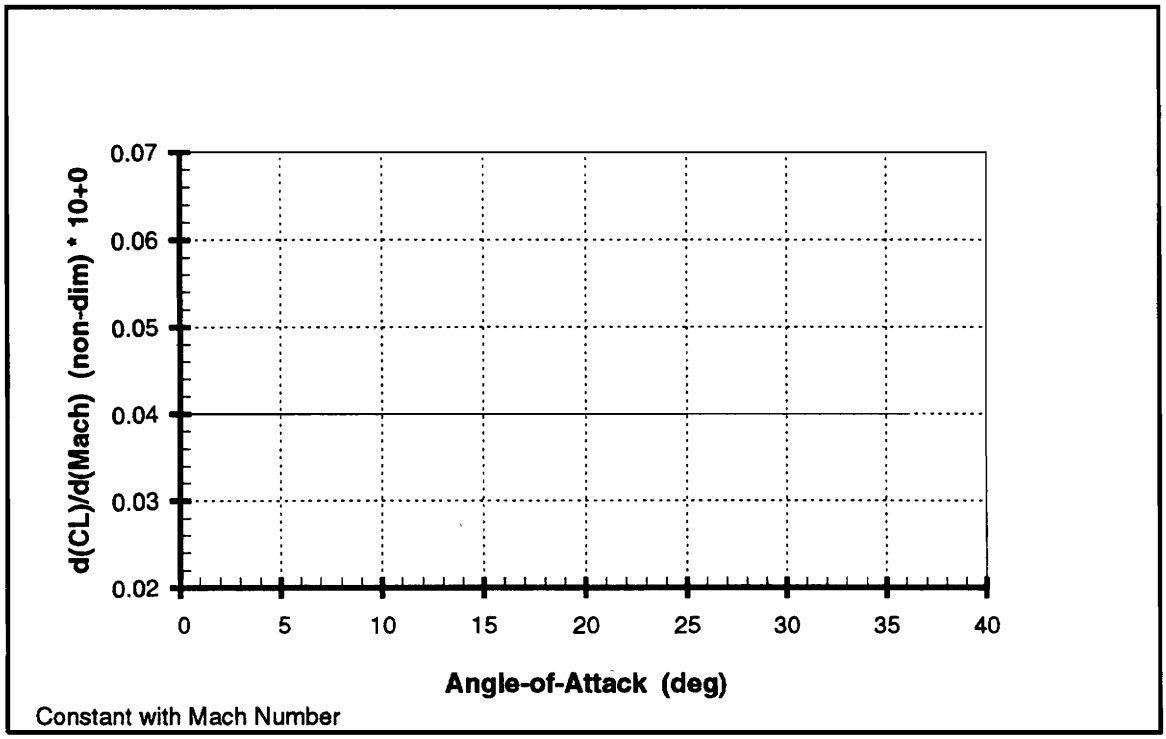

Figure B.3 Lift-Mach Derivative vs Alpha

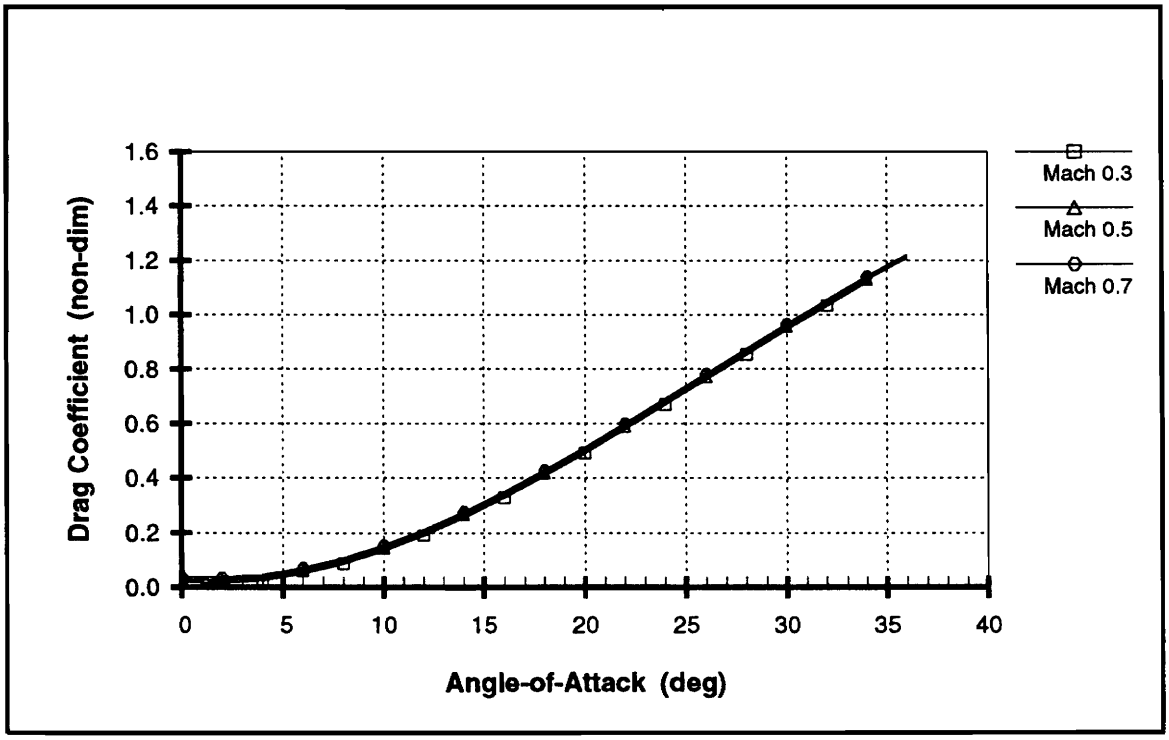

Figure B.4 Drag Coefficient vs Mach and Alpha

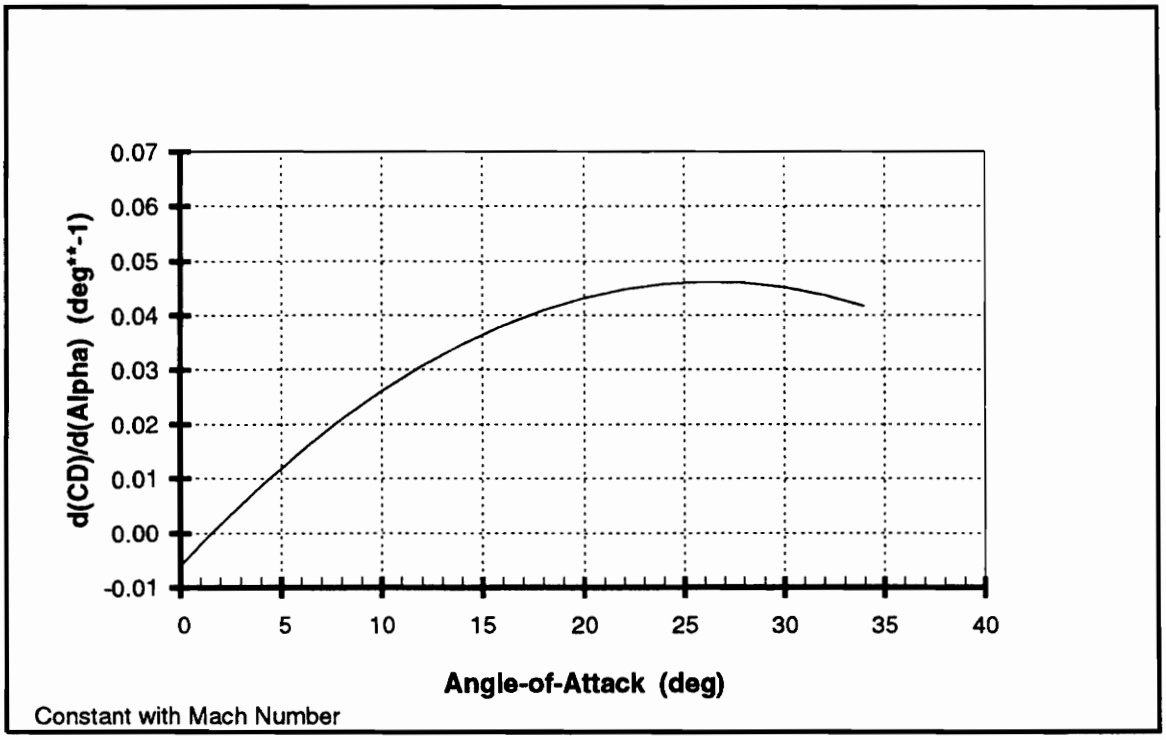

Figure B.5 Drag-Alpha Derivative vs Alpha

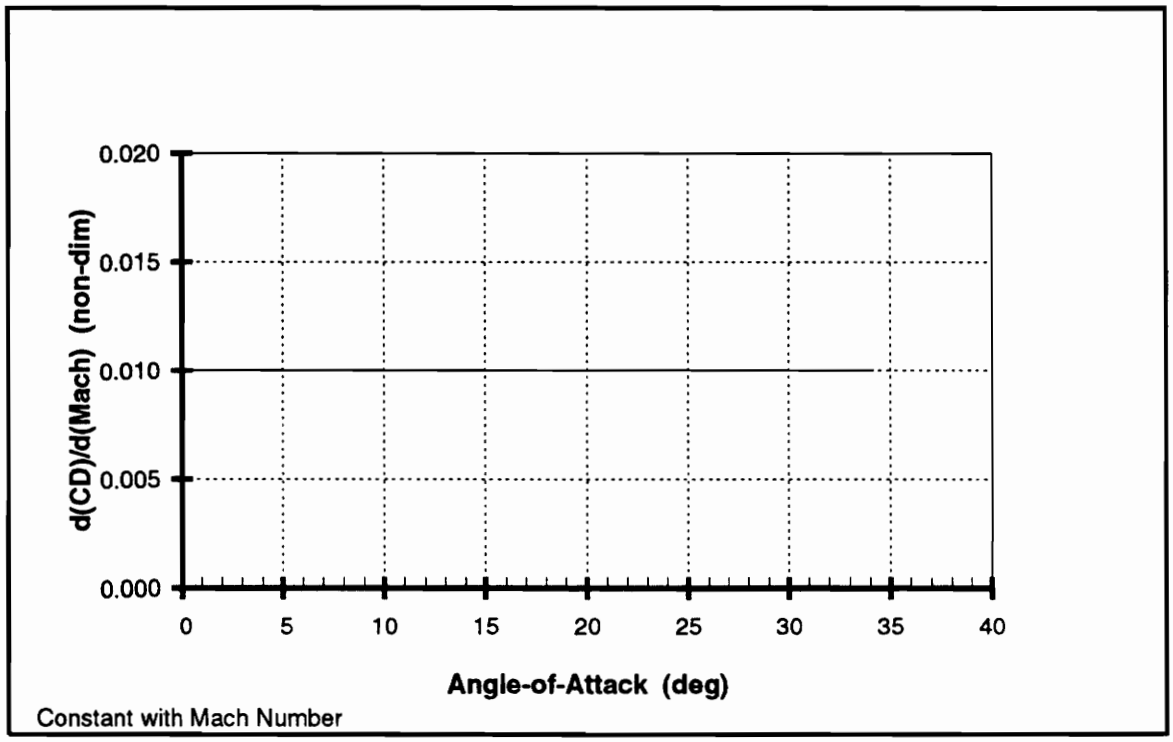

Figure B.6 Drag-Mach Derivative vs Alpha

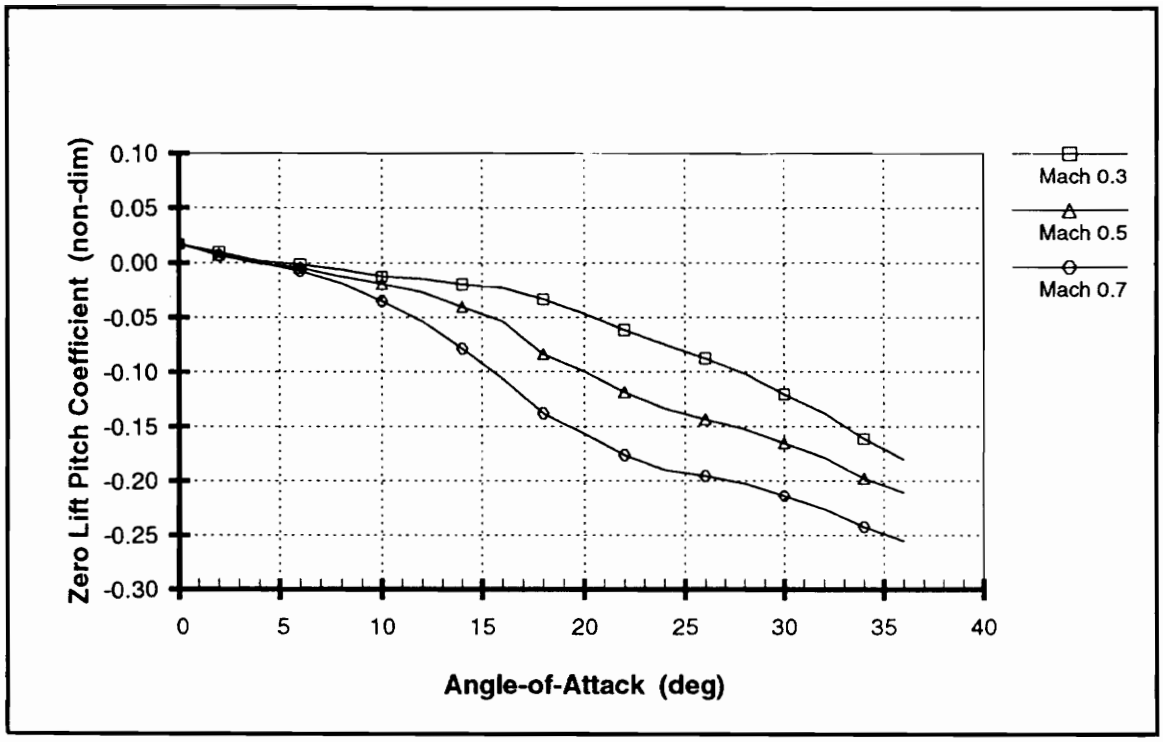

Figure B.7 Zero Lift Pitch Coefficient vs Mach and Alpha

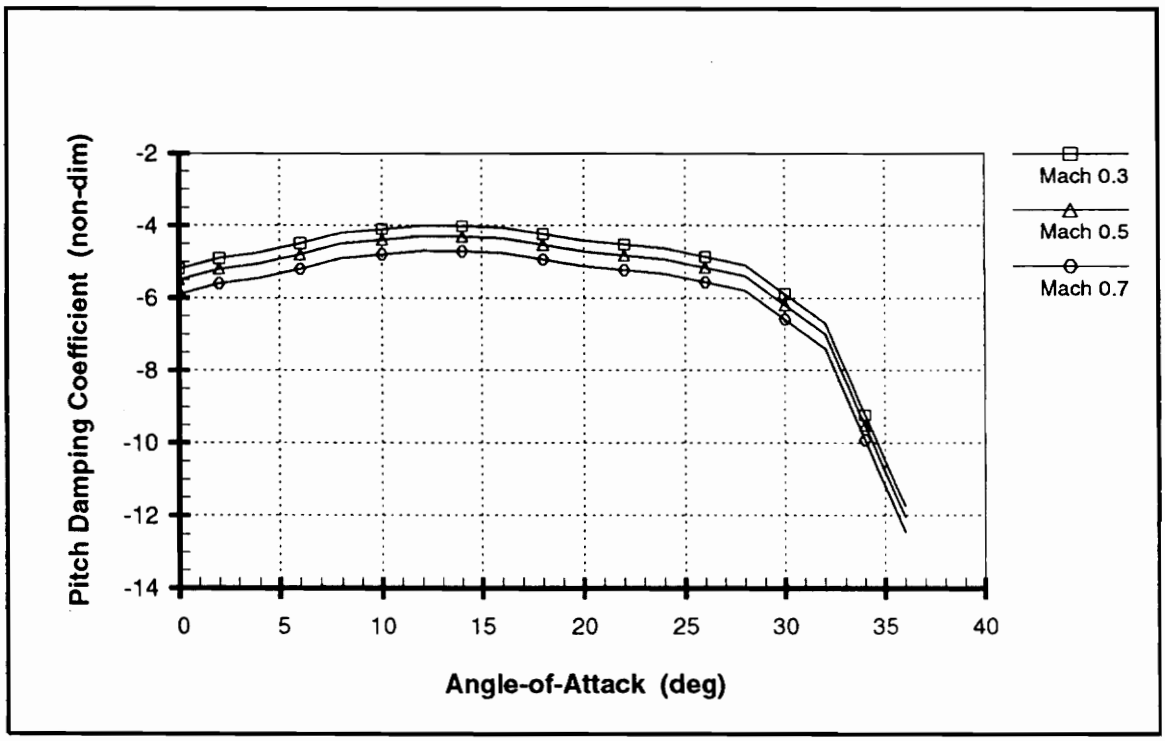

Figure B.8 Pitch Damping Coefficient vs Mach and Alpha

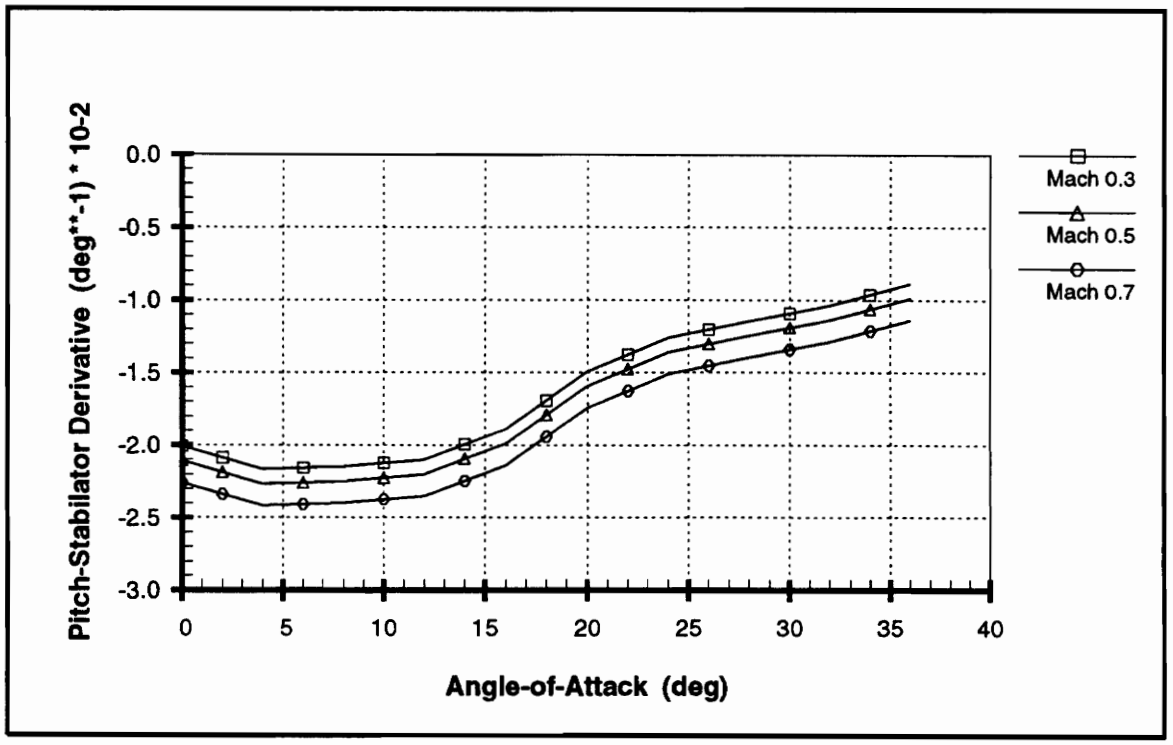

Figure B.9 Pitch-Stabilator Derivative vs Mach and Alpha

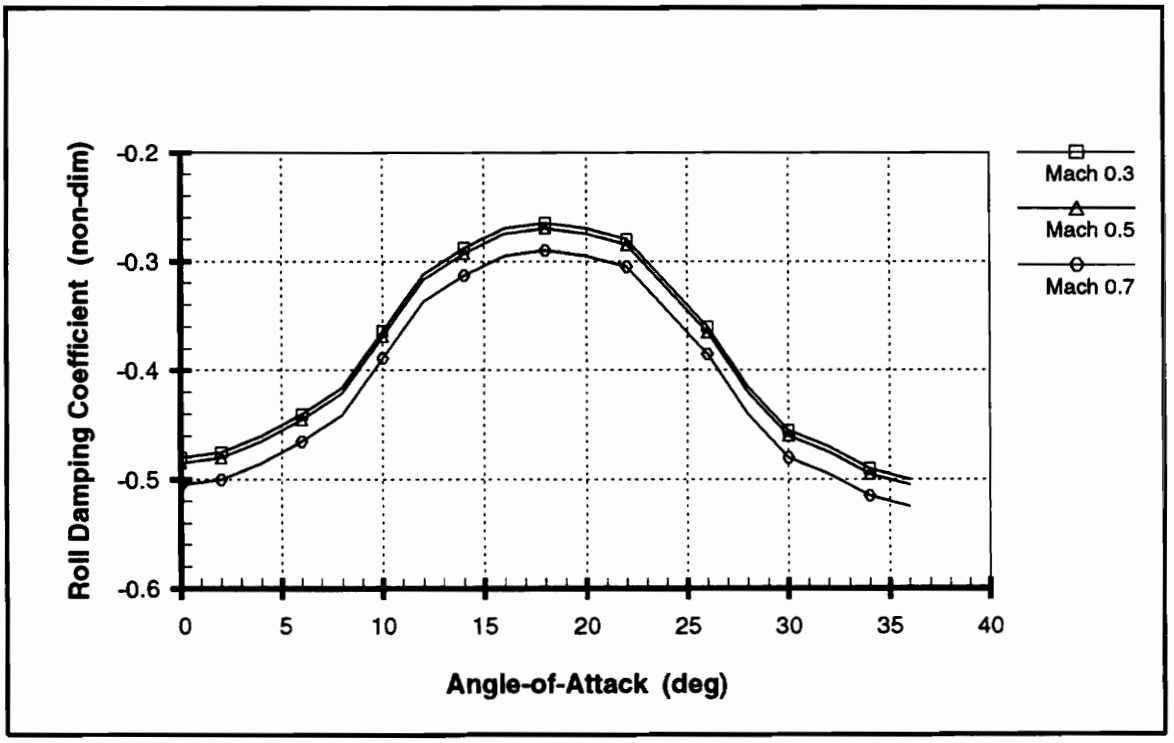

Figure B.10 Roll Damping Coefficient vs Mach and Alpha

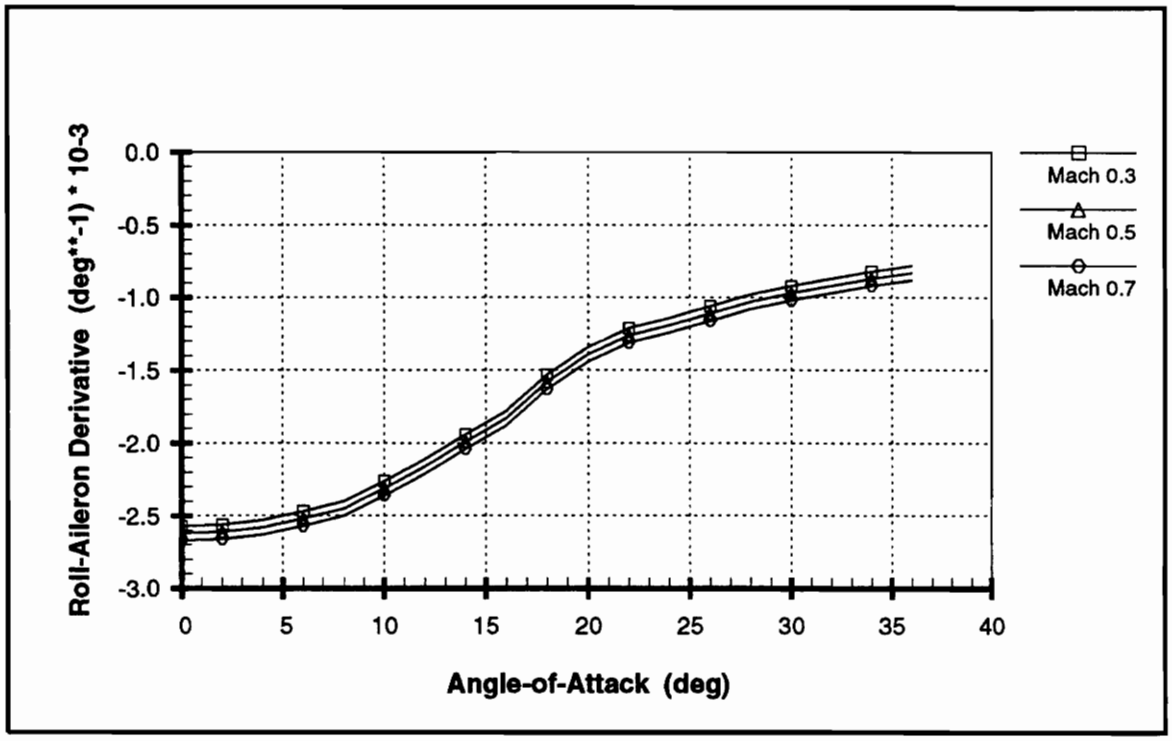

Figure B.11 Roll-Aileron Derivative vs Mach and Alpha

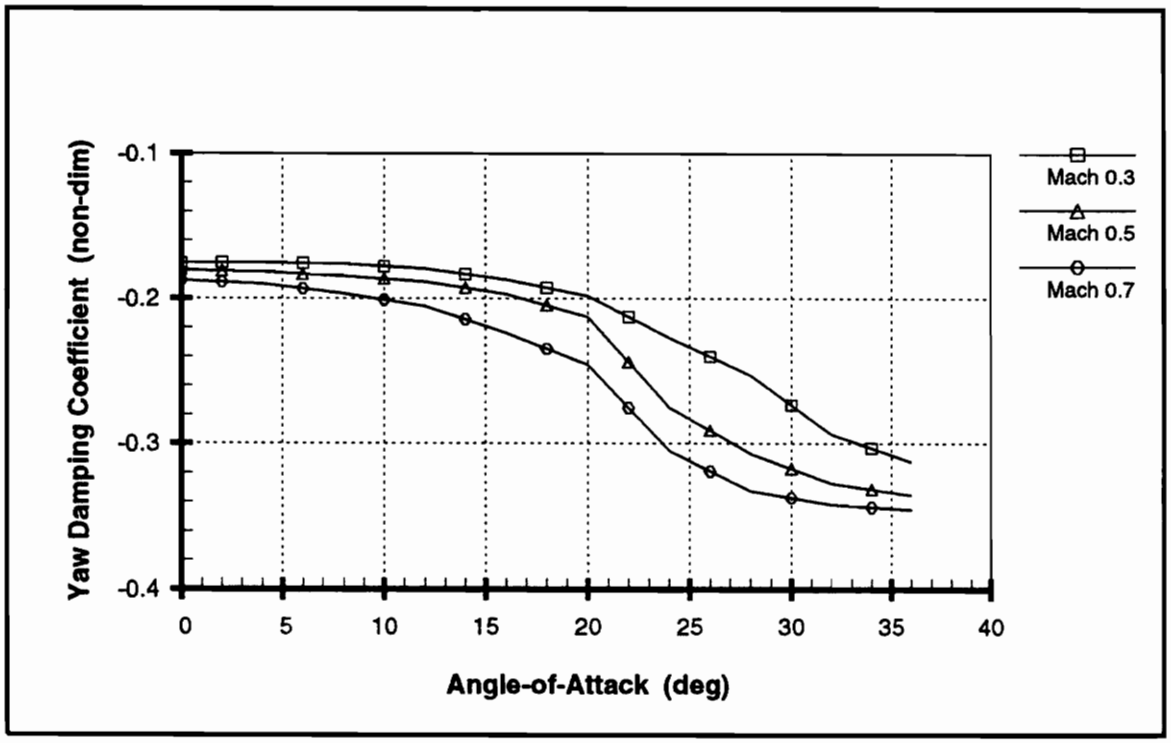

Figure B.12 Yaw Damping Coefficient vs Mach and Alpha

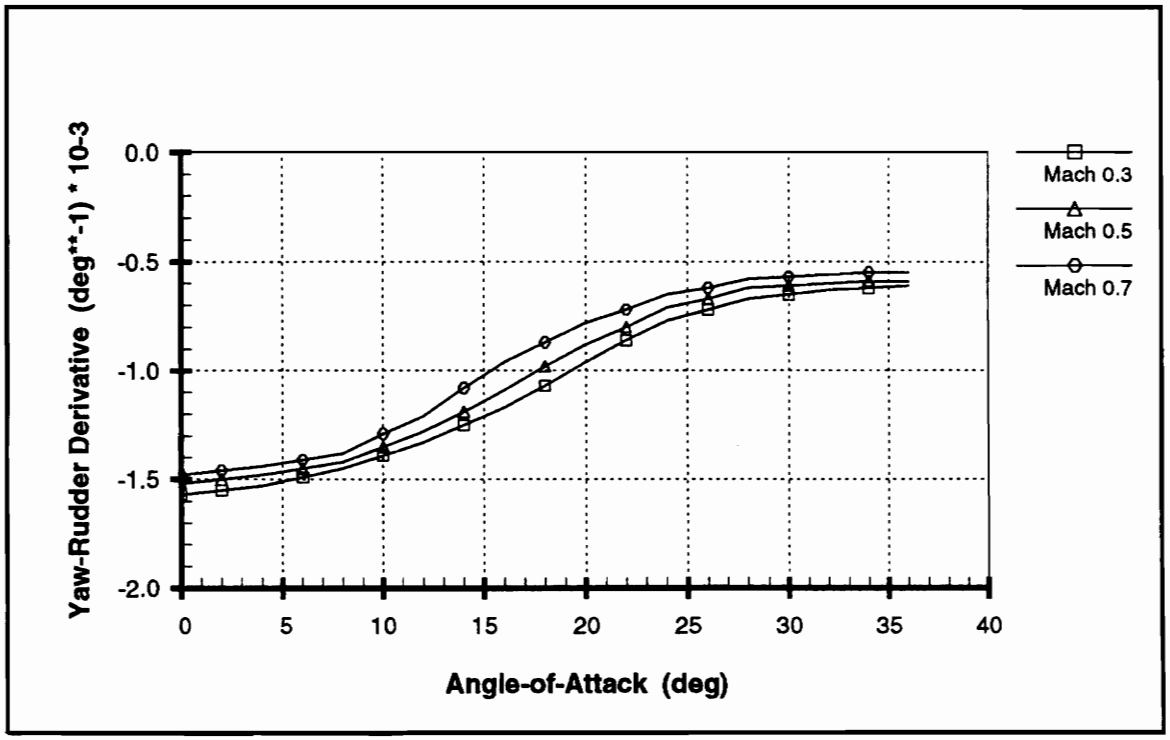

Figure B.13 Yaw-Rudder Derivative vs Mach and Alpha

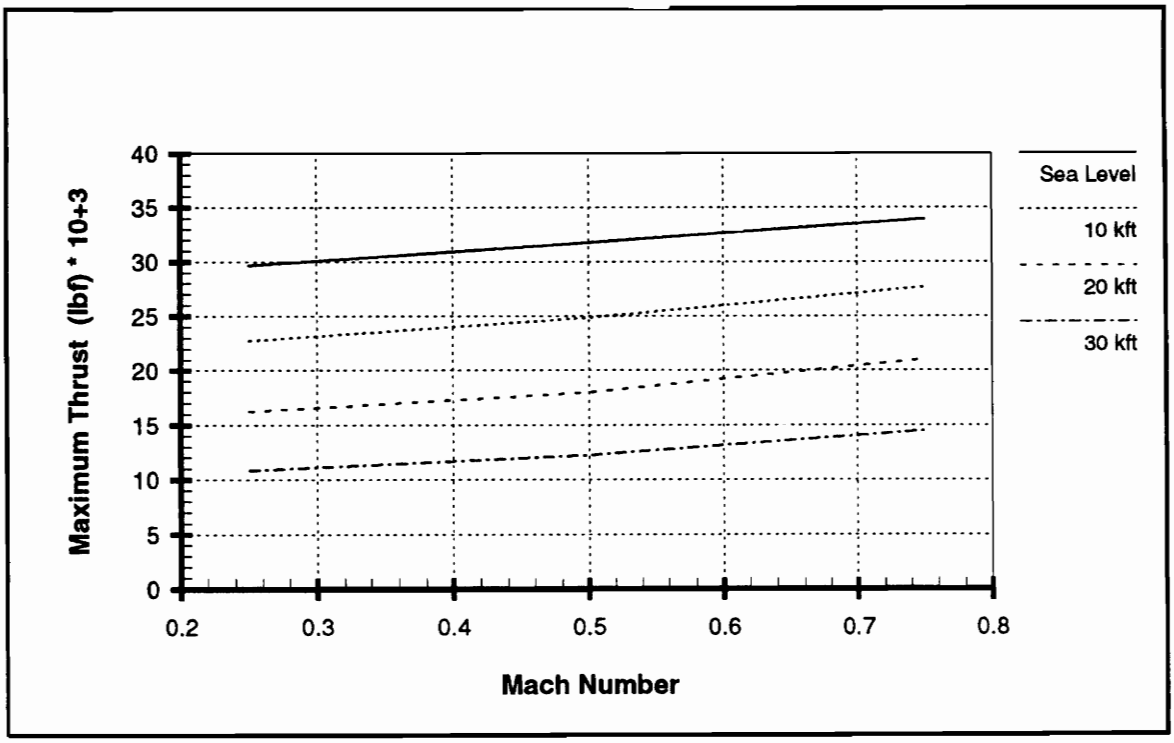

Figure B.14 Max Thrust vs Mach and Altitude

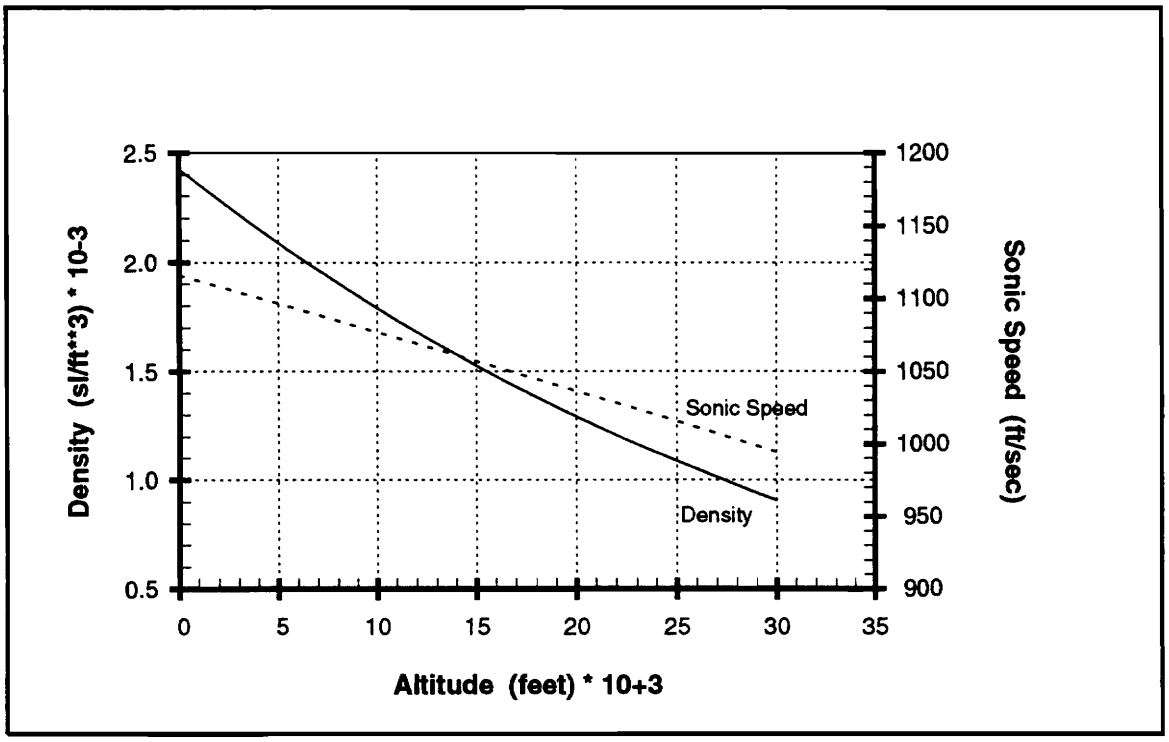

Figure B.15 Atmospheric Density and Sonic Speed

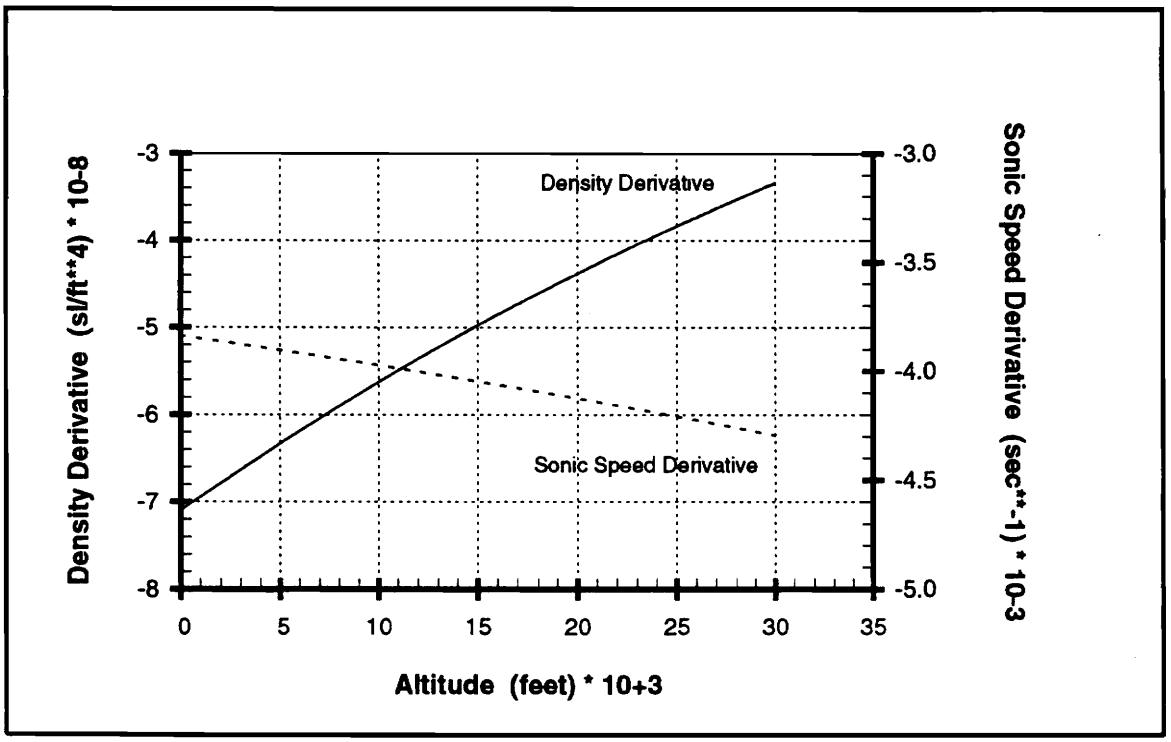

Figure B.16 Density and Sonic Speed Derivatives

APPENDIX C
BRM MOMENT EQUILIBRIUM EQUATIONS

For the sake of completeness, the coefficients for the *BRM* equilibrium equations, presented on page 36 of Chapter 4, are provided below in their complete form. For the roll equilibrium equation we have:

(C.1) $$A_l = \frac{\bar{q}Sb}{(I_z - I_y)} \frac{C_{l_p} b}{2V}$$

(C.2) $$B_l = -\tan\alpha$$

(C.2) $$C_l = -\frac{g}{V} \frac{\sin\mu\cos\gamma}{\cos\alpha}$$

(C.4) $$D_l = \frac{\bar{q}Sb}{(I_z - I_y)} C_{l_{\delta_A}} \delta_A$$

while the coefficients for pitch equilibrium are:

(C.5) $$A_m = \tan\alpha$$

(C.6) $$B_m = \frac{g}{V} \frac{\sin\mu\cos\gamma}{\cos\alpha}$$

(C.7) $$C_m = -\frac{\bar{q}S\bar{c}}{(I_x - I_z)} \frac{C_{m_q}\bar{c}}{2V}$$

(C.8) $$D_m = -\frac{\bar{q}S\bar{c}}{(I_x - I_z)} \left(C_{m_0} + C_{m_{\delta_S}} \delta_S\right)$$

and the coefficients for yaw equilibrium are:

(C.9) $$A_n = -\tan\alpha \frac{\bar{q}Sb}{(I_y - I_z)} \frac{C_{n_r} b}{2V}$$

(C.10) $$D_n = -\frac{\bar{q}Sb}{(I_y - I_z)} \left(C_{n_{\delta_R}} \delta_R + \frac{g}{V} \frac{\sin\mu\cos\gamma}{\cos\alpha} \frac{C_{n_r} b}{2V} \right)$$

APPENDIX D
POINT-MASS OPTIMAL CONTROL SOLUTION

Since the agility metrics defined in Chapter 5 were based on comparisons of the dynamic transients which exist between the body-rate model (*BRM*)and the point-mass model (*PMM*) it is useful to provide the reader with the point-mass model solution to the optimal flight problem. This then is the topic of the current Appendix. With the *BRM* solution to the problem we employed γ, χ, α and μ as state variables and p and q as control variables. However, the *PMM* solution makes use of $\gamma$and χ as state variables and the load-factor, n (ie α), and bank-angle, μ, as control variables. Also, whereas the *BRM* solution required multiple arc structures, we find that the *PMM* solution consists of a single unconstrained, non-singular arc.

The state equations for the *PMM* have the same form as the corresponding state equations for the *BRM ie*;

(D.1) $$\dot{\gamma} = \frac{g}{V}(n\cos\mu - \cos\gamma)$$

(D.2) $$\dot{\chi} = \frac{g}{V}\frac{n\sin\mu}{\cos\gamma}$$

The Hamiltonian is then given as;

(D.3) $$H = \lambda_\gamma\dot{\gamma} + \lambda_\chi\dot{\chi}$$

and the co-state equations are;

(D.4) $$\dot{\lambda}_\gamma = -\frac{g}{V}\sin\gamma\left(\lambda_\gamma + \lambda_\chi \frac{n\sin\mu}{\cos^2\gamma}\right)$$

(D.5) $$\dot{\lambda}_\chi = 0$$

The boundary conditions at the initial time are;

(D.6) $$\gamma(t_0) = \chi(t_0) = 0$$

and the transversality condition requires the following conditions at the final time;

(D.7) $$\lambda_\gamma(tf) = 0; \qquad \lambda_\chi(tf) = 1$$

The controls for the *PMM* solution are limited as follows;

(D.8) $$0 \le n \le n_{max}$$

(D.9) $$-\pi \le \mu \le \pi$$

The control dependent terms of the Hamiltonian are;

(D.10) $$H_{CD} = \frac{g}{V} n\left(\lambda_\gamma \cos\mu + \frac{\sin\mu}{\cos\gamma}\right)$$

Examining (D.10) we see that since *n* appears linearly, the value of *n* at the minimum of the Hamiltonian will be at its lower or upper bound at all times. If the term in parenthese is negative, then *n* will take on its maximum value and vice versa. To determine the optimal value for the bank-angle we apply the minimum principle;

(D.11) $$\frac{\partial H_{CD}}{\partial \mu} = \frac{g}{V} n\left(\frac{\cos\mu}{\cos\gamma} - \lambda_\gamma \sin\mu\right) = 0$$

In order to satisfy (D.11) it is obvious that either n or the term in parentheses must be zero, since $n = 0$ is a trivial solution we assume the following holds true;

$$\text{(D.12)} \quad \lambda_\gamma \cos\gamma = \frac{\cos\mu}{\sin\mu}$$

which results in an optimal control for the bank-angle of the form;

$$\text{(D.13)} \quad \mu(t) = \tan^{-1}\left(\frac{1}{\lambda_\gamma(t)\cos\gamma(t)}\right)$$

Since (D.13) involves a $\tan^{-1}$ term, quadrant resolution is necessary. One way to resolve the quadrant is to apply the 2nd order condition of optimality, specifically we require that;

$$\text{(D.14)} \quad \frac{\partial^2 H_{co}}{\partial\mu^2} = -\frac{g}{V}n\left(\frac{\sin\mu}{\cos\gamma} + \lambda_\gamma\cos\mu\right) \geq 0$$

since $\frac{g}{V}$ and n are both greater than zero at all times, the condition becomes;

$$\text{(D.15)} \quad \frac{\sin\mu}{\cos\gamma} + \lambda_\gamma\cos\mu \leq 0$$

The quadrant for μ is then chosen so as to satisfy the relation in equation (D.15).

VITA

The author was born in Taranto, Italy on 9 February 1960 while his parents were on temporary overseas assignment. He spent most of his youth in Alabama and Florida before attending Auburn University in Auburn, AL where he received a Bachelor of Science degree in Aerospace Engineering in 1983. Upon receiving his undergraduate degree, the author was married to Cathy Leigh Hinson of Birmingham, AL and accepted his first professional assignment with TRW's Ballistic Missiles Division in San Bernardino, CA.

The author spent the first six years of his career at TRW, first serving as a Systems Analyst and finally as a Section Head during his last year of service. In the Fall of 1989 the author chose to leave TRW in order to pursue graduate work at Virginia Polytechnic Institute and State University. Upon completing his classwork in the Fall of 1990 the author accepted a job with Sparta Inc. of Huntsville, AL where he currently works as a Program Manager in the Foreign Systems Division. This thesis represents the final requirements towards the completion of the degree of Master of Science in Aerospace and Ocean Engineering.